TARGETING INFLAMMATION AND FIBROSIS IN LIVER INJURY MOUSE MODELS BY MODULATING MICRORNA-155 EXPRESSION USING PASSIVE LIVER TARGETING LIPID NANOPARTICLES

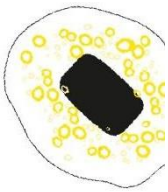

Vishal Tuli (S2664364)

Biomedical Engineering (Bioengineering Technologies)

MASTER'S THESIS

Faculty of Science and Technology (TNW)

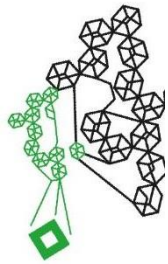

COMMITTEE

Chair: Dr. Ruchi Bansal

External Examiner: Dr. Verena Schwach

Daily Supervisor: Drs. Eline Geervliet

TLR Translational Liver Research

MCBP

UNIVERSITY OF TWENTE.

Acknowledgement

I would like to express my immense gratitude towards my PI, Dr. Ruchi Bansal for giving me the opportunity to pursue this project in the TLR lab. Without her constant support and guidance, the journey for this project would have been exponentially more perilous. I thank her for entertaining my far outreaching theories and ideas and always lending an ear in the capacity of a mentor. I would also like to thank Drs. Eline Geervliet, my daily supervisor, who was always there whenever I needed her, clearing doubts and sharing her experience and of course, for helping me find stuff at the lab (which I was selectively blind for). I have had the opportunity to learn numerous concepts and lab skills under her guidance.

I would also like to extend my gratitude towards the PhD scholars of TLR group, Marit and Richell for helping troubleshooting experiments and entertaining my doubts. They fostered an inclusive and nurturing environment for learning, which is much appreciated. I would also like to thank Abigail Groenenboom, Diana Andreoli and Maissa Satti for being supportive colleagues and for the most random refreshing conversations between breaks. I would especially like to thank members of the “International Hunger” and my family for being a support system throughout this journey.

I finally would like to thank the administrative and technical staff of the MCBP group for their help in realizing this project.

Table of contents

List of Abbreviations

Abbreviation	Full Form / Explanation
NAFLD	Non-Alcoholic Fatty Liver Disease
NASH	Non-Alcoholic Steatohepatitis
ROS	Reactive Oxygen Species
DAMP	Damage-Associated Molecular Pattern
PAMP	Pathogen-Associated Molecular Pattern
PRR	Pattern Recognition Receptor
LPS	Lipopolysaccharide
TLR	Toll-Like Receptor
IL1β	Interleukin-1 Beta
TNFα	Tumor Necrosis Factor Alpha
IL6	Interleukin-6
miRNA	MicroRNA
antimiR	AntimicroRNA
bp	Base Pair
RISC	RNA-Induced Silencing Complex
UTR	Untranslated Region
TGF-β	Transforming Growth Factor Beta
C/EBPβ	CCAAT/Enhancer Binding Protein Beta
HCC	Hepatocellular Carcinoma
NF-κB	Nuclear Factor Kappa B
SMAD4	SMAD Family Member 4
ISRE	Interferon-Stimulated Response Element
IRF	Interferon Regulatory Factor
SHIP1	SH2 Domain-Containing Inositol Phosphatase 1
BCL6	B-Cell Lymphoma 6
LCRα	Locus Control Region Alpha
IL13	Interleukin-13
SMAD2	SMAD Family Member 2
LNA	Locked Nucleic Acid
ZEN	N,N-diethyl-4- (4-nitronaphthalen-1-ylazo)-phenylamine
RNAi	RNA Interference
LNP	Lipid Nanoparticle
siRNA	Small Interfering RNA
ATTR	Amyloid Transthyretin
MC3	Dlin-MC3-MCA
DSPC	Distearoylphosphatidylcholine
DOPC	Dioleoylphosphatidylcholine
DOPE	Dioleoylphosphatidylethanolamine
PEG	Polyethylene Glycol
RES	Reticuloendothelial System
MV	Microvesicle
EV	Extracellular Vesicle
DiO	3,3'-Dioctadecyloxacarbocyanine Perchlorate

DiR	1,1'-Dioctadecyl-3,3,3',3'-Tetramethylindotricarbocyanine Iodide
NC-miRNA	Negative Control MicroRNA
RNA	Ribonucleic Acid
N:P	Nitrogen to Phosphorus ratio
PBS	Phosphate-Buffered Saline
NaCl	Sodium Chloride
MWCO	Molecular Weight Cut-Off
DLS	Dynamic Light Scattering
INF-γ	Interferon Gamma
IL4	Interleukin-4
P/S	Penicillin-Streptomycin
FBS	Fetal Bovine Serum
DMEM	Dulbecco's Modified Eagle Medium
RPMI	Roswell Park Memorial Institute Medium
CCL_4	Carbon Tetrachloride
BSA	Bovine Serum Albumin
DMF	Dimethylformamide
cDNA	Complementary DNA
qPCR	Quantitative Polymerase Chain Reaction
FACS	Fluorescence-Activated Cell Sorting
RIPA	Radioimmunoprecipitation Assay
ELISA	Enzyme-Linked Immunosorbent Assay
HBSS	Hank's Balanced Salt Solution
FGF2	Fibroblast Growth Factor 2
AMSC	Adipose-Derived Mesenchymal Stem Cell
mV	Millivolt
OA/PA	Oleic Acid/Palmitic Acid
ApoE	Apolipoprotein E
LDLr	Low-Density Lipoprotein Receptor
ECM	Extracellular Matrix
IP	Intraperitoneal
IV	Intravenous
iNOS	Inducible Nitric Oxide Synthase
MSC	Mesenchymal Stem Cell
MRC1	Mannose Receptor C-Type 1
ARG1	Arginase 1
IL10	Interleukin-10
LSEC	Liver Sinusoidal Endothelial Cell
MMP	Matrix Metalloproteinase
TIMP	Tissue Inhibitor of Metalloproteinases
LAL-D	Lysosomal Acid Lipase Deficiency
NADPH	Nicotinamide Adenine Dinucleotide Phosphate
HCV	Hepatitis C Virus
HLA	Human Leukocyte Antigen
ASK1	Apoptosis Signal-regulating Kinase 1

PDGF	Platelet-Derived Growth Factor
SOCS1	Suppressor Of Cytokine Signaling 1
AEC	3-Amino-9-Ethylcarbazole
PCR	Polymerase Chain Reaction
DNA	Deoxyribonucleic acid
mRNA	messenger ribonucleic acid
PDI	Polydispersity index
nm	nanometer
FLAPS	Fluorescent light-up aptamers
EV	Extracellular vesicles
STAT3	Signal transducer and activator of transcription 3

Abstract

Chronic liver injuries are a major health risk worldwide and responsible for over 1.2 million deaths globally each year. They can be caused by a variety of etiologies such as alcohol abuse, hepatitis B/C viral infections, unhealthy diet and lifestyle etc. but follow a common progression of hepatocellular damage induced inflammation and fibrosis, leading to cirrhosis and/or hepatocellular carcinoma. Even with a significant burden on healthcare, chronic liver diseases do not have a therapy showing significant benefit in terms of amelioration of inflammation or fibrosis available in the market. The differential expression of miRNAs has been explored as a potential diagnostic tool as well as a therapeutic target in liver diseases. miRNAs are small non-coding RNAs that regulate the expression of mRNAs by binding to their 3'UTR. Of the multiple miRNAs differentially regulated in chronic liver diseases, miRNA-155 is considered as the main inflammation and fibrosis regulator, also known as a master regulator of inflammation. Lipid nanoparticles (LNPs) are one of the best non-viral delivery systems for nucleic acid and were explore for delivering antimiR-155 to the liver as a therapeutic strategy. Three different LNP formulations based on different helper lipids – DSPC, DOPC and DOPE, were engineered and characterized for differences in their physiochemical properties showing variation in zeta potential. None of the LNPs affected the metabolic activity of the cell populations treated with them. They were explored in the context of *in vitro* cellular uptake specificity in cell lines representing liver populations (RAW264.7, AML12, 3T3 and H5V) and *in vivo* organ biodistribution, in an acute liver injury mouse model. DSPC LNPs showed the best results in passive targeting of the liver and were employed to deliver antimiR-155 in a therapeutic efficacy study using a semi-chronic liver injury mouse model. The antimiR-155 DSPC LNP therapy showed a trend of amelioration of inflammation and fibrosis as compared to the Negative Control – LNP (NC-LNP) treatment, presenting itself as a promising therapeutic strategy in focus of chronic liver injuries.

1. Introduction

1.1. Liver structure and function

The liver is one of the largest organs in the body, contributing about 1/50 of the total adult body weight. Apart from being one of the biggest, it is also one of the most complex and versatile organs in the human body, serving a crucial role in several essential processes such as maintaining homeostasis. The liver can be divided into five major tissue systems based on its structure and histology – hepatic lobule, biliary system, stroma, sinusoidal cells, vascular tissue(1). The parenchymal or hepatocyte population in the liver is estimated to account for 78% of the total liver volume, while the non-parenchymal population accounts for about 2.1% Kupffer cells, 2.8% endothelial cells and 1.4% stellate cells, making a total of 6.3% of total hepatic volume. The rest of the volume is attributed to the extracellular spaces(1,2).

By virtue of its positioning, the liver is involved in the synthesis and absorption of nutrients, immune response regulation, as well as filtration of xenobiotic substances. It has a huge role in the metabolic processing of biomolecules like amino acids, proteins, carbohydrates and lipids as a precursor to the synthesis of hormones as well as serum proteins like albumin, fibrinogen etc. These hormones facilitate the regulation of plasma glucose and the processing of vitamins. Another part of its detoxification functions is the processing of ammonia in the body to urea which is excreted in the urine. It is also responsible for the removal of bilirubin from the blood. The liver, being so versatile, also has the highest regenerative capability of any organ in the body and can repair itself after cases of partial hepatectomy or chemical induced injury, at a cellular level(1–3).

The portal veins and the hepatic arteries supplies blood, enriched with nutrients to the liver. The portal blood supply is connected to the pancreas, intestine and the spleen and thus, carries secretions from them to the liver as well. The portal veins account for about three-fourths of the total blood supply to the liver and the hepatic artery accounts for the rest. The liver contributes its filtration capabilities to two different perfusion circuits – the splanchnic-sinusoidal-systemic circulation and the entero-hepatic circulation. The former referring to the circulation of blood between the gastrointestinal tract, liver, spleen, and pancreas and the latter referring to the circulation of bile acids from the liver to the small intestine and back to the liver. The hepatic lobules are the functional units of the liver and amount to about 100,000 in number. They constitute a hexagonal arrangement of single layered hepatocytes (**Figure 1**). Hepatic sinusoids are the low pressure channels, with circulation of blood from portal tract to the terminal hepatic venule. The blood flows from the portal vein, into the sinusoids, perfusing the liver cell plates in the hepatic lobule, and exits through the hepatic venule to the systemic circulation(1–3).

Hepatocytes are the predominant and largest cellular components found in the liver lobules, constituting approximately 60-70% of the cell population and about 80% of the liver's total mass. As mentioned earlier, hepatocytes possess a distinctive polygonal shape with a typical diameter ranging from 20 to 30μm.

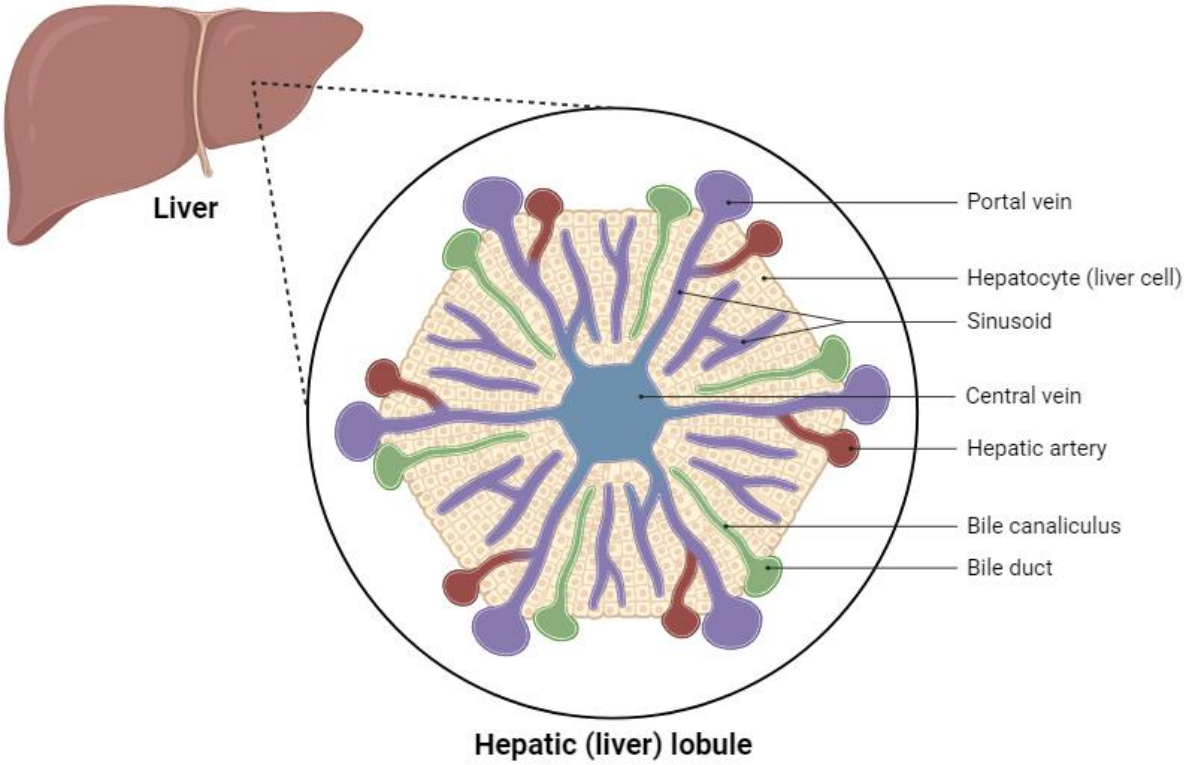

Figure 1: Structure of hepatic lobule: The hepatocytes are arranged in a hexagonal fashion to form a single layer. The sinusoids are low pressure channels allowing the flow of blood from the portal vein to the central vein(4,5) (adapted from Ricken et al.,2015)

Functionally and structurally, hepatocytes display a remarkable polarity. They possess three distinct membrane domains that serve specific purposes - the basal (or sinusoidal) domain, which interfaces with the sinusoidal blood vessels, featuring short microvilli that facilitate the exchange of molecules between hepatocytes and the bloodstream; the lateral domain, establishing the junctional complexes between adjacent hepatocytes, promoting cellular cohesion and communication; the apical (or canalicular) domain, responsible for the secretion of bile into the bile canaliculi, which subsequently merge to form larger bile ducts. The spatial arrangement of hepatocytes is characterized by their polarization, leading to their alignment in cords that form liver plates. These plates are closely positioned and facilitate the movement of substances from the bloodstream into hepatocytes for various metabolic and detoxification processes(2).

Kupffer cells, also referred to as the resident macrophages in the liver, are specialized immune cells prominently found in the sinusoids. They contribute to about 15% of the total cellular population in the liver. They, being present in the sinusoids, interact with the blood flowing through them, allowing them to capture foreign particles and pathogens. The Kupffer cells have an essential role in immune-surveillance and defense mechanism of the liver. They do so by getting activated during inflammatory conditions and secreting pro-inflammatory cytokines and chemokines like TNFα, IL6 and IL1β, which recruit other immune cells as a response(2,6,7).

LSECs or liver sinusoidal endothelial cells are specialized cells that line the sinusoidal walls in the liver. LSECs account for about 16% of the total cell population in the liver. They form the interface between the bloodstream and the liver parenchyma, creating a barrier with intracellular fenestration pores, ranging from 150 to 175nm in diameter. Their fenestrated structure permits the rapid exchange of small molecules, hormones, and nutrients between the bloodstream and hepatocytes in the space of Disse. They are equipped with scavenger receptors and mechanisms that enable them to capture and eliminate pathogens, bacteria, cellular debris, and particles that may enter the liver via the bloodstream and thus, play a significant role in the local immune response. They are also known for presenting antigens to immune cells and secreting cytokines and chemokines that act as immunomodulators(6,8). Apart from their role in local immune response, they are also involved in the regulation of blood coagulation and clotting factors. They synthesize and release von Willebrand factor, a protein essential for blood clotting, contributing to haemostasis and preventing excessive bleeding(9).

Hepatic stellate cells, also known as perisinusoidal cells and ito cells make up about 8% of the total cell population in the liver. They reside in the liver's perisinusoidal space within the space of Disse and are characterized by fibroblast-like phenotype(2). Under healthy physiological conditions, the hepatic stellate cells exhibit a quiescent state, being responsible for functions like storage of vitamin A as lipid droplets in their cytoplasm as well as maintaining the extracellular matrix (ECM) homeostasis. The ECM homeostasis is maintained by secretion of ECM proteins, matrix metalloproteases (MMPs) and tissue inhibitors of MMPs (TIMPs). However, during inflammation or liver injury, the stellate cells undergo activation, transforming into a myofibroblast-like phenotype. Activated HSCs become the primary source of excess extracellular matrix production in response to injury, disturbing the balance between production and degradation of ECM, progressing to the development of fibrosis in chronic liver diseases. The excessive ECM deposition can disrupt the liver's normal structure and function, contributing to the progression of liver fibrosis and cirrhosis(10,11). They also act as antigen presenting cells along with regulators of blood flow into the space of Disse(12). Upon the resolution of inflammation or injury, the stellate cells undergo apoptosis in order to transition into the healthy physiological microenvironment(11).

1.2. Liver injury – inflammation and fibrosis

Liver diseases account for about 1.2 million deaths worldwide per year contributing significantly to the global burden on healthcare(13). The main causes of these diseases can be listed as - ethanol abuse (alcohol associated liver disease), Hepatitis viral infections (hepatitis B and C), cholestasis as well as metabolic syndromes coupled with unhealthy lifestyle (NAFLD, NASH, etc.)(14). Apart from the mainstream diseases, ailments such as auto-immune disorders (autoimmune hepatitis, primary biliary cholangitis and primary sclerosing cholangitis), drug overdose hepatotoxicity and genetic factors (Lysosomal acid lipase deficiency (LAL-D), hemochromatosis etc.) also contribute to liver injuries(15).

Most of the liver injuries follow a common route, starting with prolonged exposure to abuse via various stimuli (alcohol, fatty diet, HCV etc.) leading to hepatocellular damage. The hepatocytes undergo necrosis and apoptosis, releasing Damage associated molecular patterns (DAMPs), pro-inflammatory cytokines, chemokines, reactive oxygen species (ROS) etc., which induce an inflammatory response. The inflammatory response corresponds to the activation of liver resident macrophages, Kupffer cells and the infiltration and maturation of circulating monocytes, causing chronic inflammation. The immune cells in the liver secrete pro-inflammatory factors, prolonging the inflammation, as well as pro-fibrogenic factors, leading to the activation of hepatic stellate cells, which causes an imbalance in the homeostasis of ECM production, ultimately leading to fibrosis(10,11,14,15).

Liver fibrosis is characterized by the excessive accumulation of extracellular matrix proteins like collagen and is the result of wound healing response of the liver, in case of liver injury. In case of acute liver injury, as seen in case of viral hepatitis infections, the necrotic and apoptotic cells are replaced by parenchymal cells amidst the inflammatory response. This process is supplemented by limited deposition of ECM as well. The persistence of liver injury as in case of chronic ailments, the liver regeneration is unable to keep up and the damaged hepatocytes are replaced with ECM composed of predominantly fibrillar collagen. The localization of fibrotic tissue depends on the ailment and its progression through the structure of the liver. It is initially found in the pericentral and perisinusoidal areas in case of alcohol induced liver injury and around portal tracts in cases of chronic hepatitis and cholestatic disorders. The chronic nature of the liver injury leads to increase in the fibrotic tissue, slowly progressing into cirrhosis(11,16).

Hepatic stellate cells are the main population that produces ECM in the case of liver injury. As mentioned earlier, in a healthy liver, the stellate cells exist in a quiescent state, inhabiting the space of Disse and primarily functioning as storage units for vitamin A. However, in response to chronic injury, they undergo an activation, transitioning into a myofibroblast-like phenotype. In the activated state, HSCs acquire contractile, proinflammatory, and fibrogenic properties, migrating to sites necessitating tissue repair. They secrete copious amounts of ECM, while also modulating ECM degradation(11,17). The stellate cells are activated by a mitogen known as platelet-derived growth factor (PDGF), released primarily by Kupffer cells(18). Characteristic observation of liver fibrosis is the alteration not only in the quantity of the ECM, but also in the quality of it by factors released by hepatic stellate cells. The accumulation and the change in the composition of the ECM is caused by the lowering the expression of ECM degrading MMPs like MMP1, the overexpression of ECM degrading MMP inhibitors like TIMP1, as well as an overexpression of proteins composing the ECM like collagen-1 and collagen-3. The continuous and prolonged fibrosis unavoidably results in cirrhosis and can even progress into hepatocellular carcinoma eventually(10,17).

1.2.1. Pathogenesis of fibrosis in context of different chronic liver injuries

As mentioned earlier, most chronic liver diseases progress by the route of hepatocellular damage induced inflammation to fibrosis, developing to cirrhosis and/or hepatocellular carcinoma (HCC)(10,17). However, there are certain pathologies more prominent in different types of chronic liver diseases, which describe their unique progression(14) (**Figure 2**).

In alcohol induced liver injury, abusing alcohol compromises the gut bacterial population and the intestinal functioning, leading to the proliferation of gram-negative bacteria. This leads to an increase in the concentration of lipopolysaccharide (LPS) in the blood flowing through the portal vein. LPS stimulates Kupffer cells by engaging the toll-like receptor 4 complex, which leads to the production of ROS via NADPH oxidase(19). In the Kupffer cells, the ROS upregulates the production of NF-κB, which causes an increase in the level of TNFα production as it is a direct downstream product. TNFα recruits other immune cells like neutrophils, monocytes etc. and also triggers ROS production in hepatocytes, causing them to go down the apoptosis cascade. ROS combined with acetaldehyde, a metabolite of alcohol are responsible for the activation of Hepatic stellate cells and initiating fibrosis(19,20).

During HCV induced liver injury, the pathogenesis is based on the unique ability of the viral particles to bypass the human leukocyte antigen presentation mediated immune response by having a part of its protein assemble with HLA-1. It infects the hepatocytes and evades immune response, causing oxidative stress by increasing the production of ROS, which leads to the recruitment of pro-inflammatory immune cells. The recruitment of pro-inflammatory immune cells as well as the ROS, both contribute to the activation of stellate cells and lead to fibrosis(21,22).

Cholestasis refers to the slowing or stagnation of bile flow through the biliary system, which can be caused by issues in the bile ducts or the liver. The pathogenesis in chronic cholestatic liver disorder is mediated by T lymphocytes, recruited by cholangiocytes(23). The cholangiocytes also release pro-inflammatory chemokine and cytokines along with fibrogenic mediators, recruiting immune cells as well as activating the myofibroblasts in the vicinity. The myofibroblasts change the ECM composition and the pro-inflammatory immune cells release more cytokines, together leading to the recruitment of stellate cells and ultimately fibrosis(24).

NASH, or Non-Alcoholic steatohepatitis is characterized by excessive fat deposition in liver leading to steatosis and hepatocellular damage with chronic inflammation and varying degrees of fibrosis, due to an unhealthy lifestyle involving high fat diet. Its pathogenesis has been associated with diabetes type-2, dyslipidemia and obesity. The most revered two hit model for NASH states that the insulin resistance combined with hyperglycemic conditions leads to increase in the concentration of free fatty acids, leading to steatosis in hepatocytes. The oxidative stress and the pro-inflammatory cytokines initiate apoptotic cascade in hepatocytes and recruit inflammatory immune cells in the second hit of the

pathogenesis. The ROS and pro-inflammatory cytokines and chemokines contribute to the activation of stellate cells and initiate the cascade leading to fibrosis(25,26).

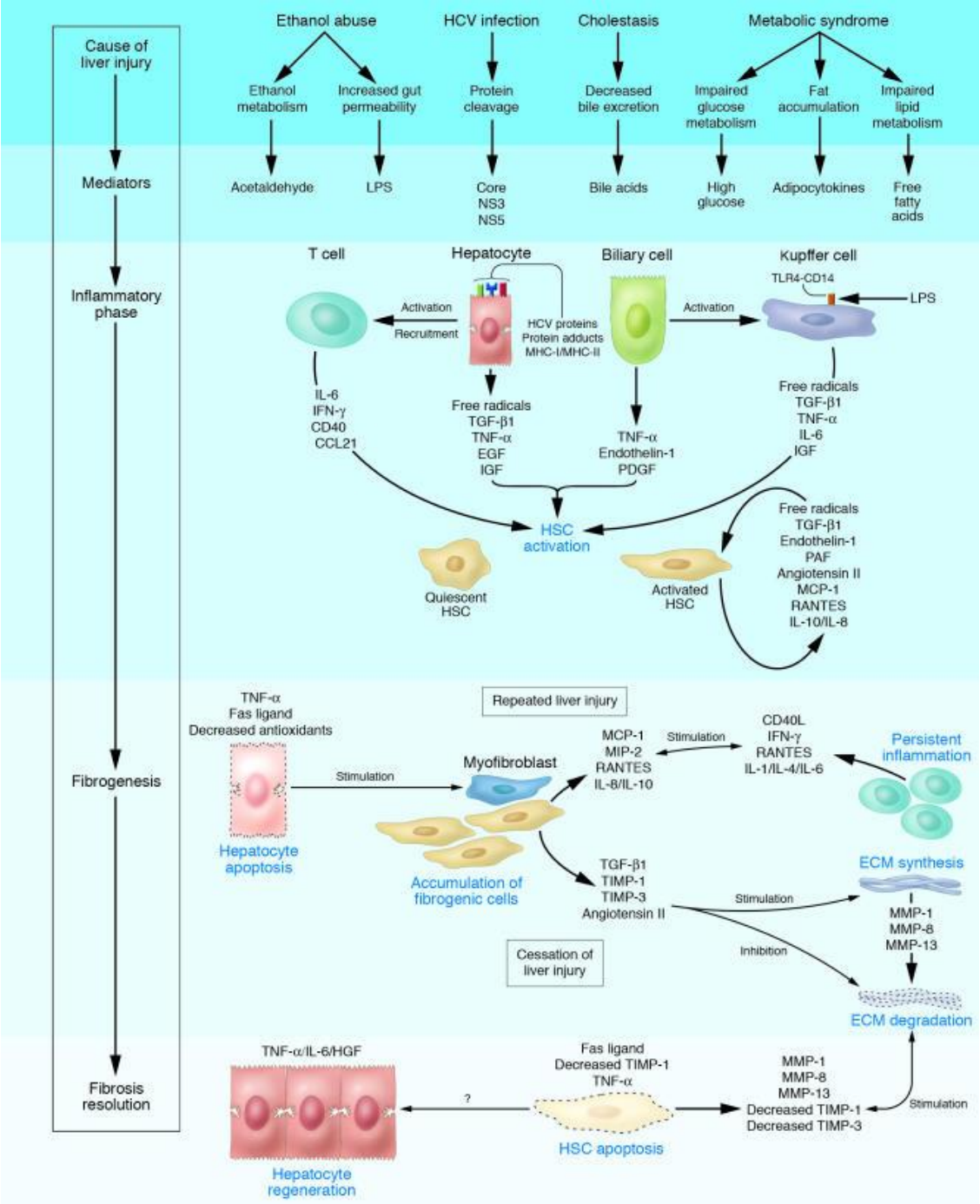

Figure 2: Cellular mechanisms involved in the pathology of Liver fibrosis based on different causes of chronic liver injury. Various types of hepatotoxic agents produce mediators that induce inflammatory response in hepatic cell populations. The damaged hepatocytes and cholangiocytes release pro-inflammatory cytokines which activate Kupffer cells and stimulate the recruitment of activated T cells. the inflammatory response leads to the activation of hepatic stellate cells, which transition into a myofibroblast-like phenotype. Activated stellate cells release cytokines in order to perpetuate their activation and regulate ECM production as well as degradation. In case of resolution of inflammation during the early stages, fibrosis is resolved.(16) (adapted from Bataller and Brenner, 2005)

1.2.2. Current and emerging therapies for fibrosis

As seen in the pathophysiology of fibrosis, there are multiple factors that affect its progression and hence, it has multiple targets that can be exploited for developing therapeutic strategies. Although it is reversible up to a certain level, if left untreated, develops into cirrhosis and may even progress into hepatocellular carcinoma(15,16,18). Many different clinical studies focus on the cellular and molecular mechanisms involved in liver fibrosis in order to develop effective treatment strategies. With the advancement in technology as well as our understanding of the condition, new therapeutics have emerged, targeting specific mechanism of progression(27).

Generally drug therapies have been the mainstream treatment for ailments and same was the case for fibrosis in the early days. There have been multiple compounds tested for their therapeutic efficacy against it but only a handful showed promising results like, Vitamin E, which is a well-known free radical scavenger and has been shown to ameliorate steatosis, hepatocellular ballooning, inflammation, and decreased levels of serum hepatobiliary enzymes considerably in a NASH model(28,29). It is now considered as an optional treatment for NASH patients but is still not preferred as the main course of action due to the absence of data on long term high concentration administration as well as its potential toxicity(30–32). Selonsertib, an ASK1 inhibitor, targeting the apoptotic signal in stellate cells showed promising results by significantly reducing fibrosis in a clinical trial of 67 NASH patients, but recently in two phase 3 trials, there was no significant antifibrotic effect observed(33).

Just like the drug based therapies, cell based therapies have also emerged as promising options, like the transplantation of endothelial progenitor cells, bone marrow progenitor cells, mesenchymal stem cells etc. in a disease model. They have shown mixed results as the transplanted cells have secondary interactions which could possibly cause complications(34).

RNA interference (RNAi) based therapies are an up and coming strategy to tackle the progression of liver fibrosis. Every ailment has a certain disease profile which can be assessed by the differential expression of non-coding RNAs in the cells. The differential expression of the non-coding RNAs is being explored as a diagnostic tool. Since these non-coding RNAs are regulatory in nature, they are also being studied as therapeutic targets. microRNAs (miRNA) are 19-23bp long RNA sequences, which regulate the expression of mRNAs by binding to them. There have been clinical studies highlighting different miRNAs having differential expression in case of liver injury as well and have been used as therapeutic targets as well(35). miRNA-23b/27b cluster has been shown to downregulate the expression of gremlin 1 protein in order to suppress stellate cell activation(36). Matsumoto et al. demonstrated the potential of miRNA-29a to suppress the expression of Collagen 1 and PDGF-C in CCl_4 induced fibrosis mouse model(37). The aberrant expression of miRNA-200 has been linked to the proliferation and migration of stellate cells and can be used as a promising target as well(38).

With all the therapeutic options mentioned above, there is a lot of hope for an effective treatment to be approved, however, none of them have yet made into the market. There are no drugs or therapies showing significant benefit, reversal of liver fibrosis or effective immunomodulation available to the patients at the moment.

1.3. miRNA Biogenesis

The canonical biogenesis of miRNA is initiated by the transcription of the pri-miRNA transcript by RNA Polymerase II, characterized by the hairpin structure (**Figure 3**). The pri-miRNA is broken down by the Drosha and DiGeorge Syndrome Critical Region 8 (DGCR8) complex to create the precursor-miRNA (pre-miRNA) by cleaving off the 3' and 5' ends off(39). The pre-miRNA is exported to the cytoplasm by the Exportin/RanGTP pathway(40). In the cytoplasm, the pre-miRNA is cleaved by Dicer to yield an RNA duplex with the sense and the anti-sense strands. Either the sense or the anti-sense strand of the mature duplex is loaded onto the Argonaute protein to form the RISC – RNA induced silencing complex, where the 20-25bp long miRNA acts as the guide(41). It does so by exploiting a 2-8 base pair long seed sequence which complements the mRNAs being targeted for degradation. These complexes bind to the 3' Untranslated region (3'-UTR) of targeted mRNAs and tag them for silencing by either blocking translation or degradation.

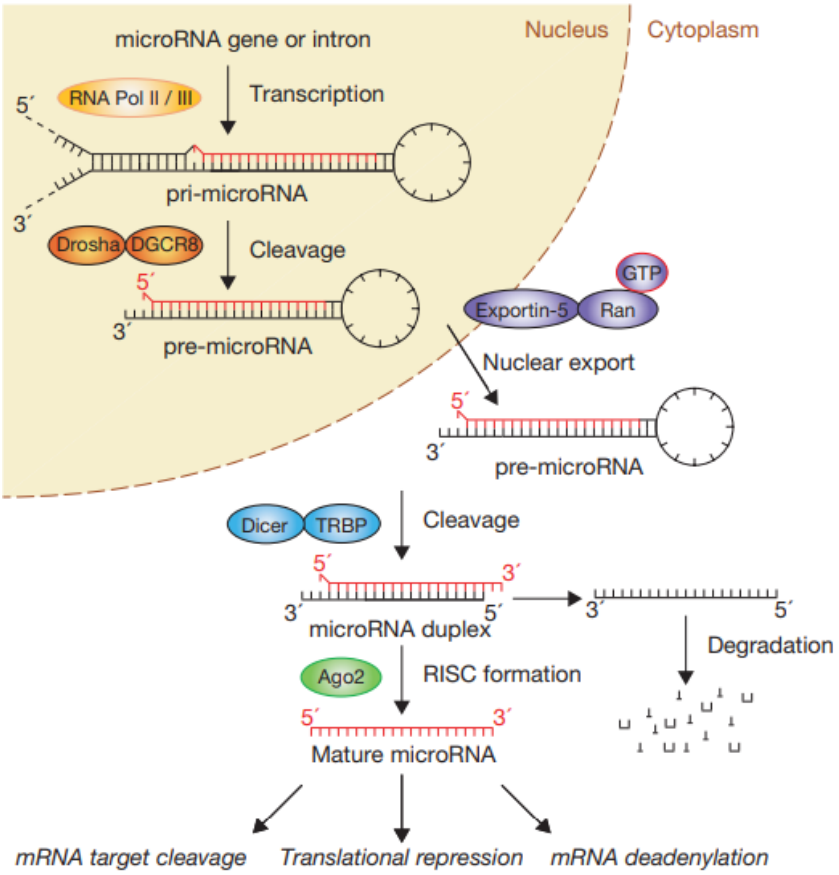

Figure 3: Biogenesis and processing of miRNA: The pri-miRNA transcript is transcribed by RNA Pol II and broken down by Drosha and DGCR8 to make pre-miRNA. The pre-miRNA is exported to the cytoplasm by Exportin/RanGTP complex and cleaved by Dicer to get a miRNA duplex. The sense strand of the duplex binds to the Ago2 protein to form the RISC and targets mRNAs to modulate their translation.(42)

1.4. miRNAs involved in liver inflammation

miRNAs have been shown to have regulatory effects on a broad spectrum of biological processes, including cell differentiation, proliferation, metabolism, development, apoptosis, secretion etc. They have also been explored in the context of liver functioning, affecting processes such as lipid and glucose metabolism, apoptosis, necrosis etc. The dysregulation of miRNAs can be induced by multiple factors, including causes of chronic liver injury like, alcohol abuse, fatty diet, genetic factors etc. Thus, the miRNA dysregulation can be affiliated with the different pathologies of these conditions(43).

Chronic inflammatory diseases, derived from atypical immune response display complex mechanisms involving changes in gene expression of immune cells. The emerging role of miRNAs in correlating their differential expression and the innate immune response strongly suggests an immunoregulatory role(44–46). There are several miRNAs, including miRNA-122, miRNA-132, miRNA-155 and miRNA-146a have shown to have a regulatory role in case of liver inflammation(43,47–51). miRNA-155 is also known as the master regulator of inflammation, owing to its multiple downstream effectors and its upregulation in multiple other ailments as well(52). In case of liver, it is considered as the main modulator of inflammation due to effects on both, innate and adaptive immunity by mediation of monocytes, macrophages, T-cells, B-cells as well as dendritic cells(53). Thus, exploiting it as a therapeutic target would enable targeting the epicenter of inflammation in liver diseases, and a decrease in inflammatory behavior would translate into lower fibrosis, decreasing chances of cirrhosis.

1.5. miRNA 155 and inflammation

miRNA-155 has been described as a master regulator of inflammation in the literature(52). It has been associated with diseases such as viral infections, bacterial infections, cancer, autoimmune disorders etc. Its expression is controlled by many different pathways with bilateral functioning, for example, TGF-β can both induce as well as inhibit its expression. There are other pathways that have unidirectional effect on its levels as well, usually pro-inflammatory increasing it and anti-inflammatory reducing it(53). The title of master regulator of inflammation stems from its multiple downstream effectors as seen in **Figure 4**. It has numerous targets which lead to a domino effect of increasing the levels of inflammatory cytokines in the microenvironment of the cells. Its increased expression has been associated with the poor prognosis of multiple different inflammation related ailments as well as metabolic dysfunction syndromes(54).

In the case of liver, the molecular mechanism described for it shows increased levels of miRNA-155 being directly correlated with the decrease in the levels of CCAAT/enhancer binding protein (C/EBPβ), leading the hepatocytes to adopt a cancerous phenotype(55). Studies on hepatocellular carcinoma (HCC) patients have shown significant increase in the level of miRNA-155 as compared to healthy individuals(56). Certain research groups have also

shown the oncogenic potential of high miRNA-155 levels during inflammation in HCC progression(57). It inhibits factors like SHIP1, SOCS1 and BCL6, which regulate the expression of chronic inflammation associated cytokines like TNFα, IL6, IL1β and IL8. It also downregulates proteins like IL13Rα and LXRα, which are involved in anti-inflammatory response pathways(54).

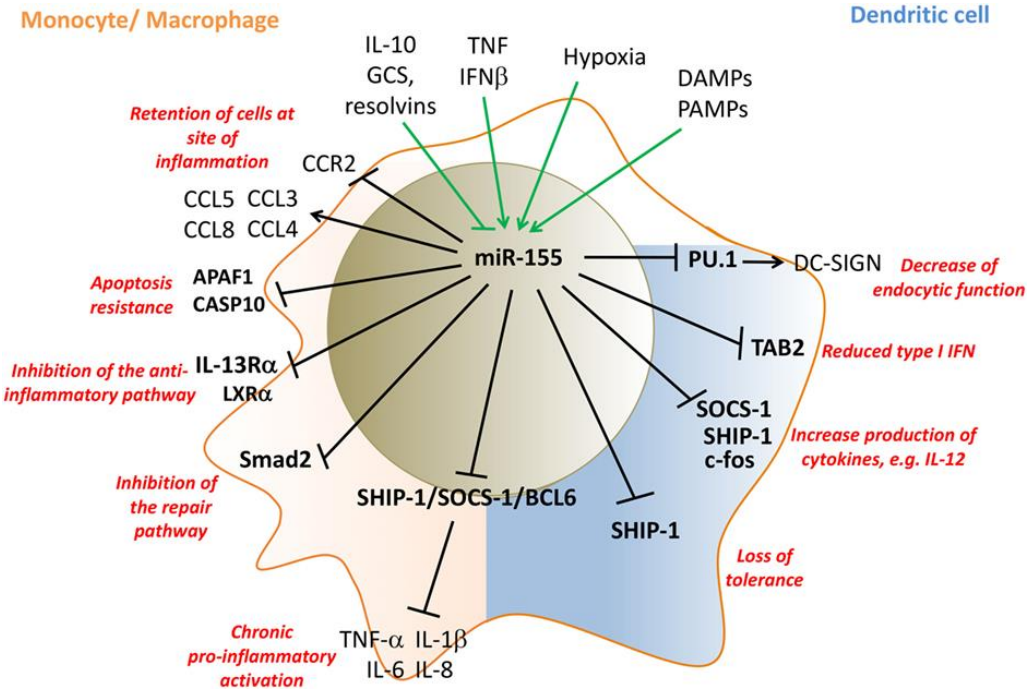

Figure 4: Multiple downstream inflammatory effectors of miRNA-155 in monocytes, macrophages and dendritic cells: miRNA-155 affects inflammation, apoptosis, anti-inflammatory responses, repair pathways as well as chronic inflammatory pathways, living up to its title of master regulator of inflammation(54)

Overexpression of miRNA-155 has been lined to HCC progression and tumorigenesis and is also associated with prognosis of HCC survival as seen in **Figure 5**(58).

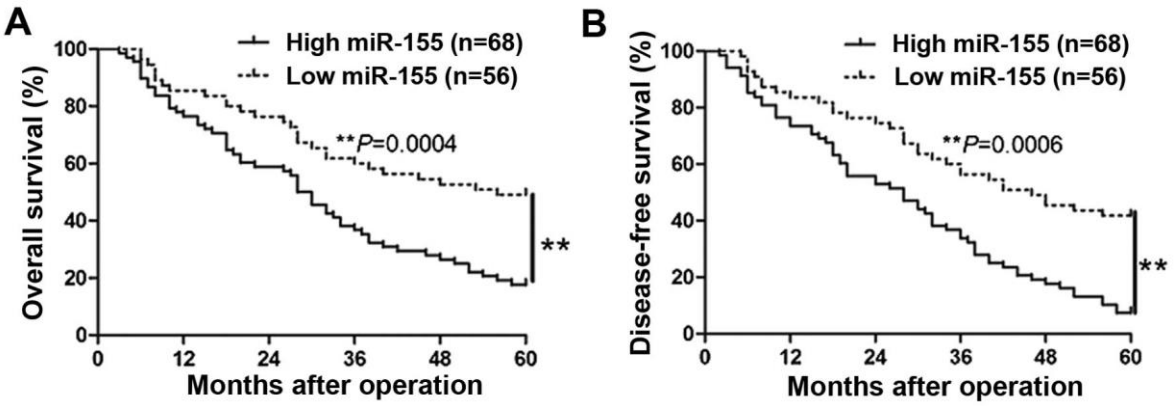

*Figure 5: Prognosis of HCC patients correlated to miRNA-155 levels assessed by Kaplan-Meier analysis. Patients with higher miRNA-155 levels showed a lower (A) overall survival and (B) disease-free survival | **P<0.01.(58)*

Zhang et al. showed that hepatitis C infection upregulated miRNA-155 levels (**Figure 6**) with the involvement of NF-κB, leading to the activation of WNT pathway and ultimately promoting carcinogenesis. miRNA-155 has many sites already characterized for transcription factors such

as NF-κB, SMAD4, ISRE, IRF etc. which play major roles in inflammation(59). The liver has 4 major cell populations – hepatocytes, Kupffer cells, sinusoidal endothelial cells and stellate cells(2).

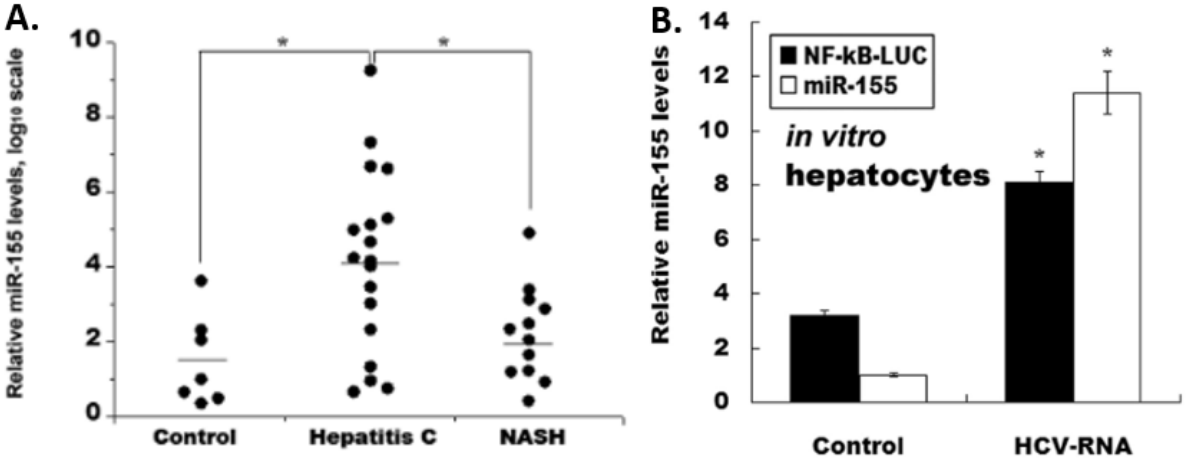

Figure 6: Correlation of HCV viral load with miRNA-155 levels (A) Significant increase in miRNA-155 levels of HCV patients as compared to healthy ones (B) Increase in miRNA-155 levels in NF- κB dependent manner in HCV patients(59)

Overexpression of miRNA-155 has been shown to induce proliferation in hepatocytes as shown in **Figure 7**(60). It induces a pro-inflammatory phenotype in Kupffer cells and leads to pro-inflammatory cytokine release. The pro-inflammatory cytokines recruit macrophages which infiltrate the liver which are also pro-inflammatory in nature, with high levels of miR-155. A study by Csak et al. showed mice fed with methionine deficient diet developing severe steatohepatitis, with increased levels of miRNA-155 in hepatocytes as well as Kupffer cells(61). The endothelial cells and stellate cells have no recorded effects of increase or decrease in the levels of miRNA-155 to the best of our knowledge.

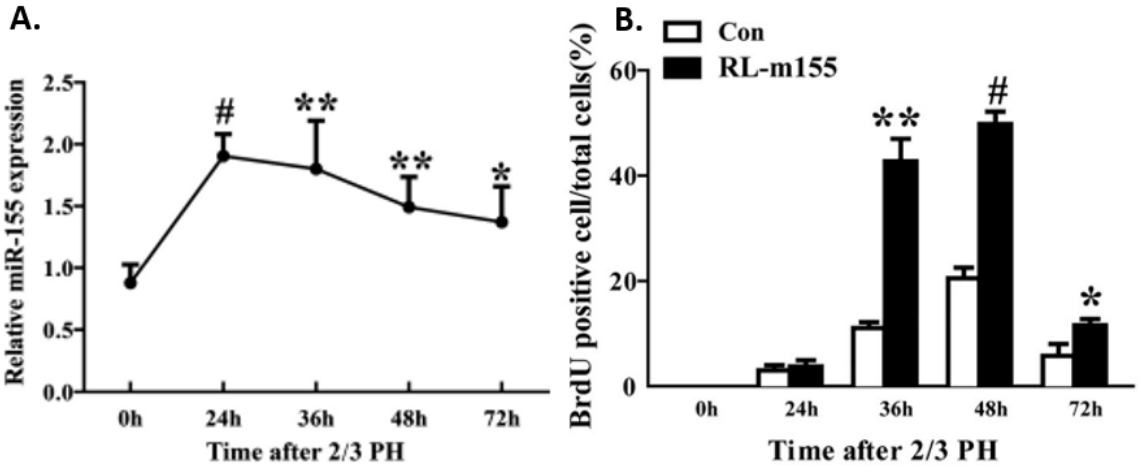

*Figure 7: miRNA-155 overexpression in hepatocytes promotes proliferation A) miRNA-155 levels in mice post 2/3 partial hepatectomy B) BrdU assay revealing higher proliferation in RL-m155 mice in comparison to ConA treated mice, correlating with elevated miRNA-155 levels. | *P<0.05, **P<0.01, and #P<0.001(60)*

miR-155 targets SOX1, SHIP1 and BCL6 in order to promote the production of pro-inflammatory cytokines such as TNF-α, IL6 and IL1β, while suppressing the anti-inflammatory

cytokines such as LCRα, IL13, SMAD2 etc. as was seen in **Figure 4** earlier. The high levels of miRNA-155 directly as well as indirectly lead to the macrophage population to be polarized to M1 – proinflammatory phenotype.

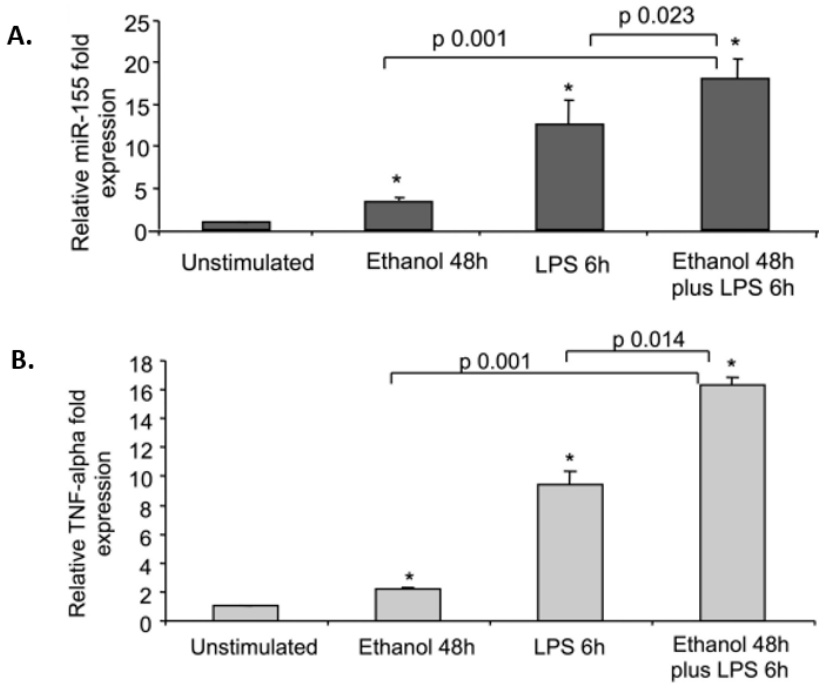

Figure 8: Correlating expression of miRNA-155 with elevated levels of TNFα in RAW264.7 macrophages treated with LPS and/or alcohol: (A) RAW 264.7 macrophages miRNA-155 levels quantified with qPCR (B) RAW 264.7 macrophage TNFα levels quantified with qPCR(62)

microRNA 155 has a central role in the propagation of inflammation in the liver and this is linearly dependent on TNFα and IL6 levels, which can be seen from the results by Bala S. et al as well as from the work of my predecessor, Miranda Türkal shown in **Figure 9**(62,63). This highlights the therapeutic target potential of miRNA-155 in ameliorating inflammation in the liver. Strategies involving regulation of miRNA-155 levels in macrophages could be promising for controlling inflammation.

1.6. MicroRNA therapies

MicroRNAs are molecules with multiple downstream targets and have been known to create a different expression profile, depending on the condition of the cell as well as the microenvironment. These expression profiles have been theorized to be used as a diagnostic marker and moving in the same direction, specific microRNAs can also be exploited as therapeutic targets(64,65). Most of the pathways influenced by microRNAs are in a feedback mechanism with no epicenters defined as causal or effectual discretely. Different disease conditions have been characterized by either over or under expression of certain microRNAs, effectively increasing or decreasing its downstream interactions. Two strategies have been devised in order to capitalize on the therapeutic potential of microRNAs – antimicroRNA (antimiR) and microRNA mimics. The antimicroRNAs are antisense oligonucleotides,

complimentary for the target miRNA, binding to it. By binding to it, the antimiR effectively blocks it from interacting with the mRNA sequences. The miRNA mimic is a sequence similar to the target miRNA and increases its population in the cell, leading to the increase in its activity in the model. These pertain to Loss of function and Gain of function therapeutic strategies respectively as visible in **Figure 9**(66).

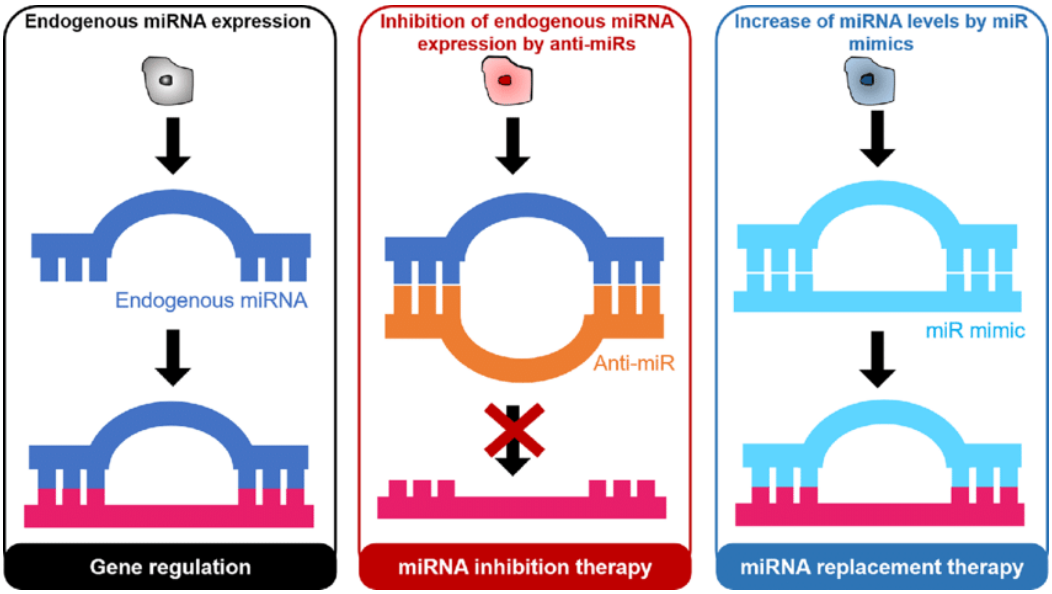

Figure 9: Graphic representation of antimir and miR mimic strategies utilized for potential therapy development: Endogenous miRNA binds to target mRNA and alters its translation, antimiRs bind to the specific miRNA sequence barring it from binding to its target mRNA, miRNA mimics increase the amount of specific miRNAs and hence increase the chances of interaction with the target mRNA(67)

antimiRs and miRNA mimics are 19-24 bp long RNA molecules, thus have a significantly short half-life. They can also be degraded by extra and intra-cellular nucleases. An ideal sequence used for miRNA therapy would have certain characteristics – high affinity to target, resistance to nucleases, low toxicity and high cellular specificity. The high affinity as well as low toxicity can be attained by modification of bases like methylation or by replacing them. There are chemical modifications which when introduced to the antimiR or miRNA mimic oligonucleotides, boast of an increased stability, and half-life, counteracting the degradation by nucleases and plasma clearance. These modifications include locked nucleic acids (LNAs), 2'-O-methoxyethyl modification and the ZEN modification in the latest generation of antimiRs. Lennox et al. showed that the "2'OMe 5'inZEN, 3'ZEN" modification pattern in different miRNA mimic sequences showed no evidence of degradation even after incubation for 4 days in liver protein extract(68). However, currently there aren't any strategies exploited to direct naked miRNA mimic and antimiR sequences to specific cell populations or organs. In order to have another barrier against degradation, immune response as well as have the capability to target specific organs or cell populations, lipid nanoparticles (LNPs) have been used as highly efficient delivery agents for such small molecule therapeutics(69).

1.7. Lipid nanoparticles

Lipid nanoparticles are one of the most advanced non-viral delivery systems for therapeutics in the market today(69). A landmark achievement in the field of drug delivery took place in the year 2018, when the first RNAi (RNA interference) based therapy, being delivered by LNPs was approved for human use. The FDA (Food and Drug Administration) approved the delivery of siRNA using lipid nanoparticles for the treatment of hereditary transthyretin amyloidosis (ATTR). The company Onpattro currently sells the therapy under the name Patisiran(70).

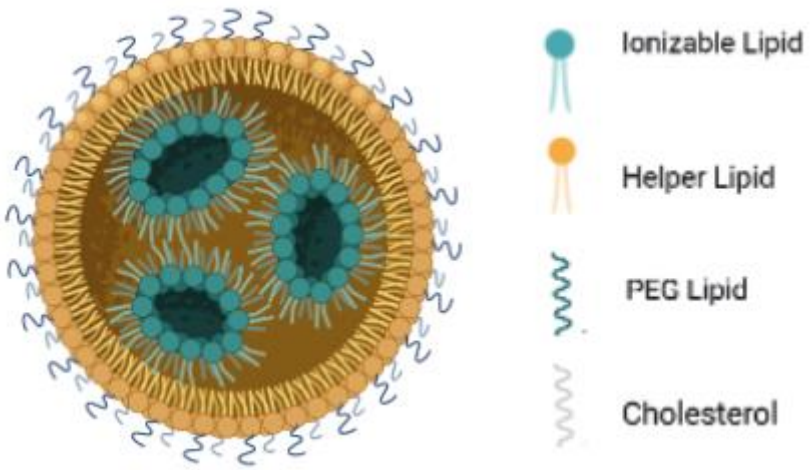

Figure 10: Composition of Solid Lipid Nanoparticles: Solid LNP formulations have ionizable lipids to trap nucleic acids, Helper lipids for easy uptake by the cell, PEG lipid to increase half-life and hydrophobicity and cholesterol to fill in the voids for a tighter packing(71)

ATTR Amyloidosis occurs when the liver produces faulty transthyretin proteins and thus the therapy delivery system focuses on the liver as well, specifically to the hepatocytes(72). The lipid nanoparticles used for siRNA delivery are composed of 4 different lipids: (6Z,9Z,28Z,31Z)-Heptatriaconta-6,9,28,31-tetraen-19-yl 4- (dimethylamino)butanoate ((DLin-MC3-DMA) (ionizable lipid)), 1,2-distearoyl-sn-glycero-3-phosphocholine (DSPC (Helper lipid)), Cholesterol and 1,2-Dimyristoyl-sn-glycero-3-methoxypolyethylene glycol (PEG-2K-C-DMG (structural lipids)) in specific proportions(70). The types of lipids used are consistent with many other formulations tested by different research groups around the world as shown in **Figure 10**. The ionizable lipids have special properties which make them positively charged at a low pH, allowing them to load negatively charged nucleic acid cargo, and become neutral at physiological pH, and finally releasing the cargo in the acidic microenvironment of the endosome. The helper lipids are usually a kind of phospholipid which helps with the endocytosis of the LNP as well as the endosomal escape of the cargo(73). As mentioned above, the Onpattro Patisiran formulation uses DSPC which is a fundamental lipid constituent of the cell membrane and comprise of saturated acyl chains. It is responsible for the rigidity and stability of the cell membrane. Somme other helper lipids used in conjunction with different ionizable lipids are - 1,2-dioleoyl-sn-glycero-3-phosphocholine (DSPC) which also a phosphatidylcholine like DSPC, however, it has unsaturated bonds in its acyl chains. As a component of the cell membrane, it is responsible for the flexibility and adaptability of it; 1,2-

dioleoyl-sn-glycero-3-phosphoethanolamine (DOPE) is a phosphatidylethanolamine unlike DSPC and DOPE. It is an essential lipid in the cell membrane on account of its role in the maintenance of the curvature. It is able to do so due to a charged ethanolamine head group and unsaturated bonds in its acyl chain(74). The PEG lipids are usually added for a stealth effect and stability, increasing the circulation time of the LNPs. Cholesterol is added for a tighter packing of the lipids by filling up any voids(73).

Targeting an organ or a cell population specifically has been a challenge that every bioengineer comes across regarding their therapeutic endeavor. Several studies have indicated that under controlled conditions, LNPs tend to be selectively taken up by different cell populations, owing to their size, charge or composition(75–77). Nanomedicines have been known to accumulate in the liver owing to its filtration functions supplemented by discontinuous vasculature, decreased blood flow rates as well as a plethora of phagocytic cell population(78,79). The Kupffer cells as well as the reticuloendothelial system (RES) in the liver are well known for their ability to phagocytose foreign entities(80,81). A group recently showed that the accumulation of their gold nanoparticles was decreased from 80% to 20% when they selectively depleted the Kupffer cells from the mice liver(82).

Right now, the only largely accepted viable strategy to target specific cell populations by LNPs is via adding antibodies specific to the cell populations or adding ligands that might be recognized selectively by them. However, active targeting strategies increase the cost of production as well as introduces another moiety onto the delivery agent which can have side effects(83). The possibility of targeting a specific organ system by merely modifying the composition of the delivery agent with previously proven safe components could be revolutionary. There have been indications of the size, charge as well as the composition of the lipid nanoparticles playing a role in their biodistribution *in vitro* (multicell population models) as well as *in vivo*(84–87). If we can understand the level of contribution of these variables, we might be able to make a leap towards targeted therapies.

2. Aim and Objectives

The introduction gives an insight into the essential role played by inflammatory reactions in chronic liver diseases. As discussed earlier, there is a void for an efficacious therapy for the ailments and exploiting miRNA can provide for a therapeutic strategy to counter it.

This thesis aims to develop on the hypothesis that that miR-155, master regulator of inflammation, can be exploited as a therapeutic target to modulate inflammation as well as fibrosis by targeting the cells in the liver as shown in **Figure 11**. LNPs, the delivery agent in this endeavor, apart from carrying the therapeutic also plays a significant role in the organ and cell specific uptake which has been explored in both, *in vitro* and *in vivo* models in this thesis. The most efficient LNPs for cargo delivery in context of passive liver targeting must be chosen for the delivery of animiR-155 and be tested for its therapeutic efficacy.

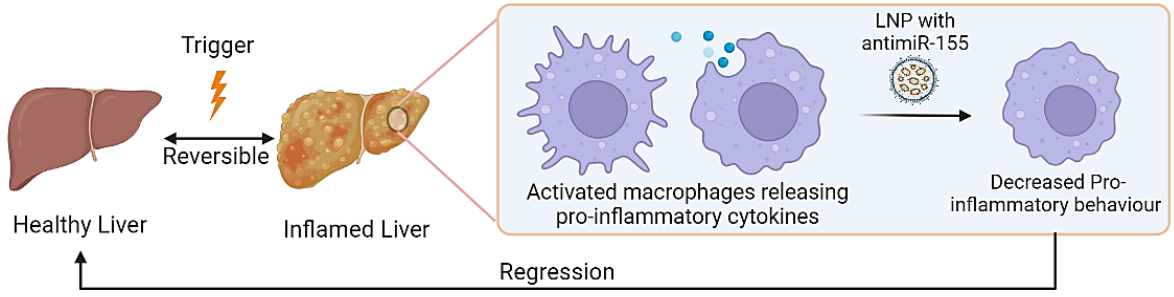

Figure 11: antimiR-155 targeting inflammatory macrophages to decrease inflammation and pro-inflammatory cytokine, thereby limiting stellate liver injury and stellate cell activation and decreasing fibrosis

In order to achieve this aim, the following objectives were formulated: -

- Engineering different LNP formulations using different helper lipids and their physiochemical characterization
- Characterization of selective uptake of the different LNP formulations by different hepato-representative cell populations
- Characterization of *in vivo* organ biodistribution of the different LNP formulations in an acute liver injury mouse model
- Testing the *in vivo* therapeutic efficacy of the selected LNP formulation with antimiR-155 cargo in a semi-chronic liver injury model

3. Strategy

As mentioned above, there are certain objectives laid out for the implementation of the ideas involved in this study.

In this study, we first discussed the pathophysiology of chronic liver diseases and the role of inflammation in fibrosis. We focused on how LNPs carrying therapeutics might passively target the liver for cargo delivery. Different LNPs were produced based on different helper lipids, claiming to have a better targeting mechanism for the liver cell. They were characterized for any differences in their physiochemical properties like size, surface charge and encapsulation efficiency, which gave an insight into potential interactions that might affect their behavior *in vitro* and *in vivo*. The formulations were then tested for their effect on the metabolic activity of different cell lines representing hepatic cell populations – RAW264.7 macrophages (representing Kupffer cells), AML12 hepatocytes, 3T3 fibroblasts (representing hepatic stellate cells) and H5V endothelial cells (representing liver sinusoidal endothelial cells).

The different LNP formulations were tested for their uptake *in vitro* using the previously defined liver representative cell lines, showing specificity for certain populations. The LNPs were also characterized for their *in vivo* organ distribution using an acute liver injury model. The results for the uptake and organ distribution were discussed in context of the physiochemical differences observed in the LNPs during characterization.

Taking into account the results from the *in vitro* uptake as well as the *in vivo* organ biodistribution of the LNPs, the most efficient formulation for passive targeting of liver was employed to deliver antimir-155 in a semi-chronic liver injury model to test its therapeutic efficacy. The therapeutic efficacy of the antimiR-155 LNPs was characterized by different analysis quantifying the progression of the liver injury. The results of the analysis and the feasibility of the treatment strategy were discussed in context of chronic liver diseases.

4. Materials and methods

4.1. Materials

DLin-MC3-DMA, Distearoylphosphatidylcholine (DSPC), 1,2-Dioleoyl-sn-glycero-3-phosphocholine (DOPC), 1,2-dioleoyl-sn-glycero-3-phosphoethanolamine (DOPE), Cholesterol, PEG-2000-C-DMG (Avanti Lipids); 1,1'-Dioctadecyl-3,3,3',3'-Tetramethylindotricarbocyanine Iodide (DiR) (ThermoFisher Scientific); 3,3'-Dioctadecyloxacarbocyanine Perchlorate (Molecular Probes); Fluidic 187 staggered herringbone microfluidic mixer (microfluidic ChipShop); NC-miRNA: 5' – GCGACUAUACGCGCAAUAUGG – 3' antimiR-155: 5'-A/ZEN/CCCCUAUCACAAUUAGCAUUA/3'ZEN/ (iDT); medical grade tubing – 0.38mm/1.09mm (Scientific commodities); Automated PHD Ultra model pump (Harvard apparatus); Vivaspin 20 amicons (Sartorius); Quant-it$_{TM}$ Ribogreen assay kit (ThermoFisher Scientific); Dulbecco's modified Eagle's medium (DMEM) (Lonza); fetal bovine serum (FBS) (Sigma-Aldrich); L-glutamine (Lonza) (Basel, CH); penicillin/streptomycin (pen/strep) (50U/ml Penicillin and 50µg/ml streptomycin, Sigma-Aldrich, St. Louis, MO, USA); Dulbecco's phosphate buffered saline (DPBS); Roswell Park Memorial Institute (RPMI) 1640 Medium (Lonza); Carbon tetrachloride (CCl_4) (Sigma-Aldrich); Olive oil (Sigma-Aldrich); tissue homogenizer (Temak Tissuemizer®); SV total RNA isolation Kit (Promega); TRIzol^{TM} reagent (ThermoFisher Scientific); iScriptTM cDNA Synthesis Kit (Bio-Rad Laboratories, Inc.) (Hercules, CA, USA); SensiMixTM SYBR & Fluorescein Mix (Bioline Reagents) (London, UK); Bio-Rad CXF-384TM Real-Time System; Zetasizer (Malvern instruments); ELISA Kits – TNFα, IL6 (RnD Systems); Lipofectamine^{TM} (Molecular Probes), Cell Strainers, Smart Strainers (100µm) (MACS); Ultracentrifuge tubes (Amicon Ultra-4, 10k) (Millipore)

Table 1: Antibody-fluorophores used for fluorescence assisted cell sorting

Antibody-Fluorophore	Produced in	Reactive with	Manufacturer
Hoechst	-	-	Invitrogen
CD45-FITC	Rat, IgG2b	Mouse	Biolegend
CD11b-PE	Rat	Mouse, human	Biolegend
F4/80-PE Cy7	Rat	Mouse	Biolegend
Tim4-AF647	Rat, IgG2a	Mouse	Biolegend
Ly6c-PERCP Cy5.5	Rat, IgG2b	Mouse, Dog, Human	eBioscience™
Ly6G-PE Dazzle 594	Rat, IgG2a	Mouse	Biolegend
CD3-PE Dazzle 594	Rat, IgG2b	Mouse	Biolegend
CD19-PE Dazzle 594	Rat, IgG2a	Mouse	Biolegend
NK1.1-PE Dazzle 594	Mouse	Mouse	Biolegend

Table 2: Antibodies used for immunohistochemical staining

Antibody	Produced in	Reactive with	Manufacturer
Collagen 1	Goat	Human, Mouse, Rat	Southern Biotech
F4/80	Rat	Mouse	BioRAD
iNOS	Rabbit	Mouse	BD Biosciences

4.2. Cell Culture

Murine AML12 hepatocytes, 3T3 fibroblasts, H5V endothelial cells were cultured in complete DMEM with 10% FBS and 1% penicillin/streptomycin. Mouse Raw 264.7 macrophages were cultured in RPMI with 10% FBS and 1% penicillin/streptomycin. All cells were cultured in a humidified incubator with 5% CO2 at 37 °C. For the Alamar blue assay, and the *in vitro* uptake studies, 250,000 Raw 264.7 cells were plated per well in 24 well plate and stimulated with 100ng/ml LPS and 10ng/ml IFN-γ for the M1 proinflammatory phenotype, 10ng/ml IL-4 and 10ng/ml IL-13 for M2 anti-inflammatory phenotype and no stimulants for M0 phenotype, all in RPMI medium supplemented with 10% FBS and 1% Penicillin/streptomycin (P/S). The stimulation was done for 24h before any other treatment was introduced into the wells. Furthermore, for the uptake study, in order to emulate fatty liver conditions, after 24h incubation of 100,000 AML12 cells, they were treated with 0.2 mM palmitic acid (PA) and 0.4mM oleic acid (OA) dissolved in isopropanol. 100µl 100mM oleic acid and 200µl of 100mM palmitic acid were added to 700µl of 1% bovine serum albumin (BSA) containing, 30% isopropanol diluted with DMEM, and mixed by vortexing. The OA/PA mix was incubated at 37°C for 15 minutes before being used for treatment. 1ml mix was prepared for each well to be treated and the OA/PA treatment was done for 24h prior to other treatments. 150,000 3T3 cells were plated per well and were starved by refreshing their media with DMEM supplemented with only 1%P/S and they were activated by refreshing the media with DMEM supplemented with 10% FBS and 5ng/ml TGFβ. The starvation and activation of the 3T3 cells was done 24h prior to any other treatment. 100,000 H5V cells were plated per well for both, the Alamar blue assay and the *in vitro* uptake study.

4.3. Lipid Nanoparticle formulations

In order to produce the different LNP formulations, lipids were mixed in mol% proportions – ionizable lipid: helper lipid: Cholesterol: PEG lipid to be 50:10:38.5:1.5. The lipids dissolved in pure ethanol, with a final concentration of 12.5mMol/ml (**Table 3**). For the *in vitro* uptake study, the lipid mix was supplemented with 1mol% DiO lipophilic dye and for *in vivo* biodistribution study, it was supplemented with 1.5mol% DiR lipophilic dye. For the aqueous phase, a total of 500µg of miRNA (NC-miRNA or antimiR-155) is dissolved in 100mM acetate buffer. The N:P ratio of the RNA containing LNPs was set to 4 by adjusting the flow rate of

components. The LNPs were produced by injecting the lipid mix and the RNA carrying buffer into the staggered herringbone chip at a flow rate ration of 3:1 (ml/min). The resulting LNPs were dialyzed overnight against PBS (pH 7.4) to remove any free dye and concentrated by using 100K MWCO centrifugal filters at 3000g for 2-3h (Amicon® Ultra, Merck).

Table 3: Components of different lipid mixes for various LNP formulations

Lipid	Molar Percentage	Molecular weight (g/mol)	Weight required (mg)
DLin-MC3-DMA	50	642.09	4.006
DSPC/DOPC/DOPE	10	790.15/734.039/744.03	0.99/0.88/0.93
Cholesterol	38.5	388.65	1.89
PEG-2000-C-DMG	1.5	2509.2	0.47
DiO/DiR	1/1.5	881.7/1013.41	0.11/0.19

4.4. LNP characterization

4.4.1. Size and Zeta potential

The size and the polydispersity index of the LNPs was measured using dynamic light scattering and the zeta potential was measured by the surface charge quantification using Malvern Zetasizer. The LNPs were diluted 1:10 with PBS and 0.9%NaCl, in separate vials, depending on the sample and for testing the size and the surface charge of the LNPs in different buffers. 15µl of the diluted samples were used per test. The volume for the former test was made up to 70µl and for the latter, it was made up to 1ml. Buffers used for diluting the LNPs for analysis were either PBS or 0.9% NaCl depending on the formulation. Specific measurement cells were used to house the LNPs for these analyses.

4.4.2. Encapsulation Efficiency

Quant-it™ Ribogreen assay was used in order to determine the encapsulation efficiency of the LNPs. 15µl of the 1:10 diluted LNPs were used for the assay. The encapsulation efficiency was measured by comparing the RNA content present in the presence and absence of TritonX buffer. 15µl of the sample LNPs were added to a well in a dark bottomed 96 well plate and the volume was made up to 250µl using TE buffer. In another well, 50µl of TE buffer was added and in the next one 50µl of TritonX buffer was added. 50µl of the diluted LNPs from the first well were added to the ones containing TE buffer and TritonX each. The plate was incubated at 37°C for 10 minutes. 100µl of 1x ribogreen dye was added to the TE and TritonX containing wells and incubated in the dark for 10 minutes. The quantification was done using a Varioskan Flash (Thermo Scientific, Waltham, MA, USA) with λ_{ex}=500 nm, λ_{em}=525 nm. The concentration was calculated using a standard curve. The loading efficiency was calculated based on the following formula:-

$$Loading\ efficiency = \frac{Total\ encapsulated\ RNA}{Total\ RNA\ input\ into\ the\ microfluidic\ system} * 100$$

4.5. Alamar Blue Assay

In order to measure the effect of the different LNPs on the metabolic activity of the different cell lines, Alamar blue assay was conducted. The different cell lines (250,000 RAW264.7 – M0, M1, M2 cells/ml; 100,000 AML12 cells/ml, 150,000 3T3 cells/ml and 100,000 H5V cells/ml) were cultured in a 24 well plate with the RAW264.7 macrophage being stimulated to the M1 and M2 phenotype, as mentioned earlier. The cells were treated with PBS, DSPC, DOPC and DOPE LNPs at a concentration of 2µg NC-miRNA/ml for a period of 24h. After 20h of incubation, amount of Alamar blue solution to be added to each well for 1x concentration was calculated and added to each well. After 4h of incubation with Alamar blue reagent and 24h of total incubation time, 100µl of media was collected from each well in a 96 well, black bottom plate and measured for emission using the Victor 3 microplate reader with λ_{ex}=530-560 nm, λ_{em}=590 nm. The fluorescence measured in wells with PBS treated populations was set as 100% viable control. Fluorescence by LNP treated wells was measured and plotted against the control population.

4.6. *In vitro* uptake study

In order to understand the different uptake of the three LNP formulations in different cell populations representing the liver cells (RAW264.7, AML12, 3T3 and H5V cells), the LNPs were tagged with DiO, a lipophilic dye. The cell lines, their seeding densities and the different experimental conditions can be seen in **Table 4**. Their stimulation and activation was done as described in **4.2**. The cells were treated with DiO labelled LNPs corresponding to a dose of 2µg NC-miRNA/ml for 4h. After the 4h, the cells were washed twice with PBS and detached using 0.1% trypsin treatment (AML12, 3T3 and H5V cells) or using disposable policeman (RAW264.7 cells) and suspended in 300µl of 2% FBS in PBS. The cells were then transferred into FACS tubes. The cells were analyzed using BD FACS Aria II flow cytometer and the FACS Diva software with the data acquisition set to 20,000 events (**Figure 12**).

The appropriate gates were set using the negative control population (**Figure 13 (a)**). The events plotted from the untreated samples were negatively selected for by the gates. The treated samples showed were expected to show a shift in the spectrum due to the fluorescence of the LNPs taken up by them.

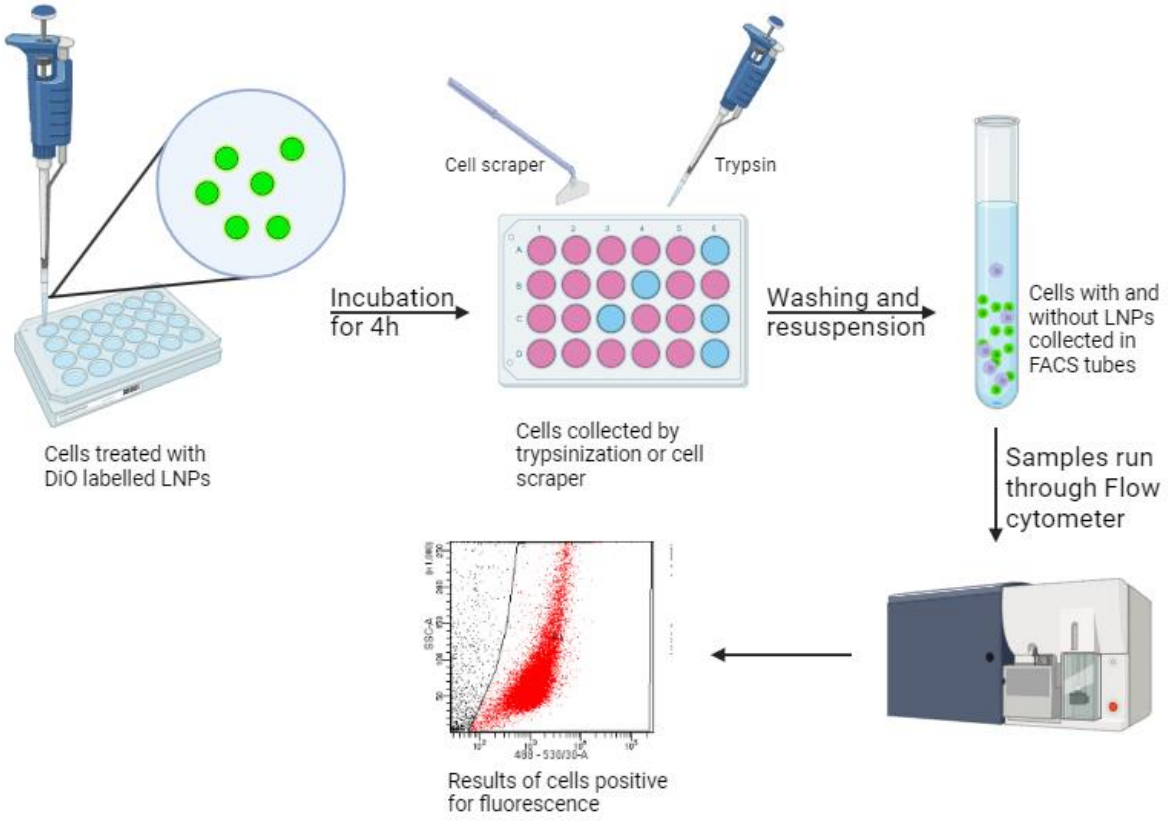

Figure 12: DiO labelled NC-miRNA carrying LNPs taken up by cells and analyzed by Flow cytometry: The different cells are treated with 2µg/ml equivalent of DiO labelled DSPC, DOPC and DOPE LNPs for 4h. The cells are washed and collected in FACS tubes. The cells are run through the flow cytometer and the data is analyzed by gating for fluorescence positive population

Table 4: Cell lines and treatment conditions for stimulation for in vitro uptake study

Cell line	Condition	Treatment
RAW 246.7 (250,000 cells/ml)	M0 (unstimulated)	-
	M1 (pro-inflammatory)	100ng/ml LPS + 20ng/ml INF-y
	M2 (anti-inflammatory)	10ng/ml IL-4 + 10ng/ml IL-13
3T3 (150,000 cells/ml)	Unstimulated	-
	Starved	No serum in media
	TGF-β activated	5ng/ml TGF-β added to media
AML 12 (100,000 cells/ml)	Unstimulated	-
	OA/PA treated	0.2mM PA +0.4mM oleic acid added to media
H5V (100,000 cells/ml)	Unstimulated	-

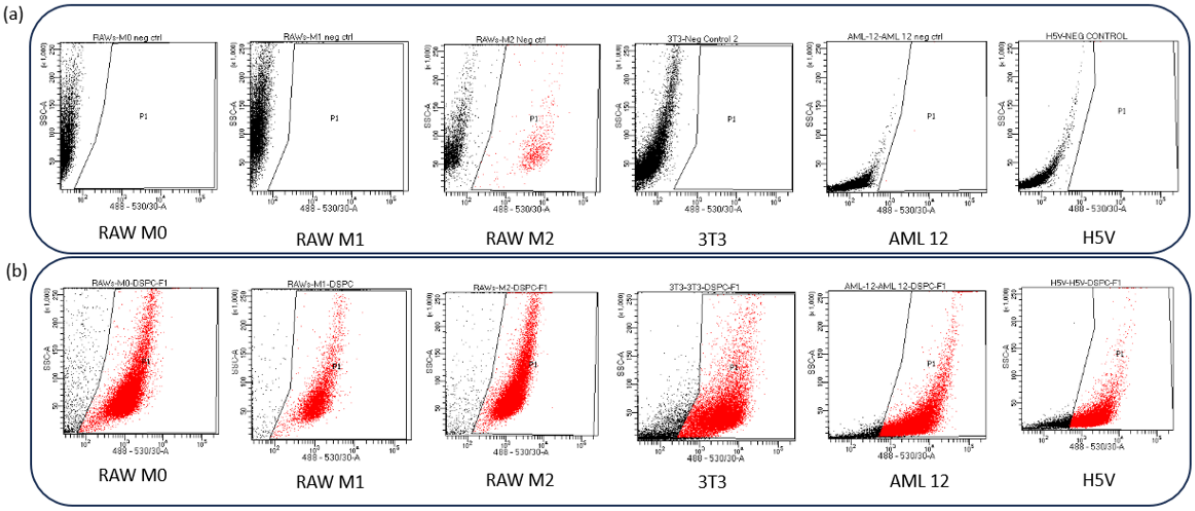

Figure 13: Gating strategy for DiO positive cells (a) Negative controls of RAW 263.7 M0, M1 and M2 phenotype, 3T3, AML 12 and H5V cells (b) Cells positive for DiO lipophilic fluorescent dye by taking up the LNPs

4.7. *In vivo* biodistribution study

The organ specific distribution of the three LNP formulations *in vivo* was tested by conducting a biodistribution study. The lipid mix used to produce the LNPs for this study was supplemented with 1mol% DiR, a lipophilic dye, with emission in the near infrared range. 20 C57BL/6J, 7 week old male mice were procured for the study. They were put on a high fat diet three days before the treatment, as the chow diet has autofluorescence. The mice were divided into 4 groups, with 5 mice each, as mentioned in **Table 5**.

Table 5: Treatment groups for in vivo biodistribution study of different LNPs

Group	Pre-treatment (IP)	LNP treatment (IV)
Healthy	Olive oil (100µl)	DiR – NC-miRNA-DSPC LNPs
DSPC	CCl_4 (0.2ml/kg)	DiR – NC-miRNA-DSPC LNPs
DOPC	CCl_4 (0.2ml/kg)	DiR – NC-miRNA-DOPC LNPs
DOPE	CCl_4 (0.2ml/kg)	DiR – NC-miRNA-DOPE LNPs

Figure 14: Timeline of in vivo biodistribution study: The disease groups were treated with CCl_4 IP 24h prior to IV LNP administration. The mice were imaged at 1h, 4h and 24h time points post LNP injection.

As shown in the timeline defined by **Figure 14**, acute liver injury was induced in the diseased groups by injecting 100µl of 0.2ml/kg bodyweight of CCl_4 (for 20g mice) intraperitonially. The healthy group was injected with 100µl of olive oil intraperitonially. 24h after the pretreatment

with CCl_4 and olive oil, the mice were injected with 100µl of DiR labelled LNP treatment corresponding to 1mg NC-miRNA/kg bodyweight (for 20g mice) intravenously.

The mice were sedated using isoflurane and imaged at time points 1h, 4h and 24h from the time of LNP treatment using the PEARL Trilogy *in vivo* imager, set at 170µm depth for signal acquisition at 778nm for the DiR labelled LNPs. The mice were sacrificed by cervical dislocation after 24h and major organs – liver, kidney, spleen, lungs and heart were excised and imaged using the same *in vivo* imager. The signal was quantified using Image studio software, version 5.2.5 by LI-COR biosciences.

4.8. *In vivo* efficacy study

4.8.1. Study design

To test the therapeutic efficacy of antimiR-155 loaded DSPC LNPs, an animal study employing a semi-chronic liver injury mouse model was conducted. 35 C57BL/6J, 7-week-old male mice were procured for the study. The mice were divided into 5 groups of 7 based on **Table 6**.

Table 6: Treatment groups for antimir155-LNP efficacy study

Group	Pre-treatment (IP)	LNP treatment (IV)
Healthy group	Olive oil	-
Disease control	CCl_4	-
Negative control	CCl_4	NC-miRNA LNPs
Therapy group	CCl_4	antimiR-155 LNPs
LNP control group	CCl_4	Naked antimiR-155

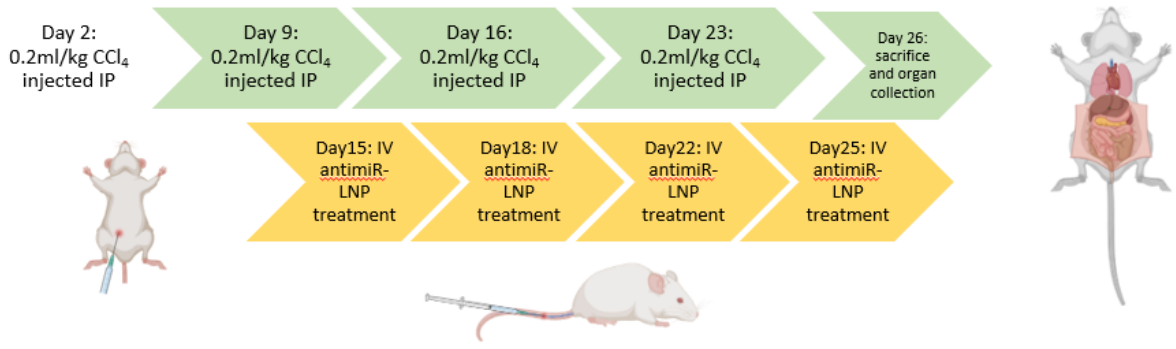

Figure 15: Timeline of antimiR-LNP efficacy study: The mice were given CCl_4 IP, once every week for four weeks. The therapy groups were administered with LNPs/naked antimiR-155 twice a week for the last two weeks of the study.

As shown in the timeline defined by **Figure 15**, the healthy group was treated with 100µl Olive oil and the rest of the groups were treated with 100µl of 0.2ml CCl_4/kg bodyweight (for 20g mice) intraperitoneally on Days 2, 9, 16 and 23. The treatment for the negative control,

therapy and the LNP control groups were administered intravenously corresponding to 1mg RNA/kg bodyweight (for 20g mice) on Days 15, 18, 22 and 25. The mice were weighed and sacrificed on day 26 by cervical dislocation and the major organs – liver, kidneys, spleen, lungs and heart were excised, weighed and cryopreserved for further analysis.

4.8.2. Fluorescence Assisted Cell Sorting

4.8.2.1. Sample preparation

The excised liver samples were cut into small pieces using scalpel and scissors and suspended in 1% BSA containing RPMI without FBS. The liver tissue pieces were transferred to the cap of TissueGrinder tubes. The tubes were overflowed with media and closed while keeping upside down. The tubes were placed in the grinding machine (TG, Fast forward discoveries GMBH) and homogenized using “optimized for liver sample” program. The homogenized samples were centrifuged right side up for 5 minutes at 300g. The pelleted samples were collected and transferred to new tubes and washed thrice with 1ml of 2% FBS in PBS along with centrifugation at 300g for 5 minutes. The cells were then fixed by treating them with a solution of 4% formaldehyde in PBS with 2% FBS for 20 minutes. The cells were centrifuged at 300g for 5 minutes and washed thrice with 2% FBS in PBS and resuspended in the same solution with a volume of 1ml. To a new vial, 100µl of fixed cells from all disease controls and healthy controls were added and centrifuged for 5 minutes at 300g. The supernatant was discarded and cells were resuspended in 1425µl of 2% FBS in PBS and 75µl of it was aliquoted in vials corresponding to individual and combination treatment of marker based antibodies as listed in **Table 7**. The samples in individual vials were centrifuged at 500g for 5 minutes and washed thrice with 2% FBS in PBS. 1µl of antibodies corresponding to **Table 7** were added to the vials and incubated at room temperature for 1h (only 30 minutes for Hoechst). After the incubation, the total volume of the vials was made up to 1ml and centrifuged at 500g for 5 minutes. The samples were washed thrice with 2% FBS in PBS and resuspended in 300µl of the same solution while being transferred to FACS tubes.

Table 7: Fluorophores and tags added to cells derived from mice liver based on different conditions for in vivo antimiR-155 efficacy study

Eppendorf number	Tag added
1	Hoechst
2	CD45-FITC
3	CD11b-PE
4	F4/80-PE Cy7
5	Tim4-AF647
6	Ly6c-PERCP Cy5.5
7	Ly6G-PE Dazzle 594
8	CD3-PE Dazzle 594
9	CD19-PE Dazzle 594
10	NK1.1-PE Dazzle 594
11	All except Hoechst
12	All except CD45-FITC
13	All except CD11b-PE
14	All except F4/80-PE Cy7
15	All except Tim4-AF647
16	All except Ly6c-PERCP Cy5.5
17	All except PE Dazzle 594 (Ly6G, CD3, CD19, NK1.1)
18	All antibody and fluorophores
19	No antibodies or fluorophores

4.8.2.2. Gating strategy

The samples missing a single fluorophore and the samples with only that fluorophore were used in conjunction to draw the gates, (eg: sample treated with All antibodies except Hoechst and sample treated with only Hoechst). The samples without the fluorophore showed the population negative for its expression and thus, a gate was drawn to exclude those events in the respective spectrum. The sample with only one fluorophore corresponding to the earlier sample was plotted on the same graph with the previously drawn gate and the strategy for gating was reconfirmed by having a population showing positive signal for the respective fluorophore. Nucleated cells were selected with the positive selection of Hoechst staining. The total leukocytes were filtered using the positive CD45 expression. Events negative for CD3, NK1.1, CD19 and Ly6G were selected by inverting the gate for them (NOT DUMP). This was done in a single step as antibodies against all four antigens had the same fluorophore and thus, were plotted in the same spectrum. The populations positive for CD11b, F4/80, Ly6C and Tim4 were gated individually based on the negative selection of events in samples not containing the respective antibody. To find liver resident macrophages, the NOT DUMP population was plotted on F4/80 vs Ly6c and events positive for F4/80 and negative for Ly6c were selected as P5. P2 was filtered out of P5 by Tim4 positive expression. P2 was plotted on

F4/80 vs Tim4 and selected as a single population, P3. For finding infiltrated monocytes, the NOT DUMP events were plotted on F4/80 vs Ly6c and cells negative for F4/80 and positive for Ly6c were selected as P1. P1 was selected as a single population P4 on a plot of F4/80 vs Tim4.

4.8.3. Immunohistochemical staining

The cryopreserved liver samples were cut into 6µm thick sections using a cryotome and placed on glass slides. The sections were dried at room temperature and fixed by acetone treatment. The sections were circled with a hydrophobic DAKO pen and rehydrated using PBS submersion. The sections were then treated with 1x primary antibodies – Goat anti mouse Collagen 1, rat anti mouse F4/80 and rabbit anti mouse iNOS and incubated overnight at 4°C. The next day, the sections were washed thrice with PBS and treated with 0.3% H_2O_2 suspended in methanol in order to block the endogenous peroxidases. The sections were washed thrice with PBS and treated with the corresponding secondary antibody, diluted in 5% mouse serum containing PBS for 1h at room temperature. The sections were washed thrice with PBS and treated with the respective tertiary antibody diluted in 5% mouse serum containing PBS for 1h. AEC solution was prepared by mixing 4.5ml of milliQ to 0.5ml 1M sodium acetate and 0.25ml of AEC dissolved in DMF. The solution was filtered through 0.45µm filter and 5µl of 35% H_2O_2 was added to it. After the tertiary antibody treatment, the sections were washed thrice with PBS and treated with AEC solution for 20 minutes. After washing the AEC solution off, the sections were counterstained using Hematoxylin for 5 minutes. The excess stain was removed by washing under tap water. The sections were rid of any excess water and were mounted using Aquatex mounting medium and cover slip. The sections were dried overnight and scanned using Hamamatsu NanoZoomer Digital slide scanner 2.0HT to create vector images of them. The vector images were analyzed using ImageJ by creating a color profile quantifying the stained areas of a section and implementing it using a batch analysis.

5. Results and discussion

5.1. Background literature

Previous research at the TLR group conducted by Miranda Türkal and Eline Geervliet established miRNA-155 as a potential therapeutic target for immunomodulation in RAW 264.7 murine macrophage cell line. The miRNA-155 levels in RAW 264.7 cells corresponded to the levels of TNFα and IL-6, well known inflammatory markers, owing to the fact that they are direct downstream effectors of the miRNA in question(62,63). PCR analysis of M1 polarized pro-inflammatory macrophages showed significant overexpression of miR-155, TNFα and IL6 transcripts as compared to the M0 and the M2 phenotypes, as can be seen in **Figure 16**. Thus, in M1 macrophages, miRNA-155 acts by regulating the expression of pro-inflammatory cytokines.

In a therapeutic strategy involving inhibition of miRNA-155, we would effectively decrease the levels of TNFα and IL6, limiting the pro-inflammatory behavior. The amelioration of inflammation would limit the damage to the liver tissue, in turn decreasing liver fibrosis and thus, mitigating the liver injury.

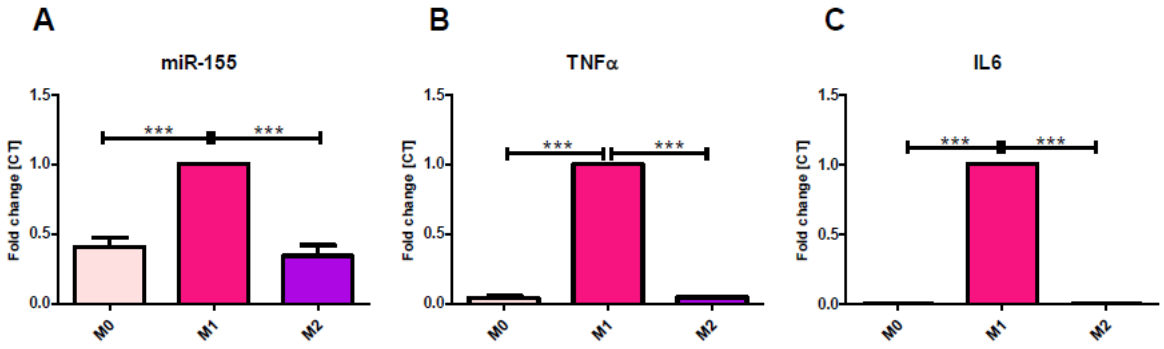

*Figure 16: Direct correlation between miR-155, TNFα and IL6 levels in M1 polarized RAW264.7 macrophages. M0 – RAW264.7 cells with no treatment, M1 – RAW264.7 with 100ng/ml LPS + 20ng/ml INF-γ for 6h, M2 – RAW264.7 cells with 10ng/ml IL4 + 10ng/ml IL13 treatment for 6h | ***p<0.001 (significance tested by unpaired t test)*

After establishing the role of miRNA-155 in M1 macrophage induced inflammation, we wanted to analyze the effect of antimiR-155 treatment. In order to achieve this, antimiR-155 was introduced in M1 stimulated macrophages using the commercially available high efficiency transfection agent, HiPerFect reagent. The antimiR-155 transfection treatment showed changes in the levels of previously described inflammation markers. The expression of miR-155, TNFα and IL6 was decreased not only at the transcript level, but also at the protein level as seen in **Figure 17**. TNFα and IL6 play a pivotal role in immune response during liver injury. They enhance macrophage activation and antigen presentation, as well as modulate the immune system via various downstream and parallel pathways. Thus, by delivering antimiR-155 to the M1 macrophages, a decrease in inflammatory behavior was observed which can be potentially exploited as a therapeutic strategy(63).

HiPerFect is a proprietary blend of cationic and neutral lipids, which encapsulates the nucleic acid cargo and efficiently delivers it inside cells. Due to the cationic nature of the lipids in the concoction, it is toxic to the cells at higher concentrations(88). It thus is not the ideal agent for delivering a therapeutic *in vivo* as well. In order to tackle this issue, we decided to explore LNPs for their drug delivery properties, while being safe to use at higher concentrations.

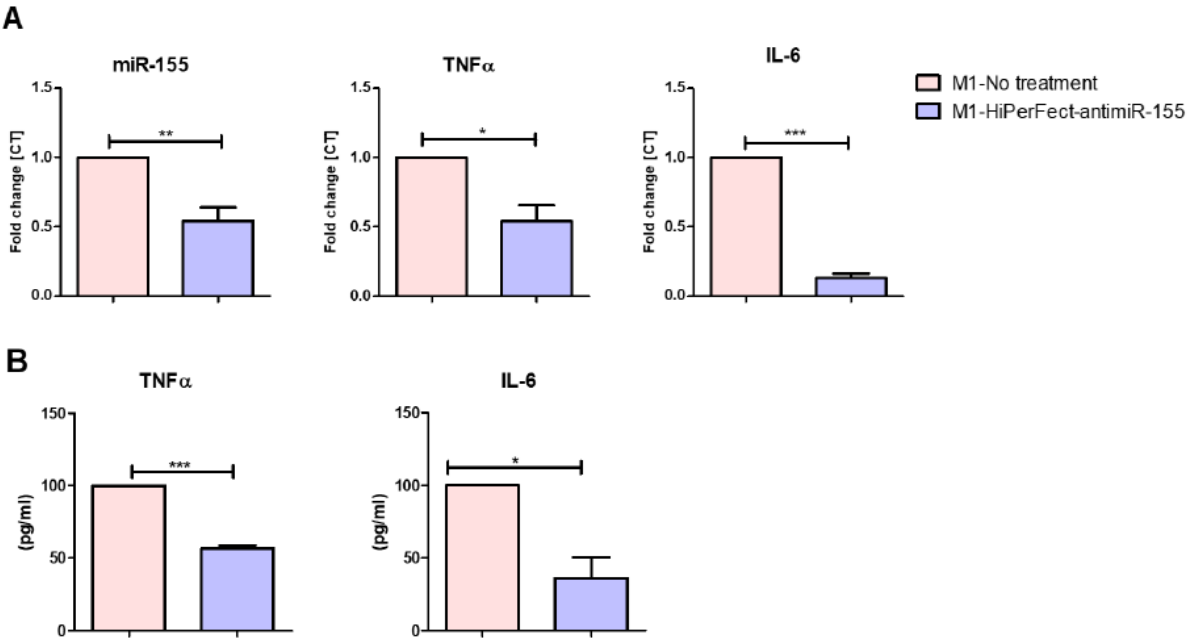

*Figure 17: Expression levels of miR-155, TNFα and IL6 in antimir-155 treated M1 macrophages. A) Transcript levels of miR-155, TNFα and IL6 after 24h of 2µg/ml antimir-155 treatment B) Protein levels of TNFα and IL6 after 24h of 2µg/ml antimir-155 treatment|Significance was determined with the unpaired t-test. *p<0.05, **p<0.01, ***, p<0.001*

Miranda Türkal, in her master's thesis, showed that the therapeutic effect of antimiR-155 delivery to M1 macrophages facilitated by DSPC LNPs followed a trend similar to when using HiPerFect based transfection (**Figure 18**), without affecting the metabolic activity of the cells. The transcript levels of miRNA-155, TNF-α and IL6 were decreased significantly and the protein levels of TNFα and IL6 were decreased significantly as well, post antimiR-155 DSPC LNP treatment. This pointed to the successful amelioration of inflammation *in vitro*, replicating the earlier results from HiPerFect based transfection treatment. This meant that the DSPC LNPs carrying antimiR-155 had the same level of therapeutic efficacy and no interference was caused by the encapsulation(63).

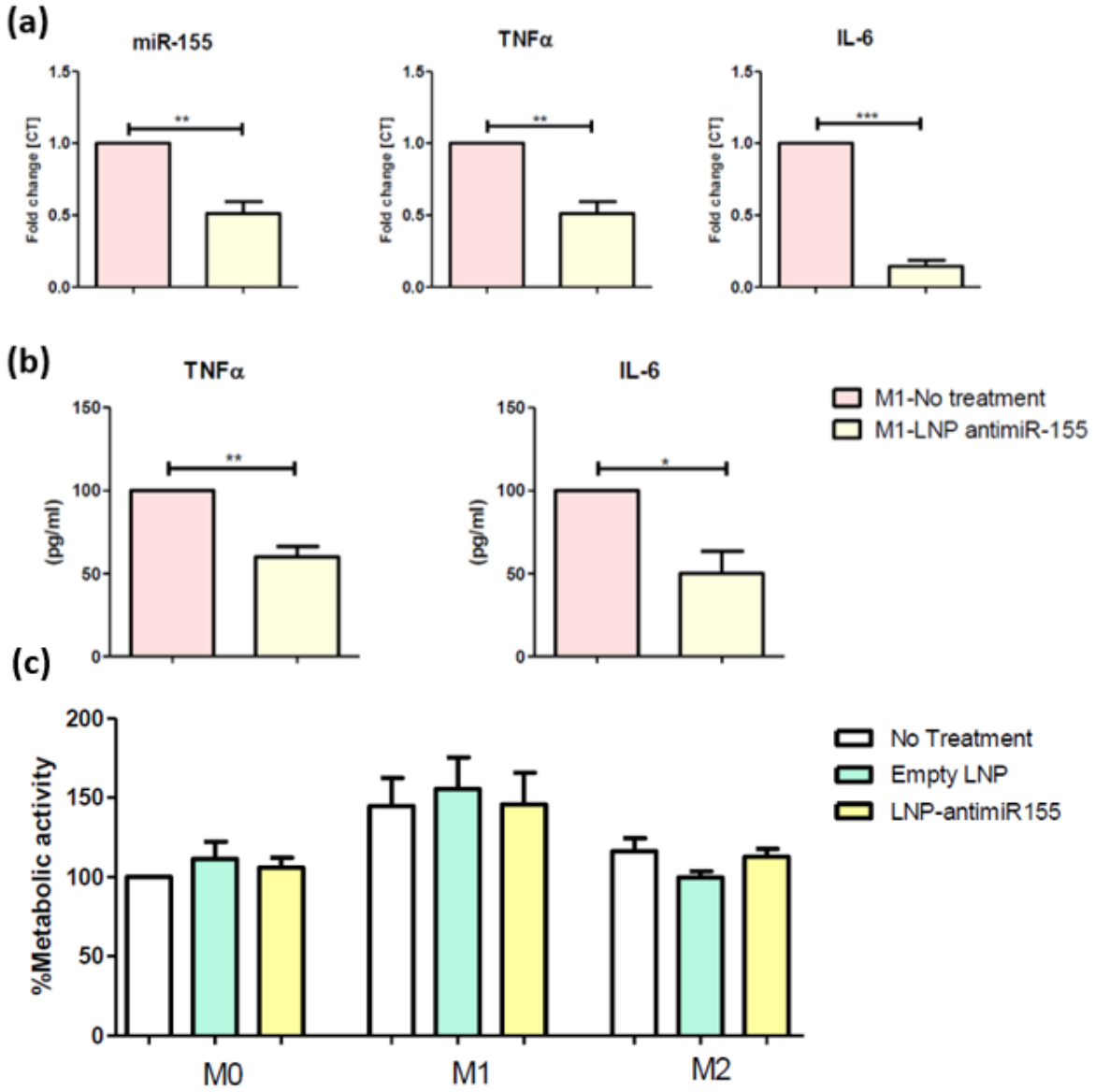

*Figure 18: Expression levels of miR-155, TNFα and IL6 in antimir-155 LNP treated M1 macrophages and the safety of the LNPs (a) Transcript levels of miR-155, TNFα and IL6 after 24h of antimir-155 LNP treatment corresponding to 2µg antimiR-155/ml (b) Protein levels of TNFα and IL6 after 24h of antimir-155 LNP treatment corresponding to 2µg antimiR-155/ml (c) Alamar blue assay for antimiR-155 carrying DSPC LNP treatment|Significance was determined with the unpaired t-test. *p<0.05, **p<0.01, ***, p<0.001*

5.2. Lipid nanoparticle characterization

5.2.1. DLS and Zeta potential

As discussed in the last section, HiPerFect is not the ideal delivery agent for cargo delivery *in vitro* as well as *in vivo*, owing to its toxicity at high concentrations. This toxicity stems from the cationic lipids present in the proprietary concoction(88). In order to circumvent this issue, LNPs employing ionizable cationic lipids were explored as a potential delivery agent. Lipid nanoparticles have been recognized as ideal carriers for nucleic acid cargo such as DNA, mRNA

as well as siRNA due to characteristics such as biocompatibility, biodegradability and encapsulation efficiency(69). Different formulations were engineered and tested for their physiochemical properties in order to achieve the same delivery efficiency as HiPerFect, without being toxic to the cells.

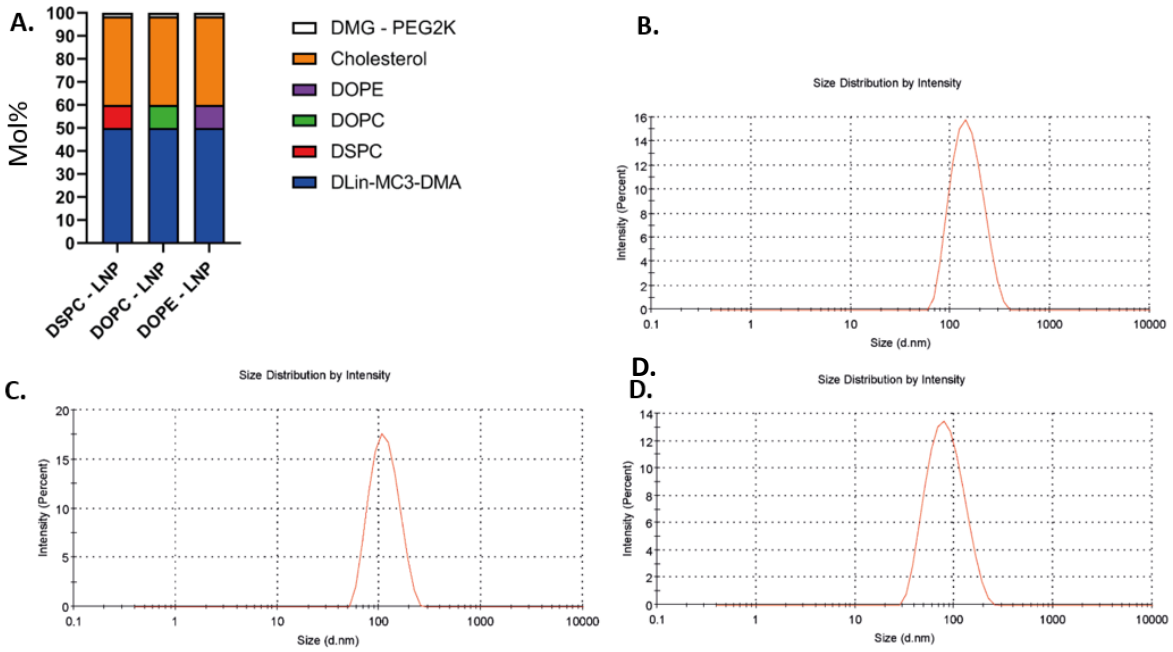

Figure 19: Characterization of LNPs: A) Composition of Lipid mix for different LNPs (DSPC, DOPC, DOPE) B) Size distribution for DSPC LNPs using DLS C) Size distribution for DOPC LNPs using DLS D) Size distribution for DOPE LNPs using DLS

Three different formulations of LNPs were engineered based on different helper lipids. Onpattro Patisiran is the gold standard for RNA-LNP therapy right now in the market. The first LNP formulation, with DSPC as the helper lipid, was based on it(70). The other two formulations had the same molar concentrations for the various components, except for using DOPC/DOPE as the helper lipids with proportions mentioned in **Figure 19 (A)**. These helper lipids were chosen based on result by Kulkarni et al. and Zhang et al, who showed that LNPs with them perform better in terms of transfection efficiency as well as passive targeting(85,86). Although, they used different ionizable lipids as well as different molar ratios for their LNPs. In order to compare the properties imparted by of the three helper lipids, the molar ratio of all the components was kept the same and only the type of helper lipid was swapped, thereby eliminating as many variables as possible(85,86). Therefore, we had the gold standard of RNA therapy delivery (with DSPC) contending with two formulations with different helper lipids – DOPC and DOPE.

DSPC, DOPC and DOPE, all three are phospholipids. DSPC and DOPC are phosphatidylcholine whereas DOPE is a phosphoethanolamine. DSPC has two saturated acyl chains which allows it to form a bilayer structure with cylindrical geometry, increasing the stability of the LNPs. DOPC and DOPE have unsaturationed acyl chains with a small head group, which together contribute to them adapting a hexagonal phase while forming a non-bilayer structures and escape from

the endosome much more easily(74). The change in these lipids also warrants a change in the physiochemical interactions of the LNPs formed(85,86). The change in the helper lipids was translated into different zeta potentials for the LNPs, which meant that they would interact with different proteins, thereby have a different protein corona. A difference in protein corona means the three LNP types would interact with different receptors on different cells, allowing for selective uptake or exclusion, which is what we intended to characterize(89).

The lipid mix used for the production of the LNPs had a concentration of 12.5mM/ml, based on multiple different studies employing the same concentrations without any adverse side effects(90–92). As observed in **Figure 19 (B, C, D)**, the size of the LNPs produced, measured using DLS, lay in the range of 70 – 140nm. Even though there were minor differences in size of the LNPs, the range which they lay in is ideal for systemic drug delivery via intravenous administration and for passively targeting the liver for accumulation of the LNP(73,93). The PDI for all the formulations lied below 0.2, which implies a narrow size distribution and high homogeneity of the LNP size. The zeta potential of the LNPs was measured to be between 5mV and -5mV, which is considered to be the neutral range, when suspended in PBS(94,95). These measurements were also conducted in 0.9%NaCl as the suspension buffer, which gave significantly more negative results for DOPC and DOPE LNPs as seen in **Table 8**. Neutral to slightly negative zeta potential of LNPs has been tied to delivery of cargo with minimal toxic side effects on the cells taking them up(96). Neural LNPs are considered the safest but due to the absence of charge, have a lower uptake. Slightly negative LNPs can interact more efficiently with phagocytic cells and hence, have a higher uptake(97). With this, we can say that the LNPs produced here are much better than the HiPerFect agent with cationic lipids mentioned earlier. Therefore, LNPs with acceptable physiochemical properties including uniform size, within the expected size range and slightly negative to neutral zeta potential were produced.

The negative values of zeta potential for DOPC and DOPE LNPs in the 0.9% NaCl suspension highlights the importance of the suspension buffer in measuring different physiochemical properties. PBS is composed of multivalent ion which when recruited to form the stern layer and the slipping plane around the LNP, would have a nonlinear relationship in terms of charge per molecule and thus, would give an inaccurate account of the zeta potential. The NaCl buffer houses only monovalent ions, which would have a linear relationship between the ions involved in forming the stern layer and the slipping plane, giving the proper result for zeta potential measurement(85,86,95). Thus, in order to get a holistic picture about the properties of nanoparticles to be used in biological context, the zeta potential measurements should be conducted in biological buffers like PBS but also in monovalent ionic buffers like 0.9% NaCl. These differences in zeta potential in different suspension buffers would translate into certain interactions being looked over or being overestimated. If only PBS was used for a certain LNP and a neutral zeta potential was reported, while NaCl would have reported a negative value, we would assume that a significant number of blood proteins would adsorb on its surface, owing to their negative charge. But, since the actual zeta value is negative, the LNP would

hardly have any of the blood proteins in its corona. This misjudgment in interactions could hinder in our understanding of the manifestation of physiochemical properties, both *in vitro* and *in vivo*.

Table 8: Physical characterization of different LNPs

LNP Type	Size (nm)	PDI	Zeta Potential (mV)	
			In PBS	In 0.9% NaCl
DSPC LNPs	137.5±2.6	0.097±0.001	-2.81± 0.88	-4.7±1.45
DOPC LNPs	105.5±1.5	0.096±0.001	-5.83±0.32	-11.07±2.65
DOPE LNPs	74.54±0.5	0.134±0.02	-2.7±1.01	-8.15±0.365

5.2.2. Encapsulation efficiency of LNPs

In order to determine the encapsulation efficiency of the LNPs in question, Ribogreen assay was performed to measure the miRNA content being loaded in them. During this assay, a known amount of LNPs are treated with TE buffer and TritonX surfactant in separate wells. The former does not affect the LNPs, but the latter being a surfactant, changes the surface tension of the LNPs, rupturing them and letting the cargo leak out(98). The Ribogreen reagent binds to the free nucleic acids and gives a fluorescent signal proportional to its concentration. The comparison between the TE suspended LNPs and the TritonX suspended LNPs gives us the encapsulation efficiency(99).

The LNPs with antimiR-155 could not have their encapsulation efficiency quantified using the Ribogreen assay due to the ZEN tag in the sequence, interfering with the fluorescent signal in the assay. Instead, the NC-miRNA was encapsulated using the same exact conditions and analyzed via the Ribogreen assay. The assay showed a 97% encapsulation efficiency and 87% loading efficiency for each of the LNP formulations, which is quite impressive considering the Pfizer's mRNA vaccine for COVID 19 boasted of an encapsulation efficiency of 88%(100–102). Since the NC-miRNA has the same length as the antimiR-155 and this being the only difference between the LNPs, they would effectively have the same encapsulation efficiency.

5.3. Effect of LNP treatment on metabolic activity

Earlier formulations of LNPs employed cationic lipid in order to have a better loading of negatively charged nucleic acids and a better uptake efficiency by interacting with the anionic cell membranes. But, they had a pitfall for being toxic *in vitro* as well as *in vivo*(103,104). The MC3 lipid used in the engineered formulations here is a type of ionizable cationic lipid, positively charged in acidic environment, which is exploited during loading of the nucleic acids as well as the endosomal escape. But it is neutral at physiological pH (pH7)(70). In order to test the effect of the LNP treatment on the metabolic activity of the different cell lines, Alamar Blue assay was conducted. Four different murine cell lines representing the major populations of the liver – RAW264.7 macrophages (M0 unpolarized, M1 proinflammatory, M2 anti-

inflammatory) (representing Kupffer cells), AML12 hepatocytes, 3T3 fibroblasts (representing stellate cells) and H5V endothelial cells were subjected to NC-miRNA LNP treatment (2µg/ml) for each of the LNPs (DSPC, DOPC, DOPE) for a period of 24h.

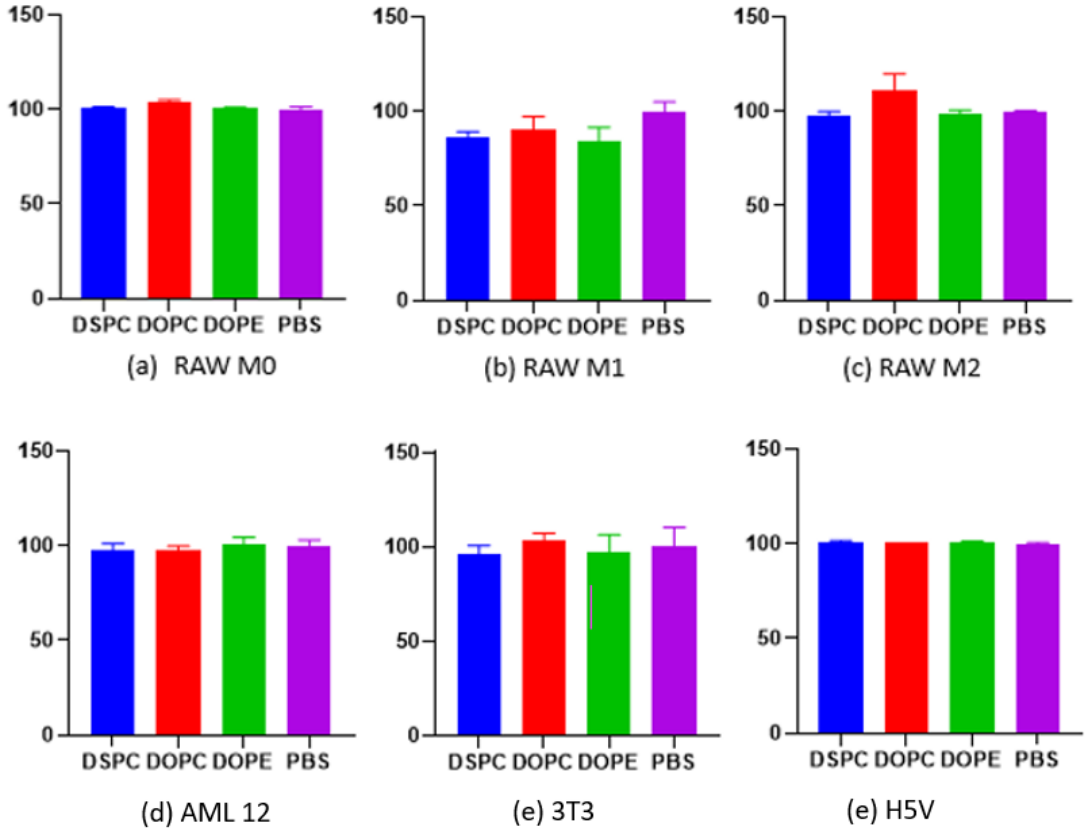

*Figure 20: Alamar blue assay results for DSPC, DOPC and DOPE LNP treatment of different cell lines. (a) RAW 264.7 M0 phenotype murine macrophages treated with DSPC, DOPC and DOPE LNPs (b) RAW 264.7 M1 polarized murine macrophages treated with DSPC, DOPC and DOPE LNPs (c) RAW 264.7 M2 polarized murine macrophages treated with DSPC, DOPC and DOPE LNPs (d) AML 12 murine hepatocytes treated with DSPC, DOPC and DOPE LNPs (e) 3T3 murine fibroblasts treated with DSPC, DOPC and DOPE LNPs (f) H5V endothelial cells treated with DSPC, DOPC and DOPE LNPs. Significance levels tested using one way ANOVA * p<0.05*

As observed in **Figure 20** No discernable change in the metabolic activity was observed in any of the cell lines and thus, we concluded that the LNPs did not affect the viability of the cells. This is also corroborated by results from Francesca et al. where MC3 based LNPs did not show any negative side effects to the doses of 5mg siRNA/kg *in vivo*(105). They were biocompatible and safe to be used for delivering therapeutic molecules.

5.4. Differential Uptake of LNPs with different helper lipids by hepatic cells

DSPC, DOPC and DOPE LNPs used for this study were incorporated with 1.5mol% DiO, a lipophilic fluorescent dye. This was implemented in order to identify the cells taking up the

LNPs (106). The dye was added to the lipid mix before the LNPs were produced and any trace of free dye was removed by dialysis, to avoid any unintended fluorescence.

Four different cell populations were used for the *in vitro* uptake study – RAW 264.7 murine macrophages, AML 12 murine hepatocytes, 3T3 murine fibroblasts and H5V murine endothelial cells. These populations represent the constituents of a functional liver system with Kupffer cells, hepatocytes, stellate cells and LSECs respectively(2). These cell lines were subjected to different stimuli in order to emulate a range of conditions found during liver injury which can be seen in **Table 4**(16).

The cell lines, with different stimuli were treated with 0.2µg NC-miRNA DiO tagged LNPs for 4h each and were analyzed via a flow cytometer. The treatment groups showed a significant shift in the spectrum of the specified channel due to the fluorescence of DiO, as compared to the untreated samples (**Figure 13**). On the accord of this shift, the gated population was deemed to be positive for the LNPs. The M2 macrophages show a small population of cells positive for fluorescence in the control samples. This could be due to autofluorescence of the cells based on byproducts specific to the M2 phenotype like a high concentration of cyclic compounds such as NADPH, aromatic compounds, or increased mitochondrial population(107). This is taken into account while analyzing the positive populations. The uptake of the cell populations was gauges on two parameters – the number of cells positive for fluorescence due to DiO emission and the intensity of the positive cells, which indicates the number of LNPs taken up per cell. The uptake of the three engineered LNP formulations per cell line are discussed in further detail below.

5.4.1. LNP uptake by AML 12 Hepatocytes

Hepatocytes make up almost 80% of the cellular population in the liver and function as the filtration units(2). AML12 murine hepatocytes were subjected to the LNP treatment in order to determine the difference in their preferential uptake. In order to emulate the fatty liver conditions, the AML12 hepatocytes were treated with 0.2mM palmitic and 0.4mM oleic acid, which are known to cause steatosis(108). For control, a population of healthy hepatocytes was also included in the experimental conditions.

In **Figure 21 (a)**, one can see that DSPC has the lowest uptake population and DOPC having the highest in both conditions. DOPE LNPs show a slight decrease in uptake in the fatty liver condition, which is significantly different from the DSPC and the DOPE LNPs. The per cell uptake shows an overwhelming level for DOPC without any change with the fatty liver condition. DSPC and DOPE LNPs show a decrease in per cell uptake with the fatty liver condition but the former does perform better in relative comparison.

The Onpattro formulation, named Patisiran uses DSPC as the helper lipid and has a well characterized mechanism of uptake for the hepatic cells, which involves the Apolipoprotein E (ApoE). The cholesterol in the DSPC LNPs recruits ApoE to coat the PEG-2000-C-DMG

molecules on the surface. The ApoE interacts with the Low Density Lipoprotein receptor (LDLr) on the hepatic cells and initiates the phagocytosis, taking up the LNP in an endosome(70).

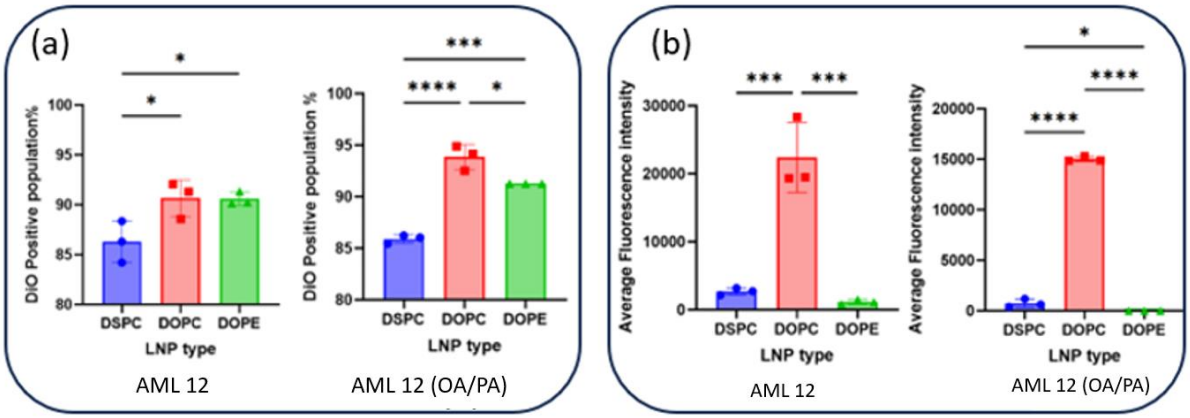

*Figure 21: (a): AML12 - Percent positive population for LNP uptake in untreated AML 12 cells; AML12 OA/PA - Percent positive population for LNP uptake in OA/PA treated AML 12 cells (b): AML12 - Fluorescence intensity plot for untreated AML 12 cells; AML12 OA/PA Fluorescence intensity plot for OA/PA treated AML 12 cells| Significance levels tested using one way ANOVA * p<0.05*

Since this method is dependent on cholesterol and PEG-2000-C-DMG in the DSPC LNPs, one would consider that the same would be applicable with respect to the DOPC and DOPE LNPs as well, but we see a significant difference in the uptake for the aforementioned treatment groups. Since the size of all three formulations lay in the range specific to liver accumulation, the only distinction in the physiochemical properties would be the zeta potential. The difference in helper lipids is hypothesized to create a different physical structure of the LNPs, thereby modifying the interactions between the different components which might be the reason for the zeta potential of the DOPC and DOPE LNPs being substantially negative as compared to the DSPC LNPs(74).

Since DOPC LNPs have a higher uptake in both, the total population as well as per cell, they might be employing a secondary pathway as well. There have been no reports so far characterizing the interaction that initiates this secondary pathway but, there have been mentions of negatively charged LNPs utilizing a secondary uptake pathway mediated via the stabilin-1 and stabilin-2 scavenger receptors in case of macrophages and endothelial cells(109). This leads to the theory that the scavenging receptors on hepatocytes might play a role in the above mentioned secondary pathway.

5.4.2. LNP uptake by RAW264.7 macrophages

RAW264.7 cells represent the resident liver macrophage population, also known as the Kupffer cells. They are hypothesized to take up a considerable proportion of the LNPs during the treatment due to their well characterized phagocytic activity(79). This is also the population we would like to target with the antimiR-155 in order to modulate the inflammatory response(19). In order to have a better understanding of which sub population of the macrophages would the LNPs target, we stimulated the RAW cells into three different phenotypes – M1 proinflammatory, M2 anti-inflammatory and M0 unstimulated.

In **Figure 22 (a),** we observe DSPC LNPs with the lowest uptake population in all three phenotypes, with the M1 population being significantly lower than DOPC and DOPE populations. The DOPC and DOPE LNPs showed comparable uptake in all three phenotype populations. **In Figure 22 (b)**, the uptake of the said LNPs per cell can be seen. DOPC LNPs dominates the per cell uptake in every phenotype population, with the DSPC and DOPE having a comparable uptake per cell. In M1 and M2 macrophage populations, the per cell uptake for all three LNPs decreases substantially as compared to the M0 phenotype population, more in the former than the latter. The relative uptake ratio per cell was however maintained in all three phenotypes.

The M2 macrophages show a higher uptake per cell than the M1 macrophages in the case of all three LNPs. This might be due to their more prominent role in clearing of debris and hence, a higher phagocytic activity(110,111). This can be attributed to an increase in the expression of receptors facilitating endocytosis, like, scavenger and lectin receptors, in the M2 polarized macrophages(110,112,113).

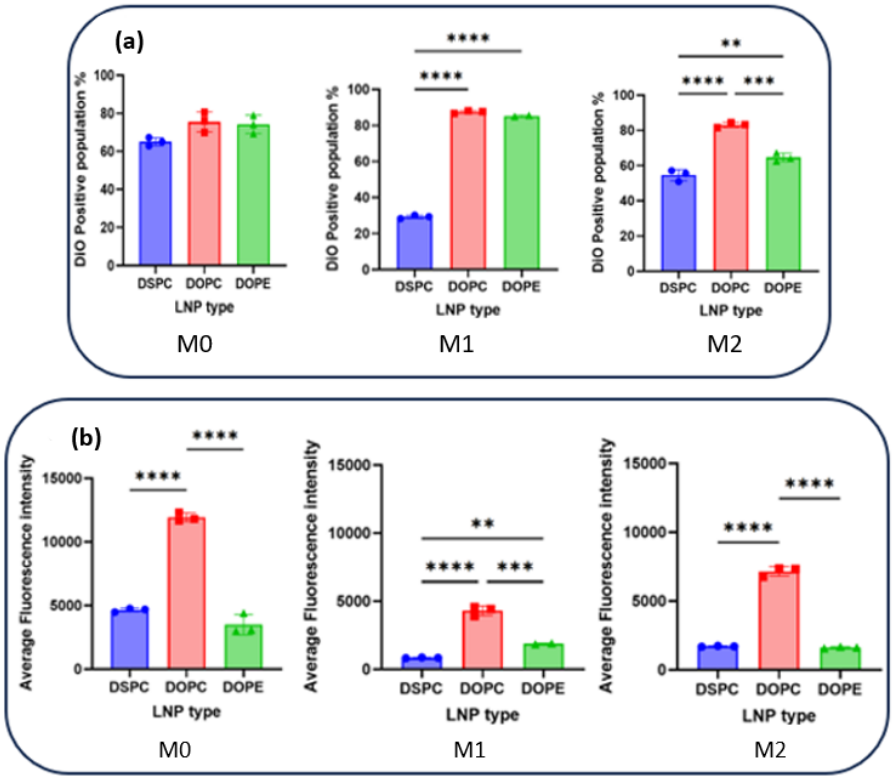

*Figure 22: a): M0 - Percent positive population for LNP uptake in untreated RAW264.7 cells; M1 - Percent positive population for LNP uptake in M1 polarized RAW264.7 cells (3) M2 - Percent positive population for LNP uptake in M2 polarized RAW264.7 cells (b) M0 - Fluorescence intensity plot for untreated RAW264.7 cells; M1 - Fluorescence intensity plot for M1 polarized RAW264.7 cells; M2 - Fluorescence intensity plot for M2 polarized RAW264.7 cells| Significance levels tested using one way ANOVA * p<0.05*

The DOPC LNPs show no inhibition or selectivity in the population or the intensity of uptake, maintaining the highest levels in both plots. The DOPE LNPs show a better uptake in the M1 phenotype than the M2. They also perform better than the DSPC LNPs in both the populations. As mentioned above, the M2 macrophages have a higher phagocytic activity, even so, the

uptake of the DOPE LNPs is higher in the M2 population(110,112,113). This could potentially point to their selectivity towards the M1 macrophages.

5.4.3. LNP uptake by 3T3 fibroblasts

The fibroblasts in this experiment are proxy for the stellate cells found in the sinusoidal walls within the subendothelial space of Disse in the liver. Their main function is to secrete collagen when activated by inflammatory mediators, in order to compensate for the damaged regions(17).

As mentioned in **Table 4,** three different conditions with the 3T3 cells were taken into consideration. The first condition refers to the non-activated 3T3 cells grown in complete media. The second refers to starved cells where the growth media did not have FBS and finally the third condition refers to their activation via TGF-β treatment. The TGF-β activates fibroblasts, making them produce extracellular matrix (ECM) and promoting proliferation(114).

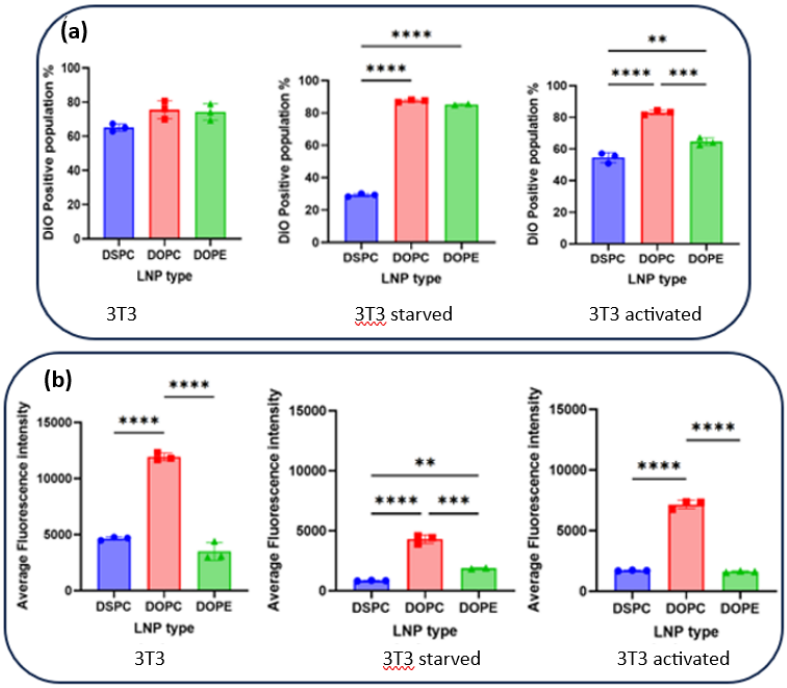

*Figure 23: (a): 3T3 - Percent positive population for LNP uptake in untreated 3T3 cells; 3T3 starved - Percent positive population for LNP uptake in starved 3T3 cells; 3T3 activated - Percent positive population for LNP uptake in TGF-β activated 3T3 cells (b): 3T3 - Fluorescence intensity plot for untreated 3T3 cells; 3T3 starved Fluorescence intensity plot for starved 3T3 cells; 3T3 activated Fluorescence intensity plot for TGF-β activated 3T3 cells | Significance levels tested using one way ANOVA * p<0.05*

From **Figure 23 (a)**, one can notice the starvation condition affects the uptake of DSPC LNPs but not the DOPC or DOPE. They maintain the same level of uptake as in the untreated population. However, there is a significant drop in the per cell uptake for all three LNPs.

Fibroblasts have been known to employ LDLr initiated endocytosis and the drop in uptake seen in starved cells could point to the fact that all three LNPs employed the ApoE-LDLr pathway. However, DOPC and DOPE LNPs did manage to maintain high levels of uptake in

starved conditions which points to an internalization pathway independent of the LDLr. Some reports have defined a Lipoprotein lipase mediated uptake of Lipoproteins, independent of LDLr, which might also be employed in the DOPC and DOPE LNPs' case as well(115). Another plausible explanation might be the involvement of yet to be characterized scavenger receptors, unaffected by the absence of serum proteins.

For the TGF-β activated population, the uptake trend seems to be close to the untreated condition, with the per cell uptake being lower, possibly due to the cells focusing on secreting ECM rather than taking up LNPs.

5.4.4. LNP uptake by H5V endothelial cells

The H5V cells represent the RES or reticuloendothelial system in the liver. They have phagocytic activity owing to their lineage being connected to monocytes(116). In **Figure 24,** one can see the population uptake for the LNPs and the per cell uptake via the intensity of fluorescent signal respectively for the three LNP populations in the H5V cell population.

DSPC and DOPC LNPs show a comparable population uptake and surprisingly DOPE has a lower uptake. DOPC dominates in the per cell uptake. However, the per cell uptake for DSPC and DOPE are comparable as in most other cell types. This could potentially be due to the fact that endothelial cells might have aversion to LNPs with phosphatidylethanolamine helper lipids, as the other two are categorized as phosphatidylcholine.

Endothelial cells are known to express scavenger receptors on their surface and there have been reports showing that anionic LNPs have a preferential uptake via them(116). Pattipeiluhu et al. showed the uptake of anionic LNPs in macrophages was mediated via stabilin 1 and 2 receptors, which are also expressed by LSECs(109,116). The DOPE LNPs however showed an unexpected decrease in their uptake which could mean that their uptake via the scavenger receptors is much slower, possibly due to an undefined rate limiting step(117).

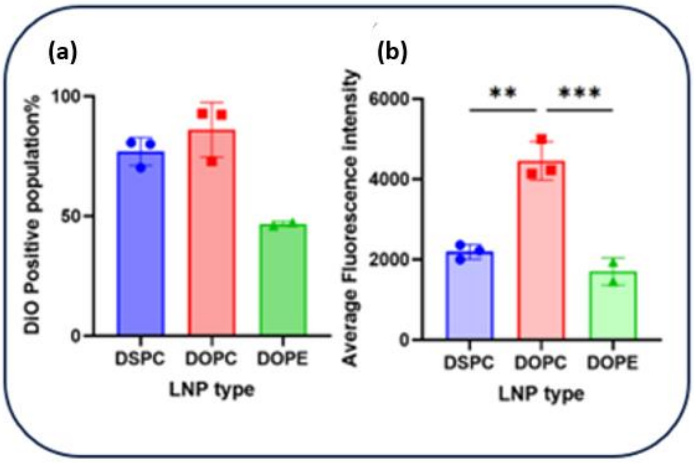

*Figure 24: (a): Percent positive population for LNP uptake in untreated H5V cells (b): Fluorescence intensity plot for untreated H5V cells | Significance levels tested using one way ANOVA * p<0.05*

5.4.5. DSPC vs DOPC vs DOPE LNP – Total signal comparison for delivery of therapy

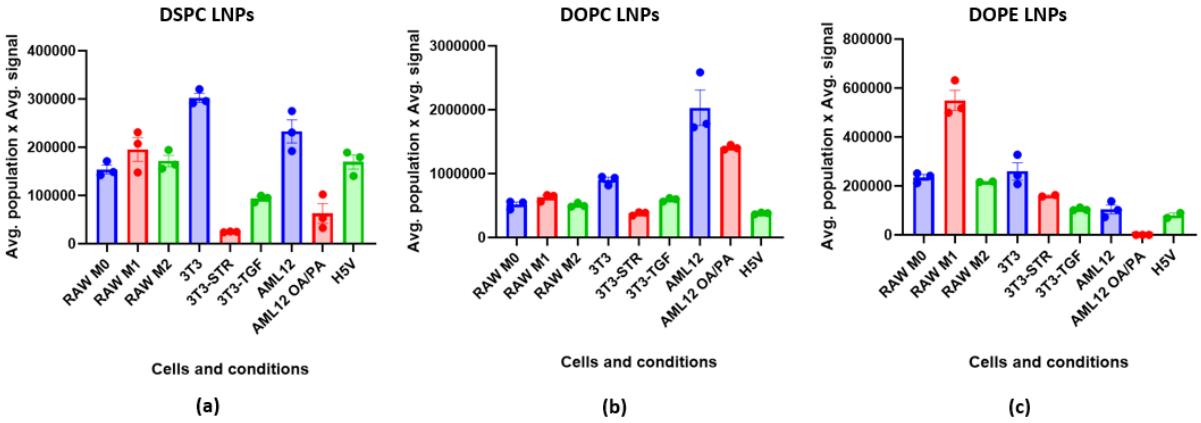

Figure 25: Total signal (average positive population x average fluorescent signal from the positive population) from the population that took up the DSPC, DOPC and DOPE LNPs (a) Total signal from the cells that took up DSPC LNPs (b) Total signal from the cells that took up DOPC LNPs (c) Total signal from the cells that took up DOPE LNPs

Besides the per cell uptake, it is essential to investigate the comparative uptake of each LNP in different cell types. In **Figure 25** we can observe all the cell populations in the experimental setup simultaneously with the three LNP populations. The graphs have their abscissa representing the average positive population combined with the average signal from the respective population, and the coordinate represents the different cell populations with their treatment conditions.

A point to note is that the scale for the three graphs is not at the same. This is due to the fact that the total signal (average positive population x average signal from the positive population) lies in very different ranges for the three LNPs and differences between their uptake would not be apparent if plotted at the same axis.

For DSPC LNPs, the highest uptake is seen in 3T3 fibroblasts, followed by healthy AML 12 hepatocytes and then the macrophages. The highest uptake being in 3T3 fibroblasts points to a gap in knowledge due to no specifically characterized interactions between them and the LNP components leading to endocytosis being mentioned in the literature. However, this does help us in deciding for a candidate to deliver antimiR-155. Bala et al. recently showed that miRNA-155 has an integral role in the activation of stellate cells via STAT3 signaling and its inhibition attenuated liver fibrosis(118).

The uptake by untreated hepatocyte (AML12) was based on the well-defined LDLr-ApoE mechanism and since this formulation was specifically designed for a therapy targeting hepatocytes, their high uptake is well within the expectations(70). The OA/PA treated hepatocytes show a decreased uptake, most likely due to the intracellular deposition of fats and steatosis, which would help target the other cell types in a diseased condition(108).

The macrophage and the endothelial cell populations have a comparable uptake, close to the level of hepatocytes. They are naturally phagocytic in nature with multiple receptors facilitating it, as mentioned earlier. Delivery to them over the other populations could help modulate the inflammation during liver injury(79,116).

The DOPC LNPs in **Figure 25 (b)** show the highest uptake in the untreated hepatocytes, followed by the OA/PA treated hepatocytes. The lower uptake could be due to the previously mentioned steatosis(108). The other cell populations have a significantly lower uptake, highlighting the high selectivity. The rest of the cell types have a somewhat comparable total signal, pointing to the non-specific uptake like trend seen in individual graphs. The scale of the plot here is much about 10x more as compared to DSPC and DOPE LNP plots. One could argue that the DSPC LNPs are highly efficient in their delivery, with the per cell uptake being substantially higher than the other due to a more efficient process of non-bilayer structure formation for endosomal escape(86).

In **Figure 25 (c)**, the DOPE LNPs show the highest total signal in M1 macrophages and the lowest in OA/PA treated hepatocytes, which makes them perfect to target pro-inflammatory macrophages in a steatosis-based disease condition for the liver. The total signal of all other populations is comparable to each other and significantly lower than that of the M1 macrophages. The most enticing reason to use this as the delivery agent for a therapy would be the low uptake in the endothelial cells, which usually have a comparable uptake to the macrophages due to scavenger receptors being expressed on their surface as the allowing for a larger portion of each dose administered to the pro-inflammatory macrophages. This would decrease the total number of doses of therapy due to high targeting efficiency.

Taking into consideration the uptake distribution for each of the LNPs in different cell lines and conditions, DSPC LNPs seem to be the best option to go forward with. They are taken up by the fibroblasts, which would help target the activation of stellate cells and the macrophages taking up the LNP would have a lower level of pro-inflammatory behavior *in vivo*. Thus, the DSPC LNPs carrying antimiR-155 would have a dual effect on tackling the progression of fibrosis during a liver injury(63,70,118).

5.5. *In vivo* biodistribution study

To study the *in vivo* organ distribution of DSPC, DOPC and DOPE LNPs in C57BL/6J mice, DiR, a lipophilic fluorescent dye was used for near infrared (NIR) imaging. About 100µl of DSPC, DOPC and DOPE LNPs equivalent to 1mg NC-miRNA/kg were administered to the mice intravenously and the signals were captured by using the PEARL trilogy whole animal NIR imaging system. An acute liver injury model including C57BL/6J mice was used for this study. The mice were imaged at 1h, 4h and 24h post LNP injections. The 1h time point is used to map out the early distribution of the LNPs and provide insights into rapid accumulation in certain

tissues, which might be indicative of potential safety concerns or off target effects. The 4h time point allows the LNPs to have sufficient time to circulate through the body, interact with

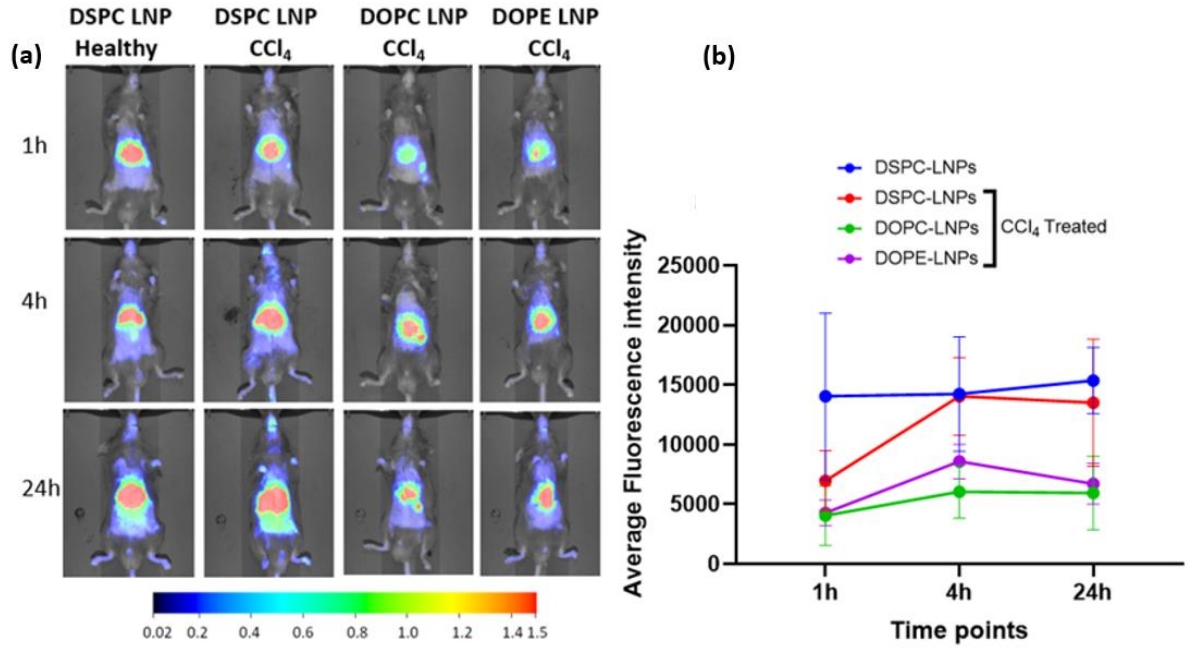

Figure 26: (a) Representative in vivo localization images for each treatment condition at 1h, 4h and 24h time points (b) Quantification of signal localized in the liver region for DSPC, DOPC and DOPE LNPs at 1h, 4h and 24h time point

different organs and tissues to reveal any patterns and trends in accumulation, clearance or redistribution. It helps understand if the LNPs have a rapid elimination or are they being retained by specific tissues. The 24h assessment provides a relatively longer term view of the LNP retention. It helps in identifying if the LNPs have a tie dependent accumulation in specific organs or if 24h was long enough for them to be cleared out of the system(119,120).

In **Figure 26 (a)**, representative images of the different groups at 1h, 4h and 24h can be observed. For DSPC and DOPC LNPs, a similar localization can be observed throughout the time points. On the other hand, for DOPC LNPs, we observe a secondary localization, possibly in the spleen which is quite evident at each of the three time points.

All three LNPs had their size in the range of 70-140nm, which is ideal for systemic administration via IV as well as passive accumulation in the liver(73,93). The zeta potential however was quite different, as seen in **Table 8**. The differential interactions with the serum proteins would be based on the zeta potential and the structural variation between PE and PC compounds used for LNP production(121). Variability in interaction with serum proteins translates into the different biodistribution of the LNPs visible in **Figure 26**.

In **Figure 26 (b)**, one can see at 1h, the CCl_4 treated groups with a low signal in the liver, possibly due to the liver injury causing vasoconstriction and compromising the accessibility(122). The signal from the healthy group was quite close to its maxima even at 1h. At 4h, the CCl_4 treated groups reached their maximum signal, hence, maximum accumulation of LNPs. At 24h, there is a slight drop in the signal in every group except the healthy, possibly

due to the LNPs attaining equilibrium with the filtration function of the liver and the blood flow, owing to the increase in iNOS levels. The iNOS levels increase in response to inflammation and is a potent antagonist for vasoconstriction(123).

Within the CCl_4 treated groups, the DSPC LNP treated group showed the highest localization in the liver at 1h, 4h and 24h. DOPC LNPs, which performed exponentially better than the other two *in vitro* had the lowest signal throughout. DOPE LNPs performed better than DOPC LNPs but significantly poorer than DSPC LNPs. Thus, DSPC LNPs performed the best in terms of highest residence time in the liver over a period of 24h.

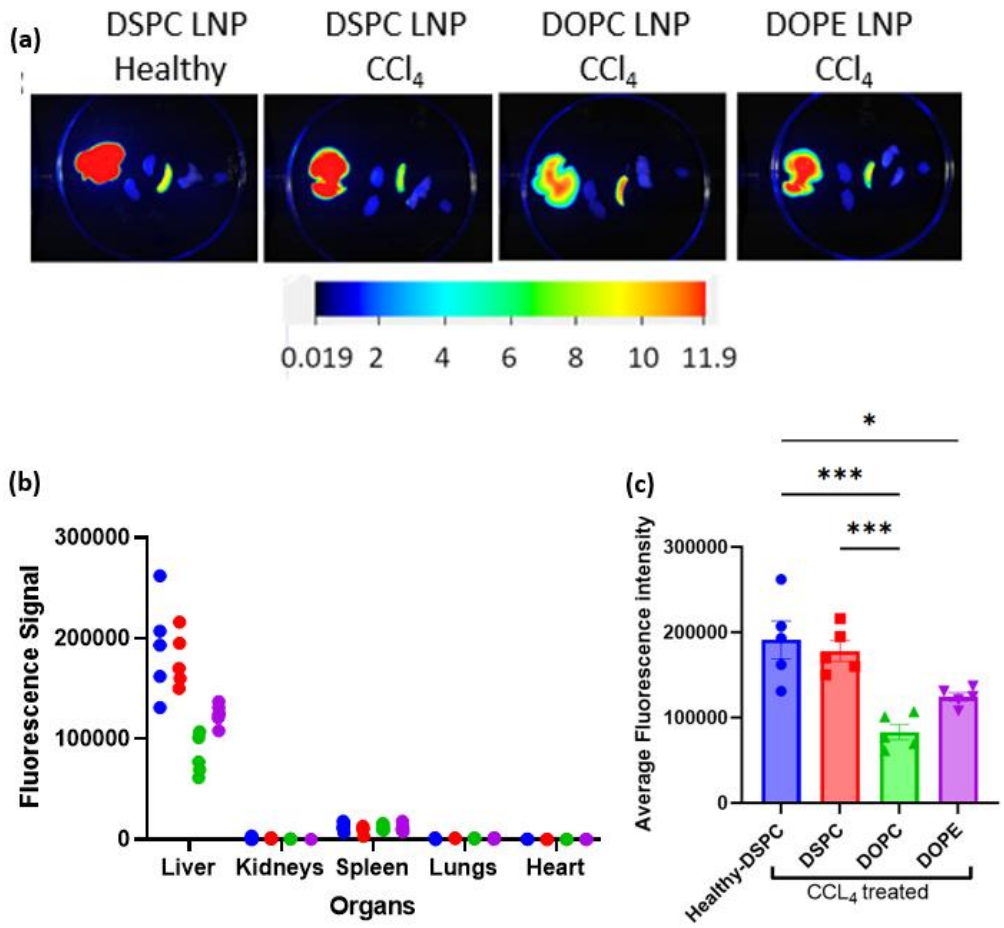

*Figure 27: (a) Representative images of fluorescent signal in excised organs from each condition in the order of (Left to right) Liver, Kidneys, Spleen, Lungs and Heart (b) Relative localization of fluorescent signal in the excised organs (c) Quantification of Fluorescent signal in the liver for each condition| Significance levels tested using one way ANOVA * p<0.05*

To get a better view of inter-organ localization of the LNPs, the major organs, namely the liver, kidneys, spleen, lungs and the heart were excised and imaged. As can be seen in **Figure 27 (a)** and **(b)**, the DOPC LNPs have a comparable signal intensity in the spleen and the liver and thus, the secondary localization is prominent in whole body images for the corresponding group. The DSPC and DOPE LNPs show the highest intensity of the signal in the liver. **Figure 27 (b)** shows the major localization of the signal being present in the liver, with some discernable signal in the spleen as well. The signal in the spleen is expected due to the high macrophage population in it, but the levels are far too low in comparison to the liver. This can be justified

by the size range of the LNPs being from 70-140nm, ideal for accumulation in the liver(73,93). The secondary accumulation in the spleen can be explained due to the high phagocytic macrophage population found over in it. In **Figure 27 (c)** we can observe the fluorescent signal in the excised livers from different treatment groups, showing the DSPC LNPs to be the best performers, with the highest fluorescent signal correlating to highest LNP accumulation after 24h. Thus, the DSPC LNPs showed the best biodistribution in regard to passive targeting of liver over the course of 24h.

Another interesting aspect of the biodistribution observed is the variation in uptake behavior of the LNPs when compared *in vitro* and *in vivo*. Since the DOPC LNPs showed the highest uptake in terms of total population as well as per cell uptake in hepatocytes *in vitro*, as observed in section 5.4.5, one would have hypothesized them to have the highest accumulation in the liver as hepatocytes make up 80% of the total liver population. They would also have the highest intensity due to the higher uptake efficiency highlighted in the previous experiment but this wasn't the case. The substantial splenic uptake of the DOPC LNPs makes them an unreliable delivery agent in the context of targeting the liver or the spleen independently. This biodistribution however goes against the results obtained by Zhang et al. and Kulkarni et al. who showed that DOPE and DOPC LNPs would perform better than DSPC LNPs in terms of preferential biodistribution in the liver(85,86). Zhang et al, showed that the replacement of DSPC with DOPE decreased splenic biodistribution by five times and increased accumulation in the liver by two times which is clearly not the case in our study. The possible explanation for this might lie in the ionizable lipids as well as the PEG lipids used in formulating the LNPs. By using different lipids, the interactions with the serum proteins changes considerably, leading to the change in their biodistribution. The ionizable lipid might have a smaller role to play here due to being localized inside the LNP structurally, but the PEG lipids are on the surface and have been characterized to interact with multiple proteins and hence, changing them would play a significant role in organ and cellular localization(124).

The DSPC LNPs had the optimal biodistribution required for passive targeting of the liver and thus, were employed for the delivery of antimiR-155 and testing its efficacy.

5.6. *In vivo* efficacy of antimiR-155 LNPs

5.6.1. Study design

After compelling evidence suggesting DSPC LNPs to be the best delivery agents for antimiR-155, an *in vivo* study based on a semi-chronic liver injury model using C57BL/6J mice was designed. The treatment timeline can be seen in **Figure 15**. The mice were injected with 0.2ml/kg CCl_4 intraperitonially once a week for four weeks, and treated with the therapeutic LNPs corresponding to 1mg miRNA/kg bodyweight of the mice in a total volume of about 100µl twice a week in the last two weeks of the study.

The mice were divided into five groups as can be seen in **Table 6**. The healthy and the disease control groups were not given any therapeutic treatments. The mice were sacrificed on day 24 and the organs were collected and cryopreserved.

5.6.2. Weight distribution over time

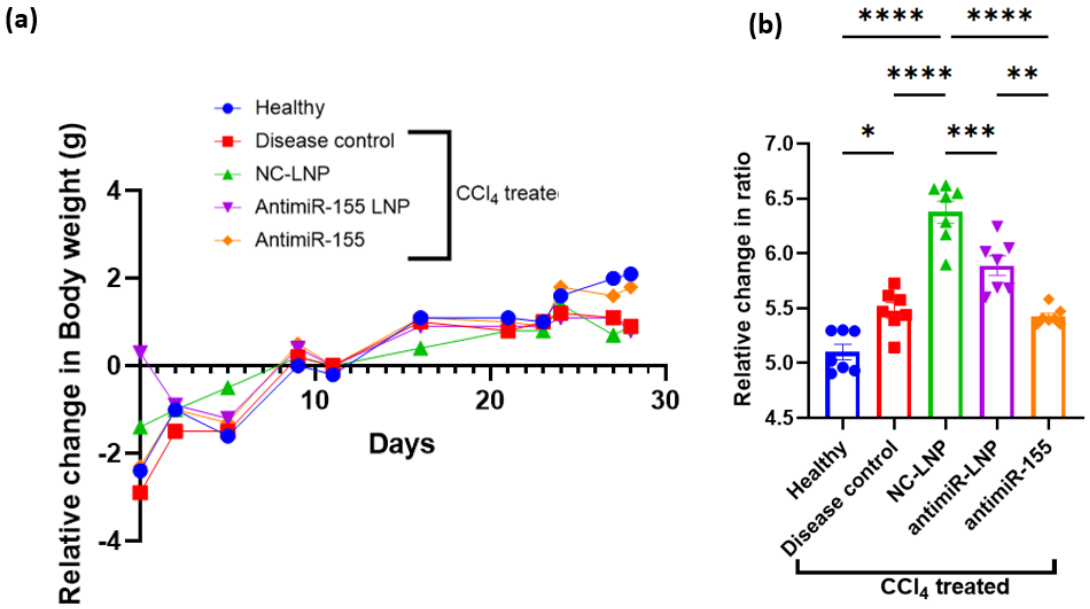

*Figure 28: **(a)** Relative change in body weight of mice over the course of study, normalized with weight on the day of first therapeutic dose **(b)** Relative change in liver weight to body weight ratio in different treatment groups| Significance levels tested using one way ANOVA * p<0.05*

The body weight throughout the study did not show any relevant significant differences, meaning that the metabolic processes in the mice were not perturbed to an extreme level. However, when observing the antimir-155 LNP treatment group individually, one can see via **Figure 28 (a)**, the bodyweight decreases up until the first therapeutic dose, after which, the bodyweight increased consistently just like the other groups. CCl_4 is a chemical agent used to induce liver injury in animal models and one of the characteristics of the loss of hepatic function during prolonged fibrogenesis is loss of weight(125). The fact that the antimiR-155 LNP treatment group showed a possible reversal of weight loss due to CCl_4 induced liver injury indicates the efficacious nature of the treatment in respect to hepatic functioning.

The liver weight to bodyweight ratio is a measure of severity of the liver injury. During the induction of liver injury by CCl_4, an increase in liver weight and a decrease in total bodyweight is a characteristic outcome(125,126). When plotted in **Figure 28 (b)** the liver to body weight ratio showed an interesting trend where the NC-LNP treated group had the highest ratio and the treatment with antimir-155 LNPs as well as naked antimir-155 had a lower ratio, the latter more pronounced than the former. These differences are significant when assessed with one way ANOVA (post hoc Tukey for multiple comparisons). An increase in the liver to bodyweight ratio could indicate prominent liver injury in the treatment groups. Thus, the naked antimiR-155 and the antimiR-155 LNP treatment groups having a lower ratio could indicate either a

less severe liver injury, or recovery of the injury due to the treatments. Considering the latter to be the more plausible explanation due to the same dosing of CCl_4 for each group, it could hint at the fact that naked antimir-155 treatment might be more efficacious as compared to antimir-155 LNPs in the context of body weight due to increased stability by 2'OMe 5'inZEN, 3'ZEN modification pattern. The naked antimiR-155 would have a sustained systemic effect due to absence of a targeting mechanism, and remain in circulation due to the modifications making it resistant to degradation by extra and intra-cellular nucleases(68).

5.6.3. FACS analysis of excised liver samples

Liver is an immune-rich organ with a diverse array of immune cells. In order to gain insight about how the monocyte/macrophage immune cell profile of the liver varied in different treatment groups, fluorescence assisted cell sorting was employed.

Small samples from the excised liver were treated as described in the methods as a prerequisite for Fluorescence assisted cell sorting analysis. As can be seen in **Table 7**, multiple fluorophores were used for tagging the cells in order to determine different populations in the sample tissue.

Figure 30 shows the plots from a sample treated with all the antibodies and the shift in the plots is clearly visible as compared to **Figure 29**, hence, affirming the gating strategy employed for separating the negative and the cells positive for the fluorophores. These cells were then represented as a function of two or more fluorophores in order to filter out different populations among them.

The gating hierarchy can be observed in **Figure 31**. The gating strategy involved selecting the nucleated cells using the Hoechst positive events, which were plotted onto a CD45 spectrum. CD45, also known as the leukocyte common antigen, is present on almost all cells covered in the immunological and hematological domain, except for mature erythrocytes and platelets(127,128). The CD45 positive cells, hence, the leukocytes, were plotted on a DUMP plot, which contained fluorophores for immune cells to be excluded from the analysis – T cells, B cells, natural killer cells, granulocytes, neutrophils etc.(129). Since the main focus of the experiment was to profile the monocyte and macrophage populations, the cells represented by the DUMP population are excluded from the analysis by inverting the gate selection. The NOT DUMP population was plotted and selected for by meticulous gating for CD11b, F4/80, Ly6c and Tim4 positive populations. The NOT DUMP population contained only monocytes and macrophages and the markers – CD11b, F4/80, Ly6c and Tim4 correspond to antigens present on the surface of these cells(130–133). By plotting the NOT DUMP events on these antigen based fluorophore spectrums, we get a sense of the level of their relative expression, which when combined with the other antigen expression levels, filters specific population of cells which can be regarded as macrophages or monocytes with a level of certainty.

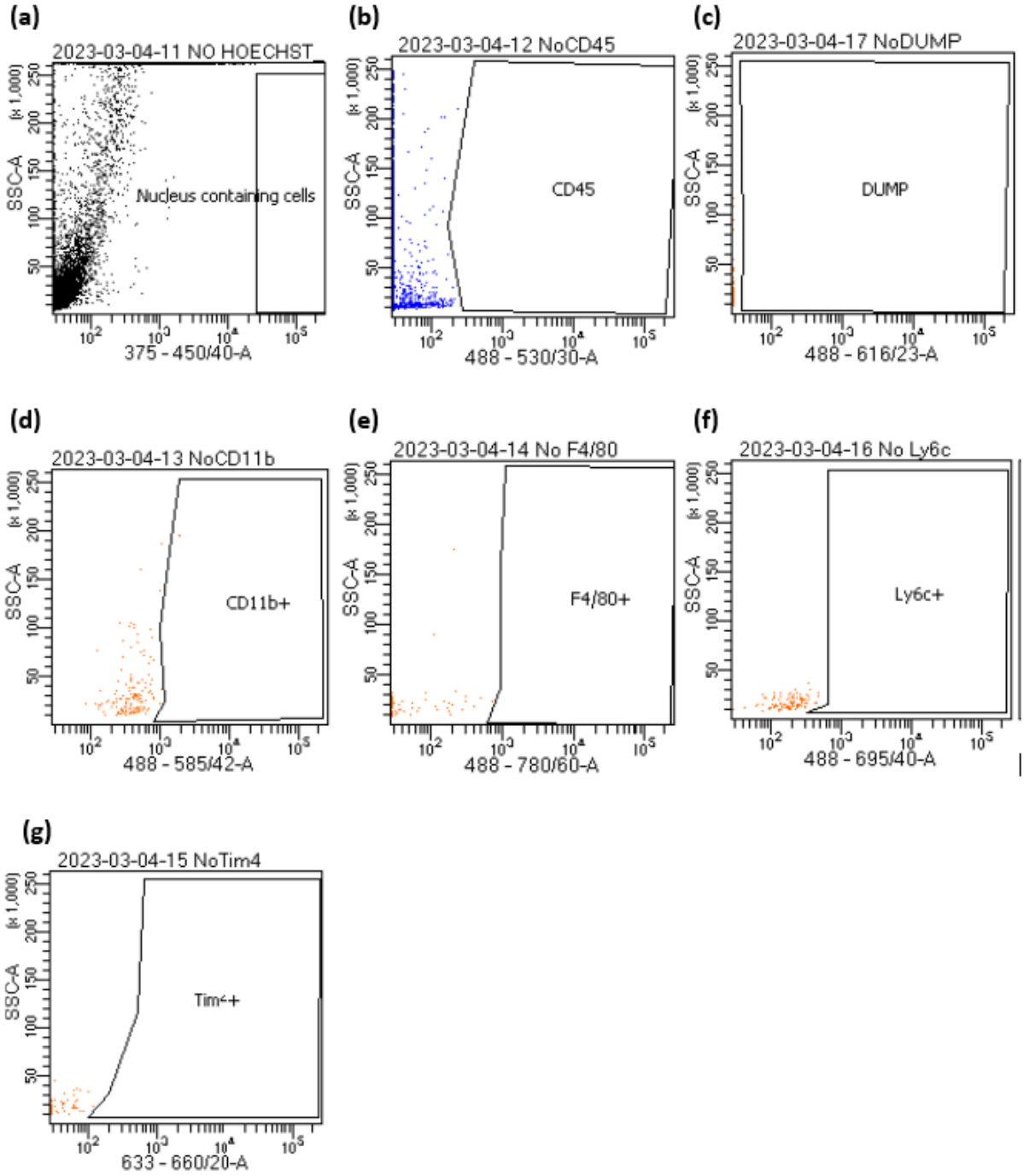

Figure 29: Negative control plots for different antibody tags (a) Liver cells treated with all antibody tags except Hoechst (b) Liver cells treated with all antibody tags except CD45 (c) Liver cells treated with all antibody tags except DUMP Abs (d) Liver cells treated with all antibody tags except CD11b (e) Liver cells treated with all antibody tags except F4/80 (f) Liver cells treated with all antibody tags except Ly6c (g) Liver cells treated with all antibody tags except Tim4

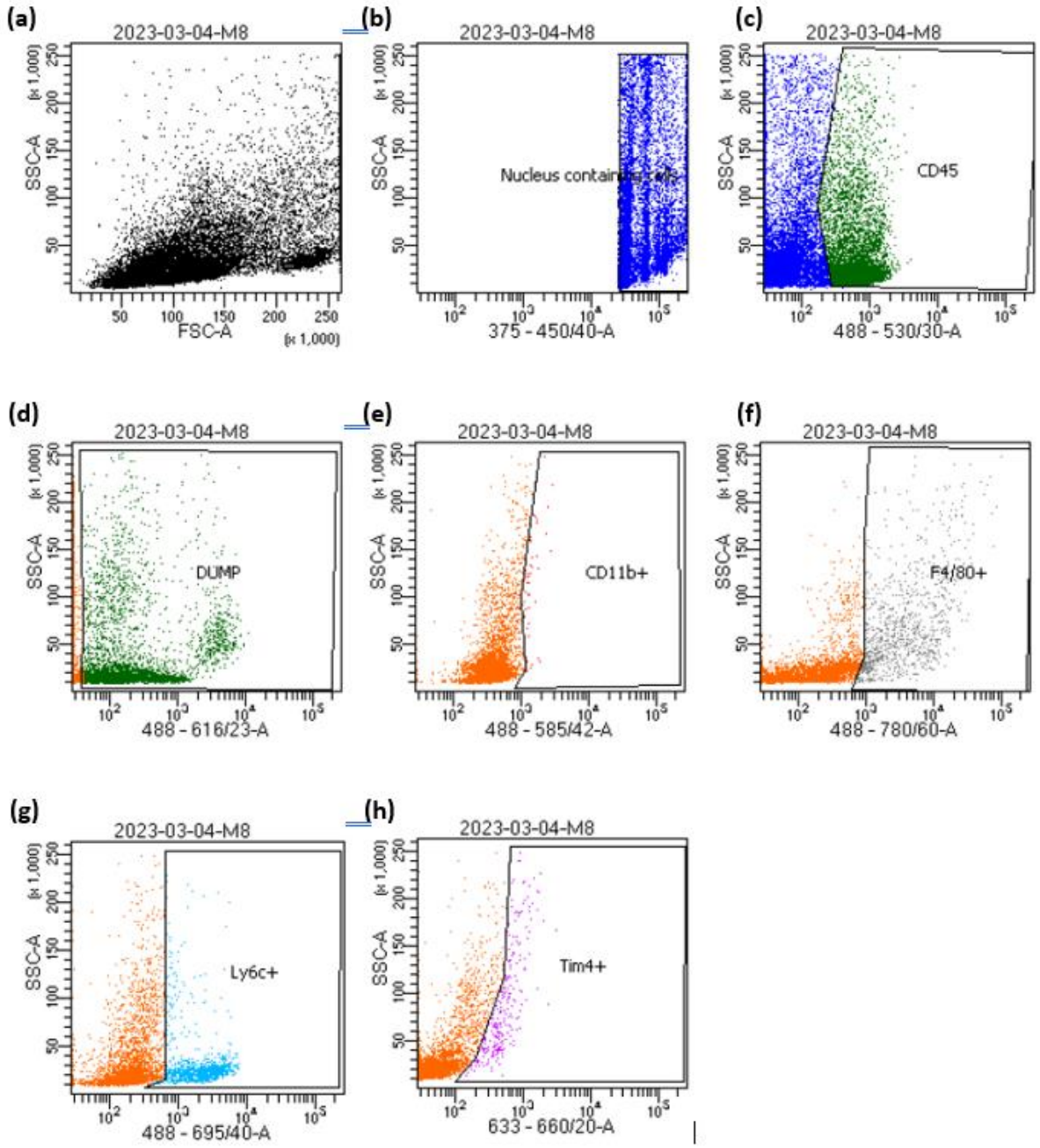

Figure 30: Populations positive for respective antigen expression plotted on fluorophore spectrum (a) Side scatter vs forward scatter of all cells visualized (b) Nucleus contain cells selected from total population using Hoechst (c) Leukocytes selected from nucleated cells based on CD45 antigen expression (d) Cells expressing Ly6G, CD3, CD19, NK1.1 antigens (DUMP) selected for from the CD45+ population and excluded from the analysis (NOT DUMP) (e) NOT DUMP population selected for the expression of CD11b antigen (f) NOT DUMP population selected for the expression of F4/80 antigen (g) NOT DUMP population selected for the expression of Ly6c antigen (h) NOT DUMP population selected for the expression of Tim4 antigen

Population	#Events	%Parent	%Total
All Events	20,000	####	100.0
Nucleus containing cells	0	0.0	0.0
CD45	0	####	0.0
DUMP	0	####	0.0
NOT(DUMP)	0	####	0.0
F4/80+	0	####	0.0
P5	0	####	0.0
P2	0	####	0.0
P1	0	####	0.0
P4	0	####	0.0
CD11b+	0	####	0.0
Ly6c+	0	####	0.0
Tim4+	0	####	0.0
P3	0	####	0.0

Figure 31: Gating hierarchy for macrophage and monocyte markers for cells derived from mice liver from miRNA-155 LNP efficacy study

5.6.3.1. Resident Macrophages

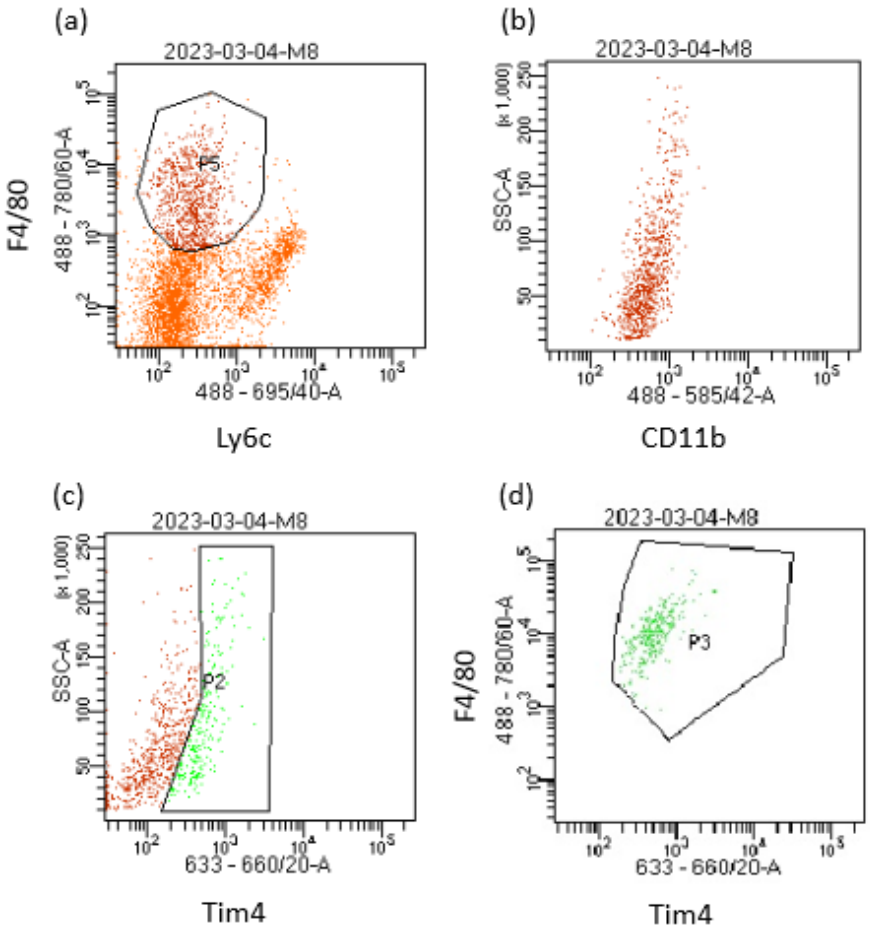

Figure 32: Isolation of resident macrophage population in liver samples – Kupffer cells (a) NOT DUMP population plotted between F4/80 and Ly6c spectrum (b) P5 plotted on CD11b spectrum (c) P5 plotted on Tim4 spectrum and positive population selected as P2 (d) P2 plotted on F4/80 vs Tim4 spectrum and selected as a single population P3

In this section, we try to find out the resident macrophage population or the Kupffer cells from the NOT DUMP population. This is achieved by looking at the relative expression of F4/80, a murine mature macrophage marker; Ly6c, a monocyte marker; CD11b, a monocyte marker and Tim4, a marker for Kupffer cells(130–133). Kupffer cells are macrophages and thus, would be expected to have a high F4/80 expression and a low Ly6c expression(132). Thus, in **Figure 32 (a)**, we see the NOT DUMP population plotted between F4/80 and Ly6c and three distinct populations are visible – F4/80+ Ly6c-, F4/80-Ly6c- and F4/80-Ly6c+. Since we are looking for macrophages, we focus on the Ly6c- population and the Ly6c+ population will be discussed in the next section. The F4/80-Ly6c- cells could likely be a special subset of dendritic cells as they are CD45 positive but do not express the markers for macrophages or monocytes(134–137). The F4/80+Ly6c- cells are gated as P5. The P5 population is then plotted on the CD11b spectrum (**Figure 37 (b)**), which shows no variation in its expression and displays P5 as a single population, pointing towards the fact that there are no monocytes present in P5. P5 is the plotted on the Tim4 spectrum to select for Kupffer cells as P2 (**Figure 32 (c)**)(130). The Tim4 negative macrophages constitute the infiltrated monocytes that matured into macrophages, replacing the Kupffer cell population as well as classical dendritic cells(130,134,138). P3 is then plotted on F4/80 vs Tim4 axes (**Figure 32 (d)**)and selected as a single population with F4/80+Ly6c-Tim4+ expression.

5.6.3.2. Infiltrated monocytes

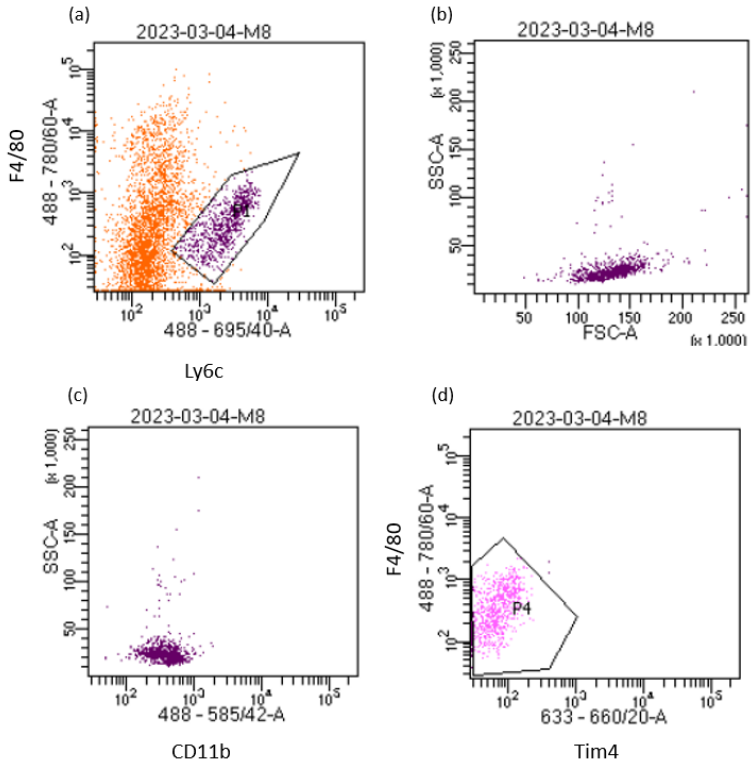

Figure 33: Isolation of infiltrated monocyte population in liver samples (a) NOT DUMP population plotted between F4/80 and Ly6c spectrum (b) P1 plotted on side scatter vs forward scatter (c) P1 plotted on CD11b spectrum (d) P1 plotted on F4/80 vs Tim4 spectrum and selected as a single population, P4

In **Figure 33 (a)**, we see the plot between F4/80 and Ly6c. For the macrophage population, we gated for the Ly6c negative population as it is a monocyte specific marker(132). Here, in order to identify the monocyte population, we gate for the F4/80-Ly6c+ population as P1(131). The F4/80 being negative points to the population not containing macrophages. P1 is then plotted in the CD11b spectrum, showing that it is a single population with no modulation in the CD11b expression(133). Side scatter vs forward scatter of P1 also reconfirms it to be a single population. F4/80 vs Tim4 plot of P1 shows low expression of both antigens, which is in line with the expectations from monocytes as they aren't mature, hence the low F4/80 expression and they aren't resident macrophages, hence the low Tim4 expression(138). The infiltrated monocyte population F4/80-Ly6c+Tim4- is then gated as P4.

5.6.3.3. Analysis of FACS

In **Figure 34** we can see P3 and P4 representing the Kupffer cells and the infiltrated monocytes on a single plot of F4/80 vs Tim4 showing the difference in Tim4 expression in the two populations(131,138).

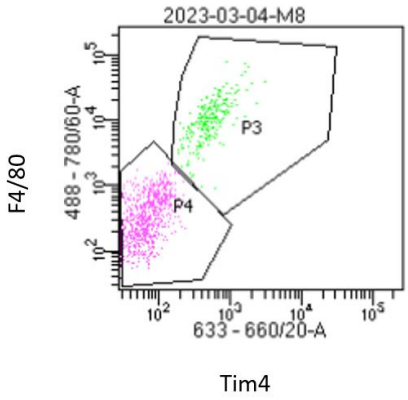

Figure 34: Kupffer cell population (P3) and infiltrated monocyte population (P4) plotted on F4/80 vs Tim4 spectrum

For the quantification of all the populations in different groups, each of them was normalized as a percentage of the total CD45+ (leukocyte) population, as can be seen in **Figure 35**(128).

The F4/80 levels, as observed in **Figure 35 (a)** are highest in the NC-LNP group, followed by the antimiR-155 LNP treated group and the disease control group. The lowest level can be seen in the naked antimiR-155 treated group. During the progression of liver injury, liver resident macrophages, Kupffer cells are replaced by infiltrating monocytes, which mature into macrophages as well. F4/80 is a murine macrophage marker and highest levels in NC-LNP group suggests two possible explanations – the population of resident macrophages and special subset of F4/80 expressing dendritic cells is high in the NC-LNP treated group or the infiltrated monocytes have matured into macrophages(130,134–138).

CD11b is a monocyte/macrophage marker, mostly leaning towards monocyte population(133). The CD11b levels in the population are highest in the antimiR-155 LNP treated group, followed by

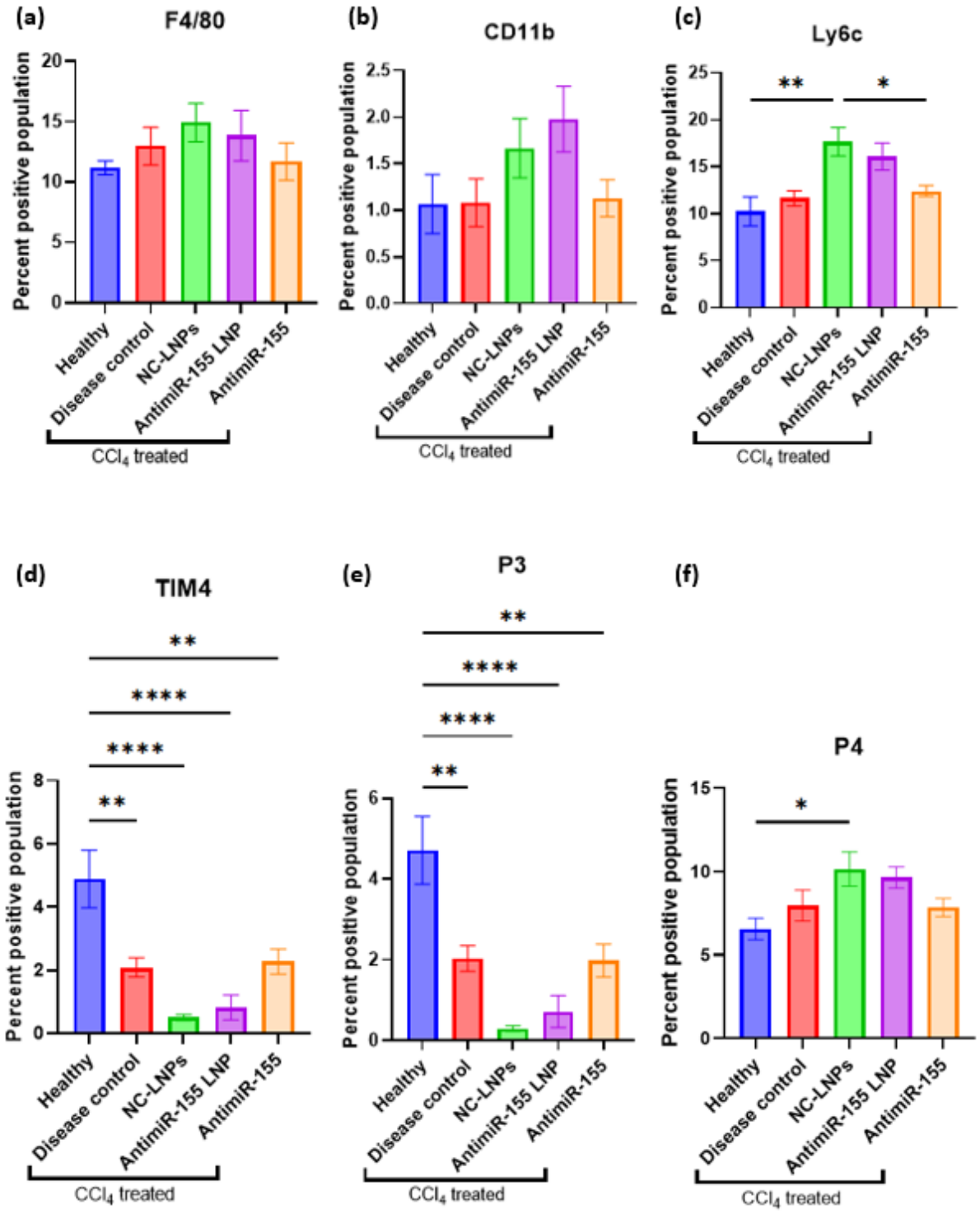

*Figure 35: Quantification of the populations isolated from FACS analysis. All populations normalized with CD45+ leukocytes in respective samples (a) F4/80 positive population percentage (b) CD11b positive population percentage (c) Ly6c positive population percentage (d) Tim4 positive population percentage (e) Kupffer cells (P3) in different groups, isolated from FACS analysis (f) Infiltrated monocytes (P4), isolated from FACS analysis | Significance levels tested using one way ANOVA * p<0.05*

NC-LNPs and the rest three groups are almost at the same level which can be seen in **Figure 35 (b)**. This does not correspond to the Ly6c based results, which quantify the monocyte population(132). Thus, the antimiR-155 LNP and the naked antimiR-155 treated groups might have macrophages expressing CD11b. But, CD11b macrophages have been shown to be pro-inflammatory in nature and their high levels are not corroborated by the iNOS staining seen in **Figure 37 (a)**(139). They could be non-classical CD11b positive macrophages which inhibit pro-inflammatory response(140).

Ly6c being a monocyte marker, can also be seen on infiltrated monocytes maturing into macrophages(130,132). Its levels as observed in **Figure 35 (c)** in the total population are highest in the NC-LNP treated group, followed by the antimiR-155 LNP treated group. The rest three groups are almost at the same level. The NC-LNP group level is significantly higher than the healthy group and the naked antimiR-155 treated groups' level is significantly lower. As the livery injury progresses, monocyte infiltration increases as well, replacing the resident macrophage population. This suggests the naked antimiR-155 treatment working better towards decreasing the infiltration of the monocytes into the liver, possibly due to the increased stability gained by 2'OMe 5'inZEN, 3'ZEN modification pattern. It has been shown to prevent degradation of miRNA mimics for up to four days while incubated in liver cell extract(68). Thus, giving the naked antimiR-155 a longer circulation time and therapeutic window.

Tim4 is a marker specifically expressed by Kupffer cells and its levels in the total population are lowest for the NC-LNP treated group, followed by the antimiR-155 LNP treated group presented evidently in **Figure 35 (d)**(130,138). Every group has significantly decreased Tim4 population as compared to the healthy. The disease control and the naked antimiR-155 treated groups are almost at the same level, with the healthy group having the highest value. These results complement the Ly6c levels in the total population. The groups with the highest Ly6c levels have the lowest Tim4 levels and vice versa, pointing to the well observed phenomenon of Kupffer cell population decreasing as the infiltration increases during a prolonged liver injury(141,142).

As mentioned above in the comparison for the Ly6c an Tim4 levels, we see cells in P3 and P4 representing the exact same trends while complementing each other as observed in **Figure 35 (e)** and **(f)**(130,132,138,142). P4 shows a significant increase in the monocyte population in the NC-LNP treated group as compared to the healthy group, which points to increased monocyte infiltration. In diseased/liver injury condition, monocytes are recruited from circulation via pro-inflammatory chemokines and cytokines. These monocytes are responsible for propagating the pro-inflammatory environment in the liver. The trend here shows decrease in the monocyte population in the antimiR-155 LNP and naked antimiR-155 treated groups as compared to the NC-LNP group, pointing to low macrophage infiltration(130,142). The trend in P3 shows antimiR155 LNP and naked antimiR-155 treated groups retaining more Kupffer cells as compared to the NC-LNP treated group, which is a characteristic of a relatively heathy liver. The Kupffer cell population in the naked antimiR-155 treated group is higher than that in

the antimiR-155 LNP treated group and the monocyte infiltration is lower, indicating that the naked antimiR-155 treatment being better. These trends point to the fact that the naked antimiR155 treatment seems to work better than the antimiR-155 LNP treatment. As mentioned earlier, this can be explained by the 2'OMe 5'inZEN, 3'ZEN modification of the sequence, which has been shown to exponentially increase the stability of miRNAs. It has been shown to prevent any degradation of the sequences for up to four days while being incubated in liver cell extracts(68). The effects of the naked antimiR-155 would be systemic due to the absence of any active targeting, and hence, the side effects cannot be accounted for when the proper localization of the therapeutic is not known. There is however a possibility that a large amount of it would accumulate in the liver due to the livers' filtration function, unintendedly passively targeting the therapy(93). Another plausible explanation could be that the effects might be systemic, but relatively short lived as compared to the LNPs. The antimiR-155 LNPs might remain in circulation longer and could have a longer, sustained effect on the amelioration of immune response. We can't say this for sure as we haven't yet compared the half-life of the LNPs and the naked antimiR-155 *in vivo* and thus, this remains a hypothesis.

While describing the level of F4/80 positive cells in the total leukocyte population, two possible explanations were put forth and looking at all the other markers, the theory of a high number of infiltrated monocytes maturing into macrophages in the NC-LNP treated group, along with a considerable population of a special subset of F4/80 expressing dendritic cells seems much more plausible. F4/80 is a murine macrophage marker and has the highest levels in NC-LNP treated group. Kupffer cells are resident macrophages in the liver, also F4/80 positive, but are replaced by infiltrated monocytes that mature into macrophages. Dendritic cells are a contributor to the hepatic immune homeostasis and have been shown to express F4/80, but not Tim4 or Ly6c, but there are non-classical subtypes that don't even express F4/80(130,134–136,142). The infiltrated monocytes maturing into macrophages do not express Tim4, which are selected against in P2 in **Figure 32 (c)**. The events which aren't selected for, are the F4/80+Ly6c-Tim4- cells, or infiltrated monocyte derived macrophages with classical dendritic cells(135–137).

5.6.4. Immunohistochemical staining

In order to look at different inflammation markers, as well as fibrosis, the secondary effect of liver injury, immunohistochemical staining was performed as per the methods defined earlier. **Figures 36, 37** and **38** shows representative images as well as quantitative graphs for the levels of different markers – F4/80, Collagen 1 and iNOS. F4/80, as previously defined, is a murine macrophage marker and can be used to quantify them in the liver sections, giving us an idea about the level of inflammation response due to the induced injury(130,142). iNOS is a marker for M1 – proinflammatory macrophages which also defines the extent of inflammatory response in the model at hand(143). Collagen 1 staining corresponds to the levels of fibrosis

observed due to the regenerative response after the injury is sustained. It quantifies the scar tissue in the liver(144,145).

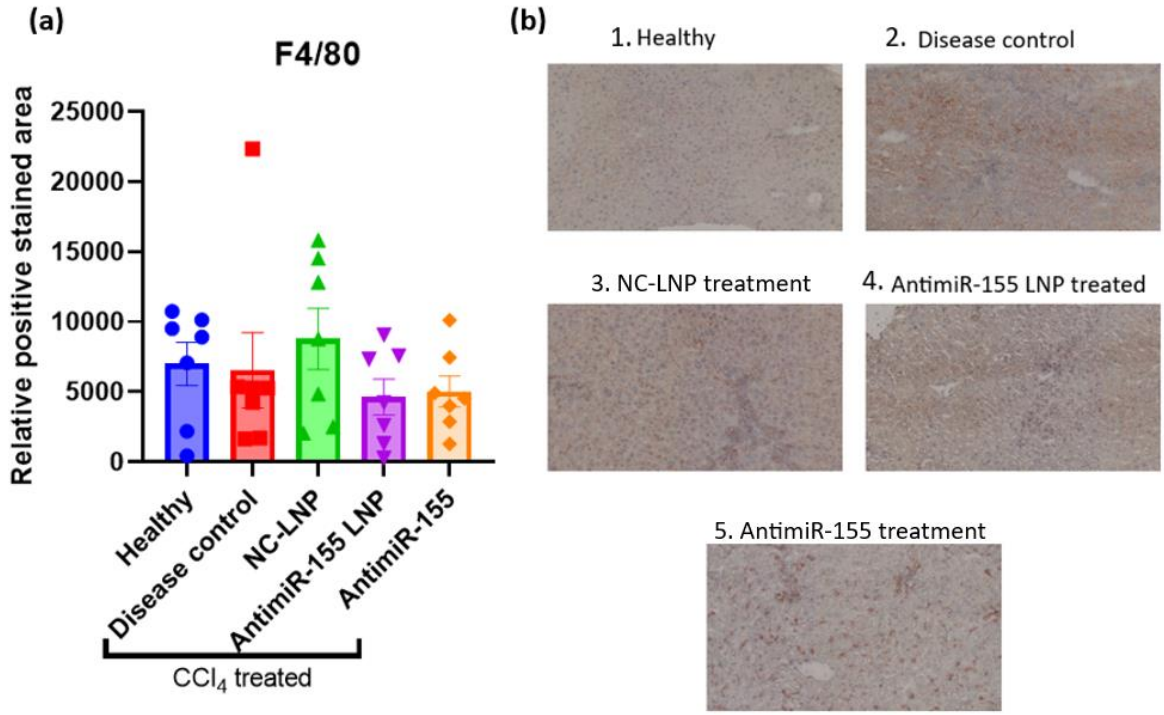

*Figure 36: (a) F4/80 antigen staining quantification (b) representative images of each of the treatment groups with F4/80 staining | Significance levels tested using one way ANOVA * p<0.05*

F4/80 was also quantified using FACS and we see a similar trend in **Figure 36 (a)** as well. The NC-LNP treated group has the highest level of F4/80 and antimiR-155 LNP treated group along with the naked antimiR-155 treated group have comparable lowest levels. The antimiR-155 delivery leads to the downregulation of miRNA-155 activity by binding to the complementary sequence. Since the miRNA-155 can't upregulate the downstream pro-inflammatory effectors like TNFα and IL6, the total inflammation in the liver goes down. The decrease in inflammation corresponds to lower number of monocytes recruited due to reduced inflammatory cytokine production(54,63,146). Since there are a lower number of monocytes that infiltrate the liver, an even smaller portion mature into macrophages. The resident macrophages, in case of liver injury are replaced by infiltrating monocyte derived macrophages(130–132,142). Thus, with the therapy groups delivering antimiR-155, we see a decrease in the total macrophage population as compared to the group delivering NC-miRNA. The results points to the NC-LNP treated group having a high number of macrophages in light of higher number of infiltrated monocytes and a large proportion of them maturing into macrophages. In antimiR-155 LNP treated and naked antimiR-155 treated groups, the level of total macrophages decreases as compared to the NC-LNP group, possibly due to a lower number of total infiltrated monocytes, or, a smaller proportion of the infiltrated monocytes being matured into macrophages. The comparable levels of F4/80 in antimiR-155 LNP and naked antimiR-155 LNP treatments could be attributed to the 2'OMe 5'inZEN, 3'ZEN modification in the miRNA-155 sequence which increases the stability exponentially(68). Thus, the naked antimiR-155 would have a

considerably longer half-life, increasing the therapeutic window, but due to the absence of a targeting system, the effects would be systemic and there might be side effects we can't account for. By looking at **Figure 35 (f)**, we can say that the antimiR-155 LNP and the naked antimiR-155 treated groups had a lower total infiltrated monocyte count as compared to the NC-LNP treated group, thus, establishing its therapeutic efficacy against monocyte infiltration.

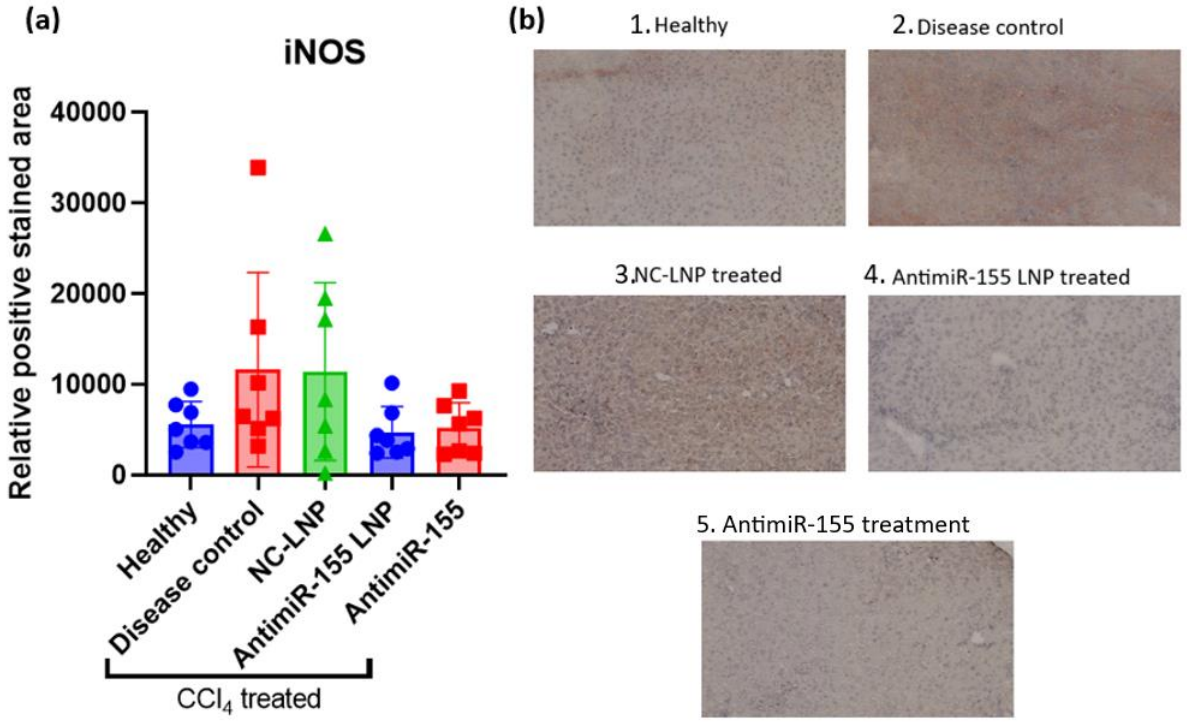

*Figure 37: (a) iNOS antigen staining quantification (b) representative images of each of the treatment groups with iNOS staining | Significance levels tested using one way ANOVA * p<0.05*

iNOS is a well characterized marker for M1 proinflammatory macrophage activation. It distinctly shows if the antimiR-155 was able to target the M1 macrophage population and decrease it or was the therapy for naught(143). The antimiR-155 delivery would bind to the miRNA-155 inhibiting any interaction with the downstream mRNAs, thereby decreasing the production of chronic inflammatory cytokines such as TNFα and IL6. It would also be unable to inhibit proteins involved in anti-inflammatory or cellular repair pathways, such as IL13Rα, Smad2 etc.. These actions together would enable the amelioration of the pro-inflammatory response, decreasing the number of M1 macrophages being recruited as well as polarizing the ones already recruited to M2-like phenotype(54,63). We can clearly see in **Figure 37 (a)** that the disease control and the NC-LNP treated groups have the highest iNOS positive population and hence, the highest M1 macrophage population showing the highest inflammatory potential. The antimiR-155 LNP treated and the naked antimiR-155 treated groups have iNOS levels even lower than the healthy group, meaning that the antimiR-155 delivery decreased the M1 macrophage population considerable, reducing the inflammation and the chances of prolonged liver injury. The strategy for the delivery of antimiR-155 in case of liver inflammation does work against the pro-inflammatory macrophages *in vivo*. It also points to the fact that the naked antimiR-155 is quite stable due to the 2'OMe 5'inZEN, 3'ZEN

modification, as described earlier, and might have the potential to decrease the inflammatory response by itself due to it, barring the systemic side effects it might elicit owing to the absence of a targeting system(68).

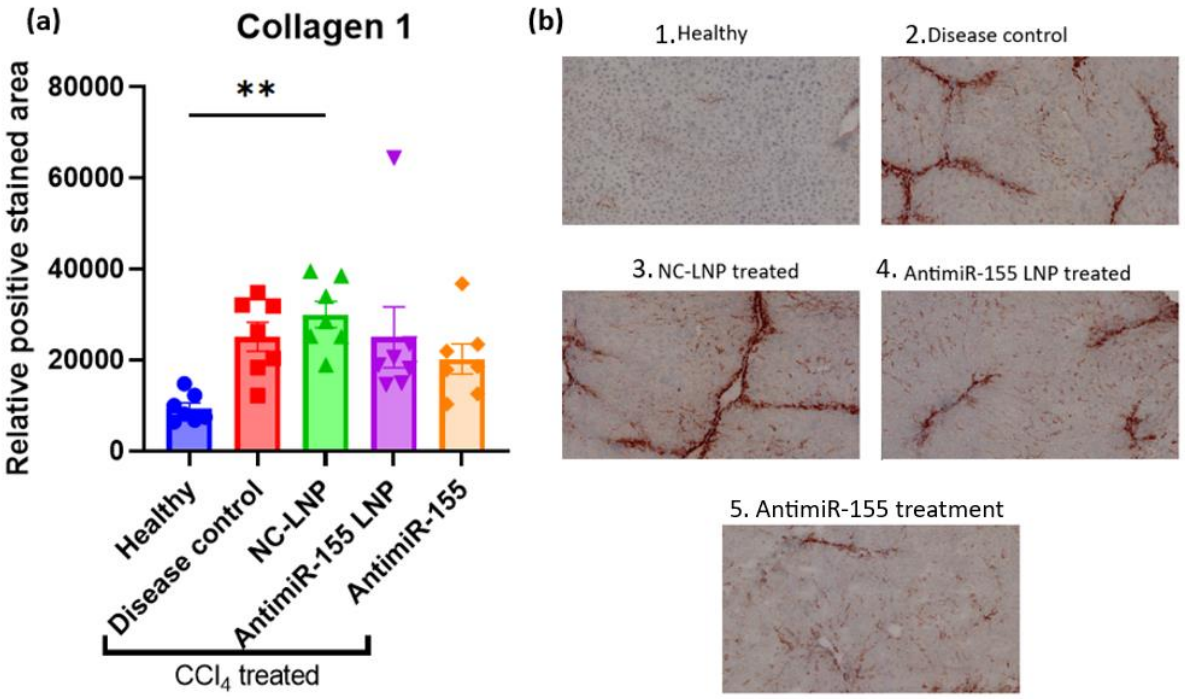

*Figure 38: (a) Collagen 1 antigen staining quantification (b) representative images of each of the treatment groups with Collagen 1 staining | Significance levels tested using one way ANOVA * p<0.05*

The collagen staining corresponds to the fibrosis in the liver(144,145). There is a discernable trend of lower collagen 1 level for antimR-155 LNP treatment and the naked antimiR-155 treatment as compared to the NC-LNP treatment in **Figure 38 (a)**. Fibrosis is a result of the wound healing response of the liver to prolonged injury. It is characterized by the imbalance in the production and the degradation of ECM, commonly regulated by the hepatic stellate cells. miRNA-155 has been shown to play a significant role in accentuating inflammation in case of chronic liver diseases. The prolonged liver injury causes immune cells to release factors that activate hepatic stellate cells, transforming them into a myofibroblast-like phenotype which release copious amounts of ECM(10,16,144). Apart from the regulatory role in inflammation and indirect involvement in hepatic stellate cell activation, Bala et al. recently showed that miRNA-155 also plays a role in directly activating the stellate cells. They showed that miRNA-155 KO mice had lower levels of TGFβ, a master profibrogenic cytokine in miRNA-155 KO mice as well as mice with miRNA-155 inhibition, as compared to the WT-CCl_4 treated mice. STAT3 protein is a part of an essential signaling pathway in fibrosis and is regulated by miRNA-155. The levels of phosphor-STAT3 were shown to be higher in disease controls as compared to miRNA-155 inhibited mice as well as miRNA-155 KO mice(118). Thus, the antimiR-155 LNP and naked antimiR-155 treated mice showed reduced levels of fibrosis as compared to the NC-LNP treated mice due to lower levels of perturbation in ECM homeostasis by miRNA-155. The naked antimiR-155 treated group shows slightly better results in lowering

the fibrosis as compared to the antimiR-155 LNPs and this could be due to the fact that it has 2'OMe 5'inZEN, 3'ZEN modification pattern, shown to have exceptional stability, and quite possibly is accumulated in the liver in a large amount owing to its filtration function(68,93). But since the naked antimiR-155 does not have a targeting ligand or selectivity for uptake, it would cause a systemic effect leading to side effects not yet accounted for, thus, the antimiR-155 LNPs would be the better choice to go for passive targeting even with lower therapeutic efficacy.

6. Conclusion

The progression of chronic liver injuries goes through a route of prolonged inflammation, induced by hepatocellular damage, followed by fibrosis, developing into cirrhosis and/hepatocellular carcinoma. Currently there aren't any therapies approved by national or international regulatory bodies showing significant benefits towards reversal of fibrosis or effective immunomodulation in case of chronic liver diseases. Certain strategies have shown promise in clinical trials but none have been able to make it to the market, necessitating the need of alternate therapeutic strategies. miRNAs have been explored as diagnostic tools due to their differential expression in diseases and now are also being studied as therapeutic targets for the same reason. They are small non-coding RNAs, 19-23 bp long which regulate the expression of mRNAs by binding to their 3'-UTR. Multiple different miRNAs have been linked to the progression of inflammation and fibrosis in chronic liver diseases and miRNA-155 takes the ball due to multiple downstream effectors like IL6, TNFα, IL13Rα, Smad2 etc. involved in the prolonging the inflammation. In this study, we developed a therapeutic strategy to tackle inflammation and fibrosis in case of liver injury exploiting miRNA-155 as a therapeutic target and decreasing its levels in the liver.

In order to deliver the antimiR-155, HiPerFect reagent was used but discarded promptly due to its toxicity in high concentrations. Lipid nanoparticles, being one of the best non-viral delivery system for nucleic acids were explored for the antimiR-155 delivery. Three different LNP formulations were engineered based on different helper lipids – DSPC, DOPC and DOPE and characterization showed considerable differences in zeta potential with DOPC LNPs being the most negative, DSPC LNPs being neutral and DOPE LNPs laying between the two. The three formulations showed no effect on metabolic activity of different cell lines representing liver cell populations – RAW264.7, AML12, 3T3 and H5V cells. An uptake of the three formulations in different cell lines representing liver populations was done in order to understand cellular preference in uptake. It revealed that the DOPC LNPs were highly efficient in being taken up by all cell types, almost by a factor of 10, as compared to the other two. DOPC LNPs showed a selectivity for hepatocytes, DOPE LNPs showed a selectivity for M1 macrophages and DSPC LNPs showed selectivity for fibroblasts, followed by hepatocytes and macrophages. An *in vivo* organ biodistribution study in an acute liver injury model revealed DSPC LNPs to have the highest accumulation in the liver as compared to DOPC and DOPE LNPs. DSPC LNPs were chosen for the delivery of antimiR-155 for an *in vivo* therapeutic efficacy study in a semi-chronic liver injury model. The bodyweight distribution did not show any significant changes over the period of the study in any of the groups. The bodyweight to liver ratio however showed a trend of reduction in the antimiR-155 LNP and naked antimiR-155 treatment groups. FACS analysis showed the NC-LNP treatment group to have the highest amount of infiltrated monocytes and the lowest amount of Kupffer cells, pointing to the highest level of inflammation. The antimiR-155 LNP and naked antimiR-155 treatment groups showed a higher level of Kupffer cells and a decreasing trend for infiltrated monocytes, showing signs of amelioration of inflammatory response, more prominent for the latter than the former.

Immunohistological staining revealed that NC-LNP treated group had the highest amount of macrophages, corroborating the results from FACS analysis. The antimiR-155 LNP and naked antimiR-155 showed a decreasing trend for macrophage population pointing to their therapeutic efficacy. iNOS levels, correlating to M1 macrophage population, were again highest in NC-LNP and the CCl_4 treated groups, with antimiR-155 LNPs and naked antimiR-155 treatments showing a decreasing trend. Collagen 1 levels, correlating to the severity of fibrosis showed highest levels in NC-LNP treated group with a decreasing trend in antimiR-155 LNP and naked antimiR-155 levels, with the latter showing lower levels. The therapeutic efficacy of the antimiR-155 treatment was prominent but the naked antimiR-155 overshadowed the antimiR-155 LNP treatment. This can be attributed to the 2'OMe 5'inZEN, 3'ZEN modification offering exceptional stability to the antimiR. Further studies are required to characterize the side effects associated with naked antimiR-155 administration. Thus, antimiR-155 delivered using DSPC LNPs presents as a promising therapy for targeting inflammation and fibrosis in context of chronic liver diseases.

7. Future perspective and recommendations

In this study, DSPC LNPs were employed to deliver antimiR-155 to liver via passive targeting in order to test their therapeutic efficacy in context of chronic liver injuries. While testing for the selective uptake of the different LNP formulations, the DSPC LNPs had the highest uptake in the 3T3 cells, representing the hepatic stellate cells. In order to characterize the effects and possible therapeutic efficacy of antimiR-155 delivery to 3T3 cells, an *in vitro* efficacy study should be conducted. The study should take into account the factors involved in the homeostasis of ECM like MMP1 and TIMP1, and measure their differential regulation in TGFβ activated 3T3 cells to characterize the dysregulation. The effects of antimiR-155-DSPC LNP treatment should be observed based on the same factors in order to see if it directly makes a significant difference or is the therapeutic efficacy of the treatment, in context of hepatic stellate cells limited to a downstream effect of immunomodulation.

During the analysis of the *in vivo* efficacy study for the antimiR-155 LNPs, the naked antimiR-155 treatment group performed better, which can be attributed to the 2'OMe 5'inZEN, 3'ZEN modification offering exceptional stability to it. Lennox et al. showed miRNA mimics with this modification to be stable while incubated in liver cell extracts for up to 4 days. In order to test for the biodistribution as well as the stability and half-life of the naked antimiR-155, an *in vivo* study needs to be conducted with fluorescently tagged antimiR-155. This can be achieved with fluorescent light-up aptamers (FLAPS). The study would be time dependent with mice sacrificed after regular intervals from the administration of a single dose of the antimiR-155. The organ as well as the cellular biodistribution would be analyzed using *in vivo* imaging and FACS as well as immunohistochemistry combined with FLAPS. This would give us information about the possible systemic effects of naked antimiR-155 administration and the circulation half-life *in vivo*.

Lastly, I would like to recommend testing different doses of the antimiR-155 LNP treatment in the semi-chronic liver injury mouse model. Right now, the antimiR-155 LNP treatment did show effects in decreasing inflammation and fibrosis but they weren't significant. Thus, a dose dependent study with concentrations going up to 5mg antimiR-155/kg bodyweight (upper limit for MC3 lipid tested without side effects) would give us insight into what the optimal dosage should be for the best possible effect for ameliorating inflammation and fibrosis in the context of chronic liver diseases. The same parameters used in the study described in this thesis could be used to analyze the effects.

8. Appendix A - Testing Mesenchymal stem cell derived extracellular vesicles for mitigating inflammation in RAW264.7 macrophages

8.1. Introduction

Extracellular vesicles are an umbrella term used to describe nanovesicles of various sizes – exosomes (30—120nm), microvesicles (MVs) (50 nm–1μm), and apoptotic bodies (500–1000 nm). They are released from many different cell populations in the body depending on the cellular stimulus(147,148). These vesicles have been known to carry cytokines, genetic material as well as other cargo to facilitate juxtracrine and paracrine signaling, and have been demonstrated to play a pivotal role in physiological and pathological processes like immune surveillance, tissue repair, tumorigenesis etc. depending on their cargo(149–151). EVs, due to their biocompatible nature and the natural ability to carry RNA, are an attractive bio-nanovesicle platform for drug and gene delivery(148).

Mesenchymal stem cells (MSCs) are multipotent adult stromal cells, capable of differentiating into multiple different lineages, found in various tissues in the body including bone marrow, adipose tissue, etc. They are known to play a role in the mitigation of immune response and restoration of damage and thus, have garnered an interest in the field of regenerative medicine based on their multipotency as well as their trans differentiation properties using different stimuli(152,153). Although MSCs play a pivotal role in tissue repair, they have a low grafting efficiency and poor survival when introduced in to the injured tissue. They also carry the potential for malignant transformation, limiting their therapeutic uses(154). However, studies have shown that the exosomes released from the mesenchymal stem cells, under specific stimuli play a larger role in the regenerative properties than their trans differentiation properties. These extracellular vesicles (EVs) have also been shown to ameliorate the inflammation caused by M1 pro-inflammatory macrophages by polarizing them to the M2 anti-inflammatory phenotype via the transactivation of ARG1 and STAT3(155). The cargo characterization of exosomes from activated MSCs have shown miRNA-34a-5p and miRNA-146a-5p (miRNAs involved in M2 polarization) to be present in them and thus, there is a potential that the MSC EVs could be exploited as carriers for antimiR-155(156). Considering their anti-inflammatory as well as regenerative potential, therapies with EVs from MSCs could be an effective strategy for immunomodulation by factors present in them and doubling down as delivery agents for antimiR-155.

8.2. Methods

8.2.1 Adipose tissue derived Mesenchymal stem cell isolation and culturing

The protocol describes is adapted from Chen et al(157). The epididymal tissue was resected and excised from healthy C57BL/6J mice. It was washed with saline and stored incubated in DMEM with 10%FBS and 1% Pen/Strep for 15 minutes. The tissue was put in a petri dish, washed with HBSS and cut into small pieces using a scalpel and scissors. The tissue pieces were put into a new vial. The tissue containing vial was centrifuged at 200g for 10 minutes

and the supernatant was discarded. 2mg/ml collagenase type 1 made in HBSS, was added to the vial to cover the tissue completely and the vial was vortexed to have maximum surface area exposed to the enzymatic digestion. The vials were incubated at 37°C for 1h with constant shaking. The cell suspension was then pushed through a 70µm cell strainer. The strained cells were suspended in PBS and centrifuged at 400g for 10 minutes at 4°C. The supernatant was removed and the cells resuspended in PBS again. The centrifugation and resuspension were repeated thrice and after the final time, the cells were resuspended in 5ml of DMEM supplemented with 10%FBS, 1%Pen/Strep and 5ng/ml FGF-2 and incubated in a T25 flask. The third to fifth passage cells were used for experiments.

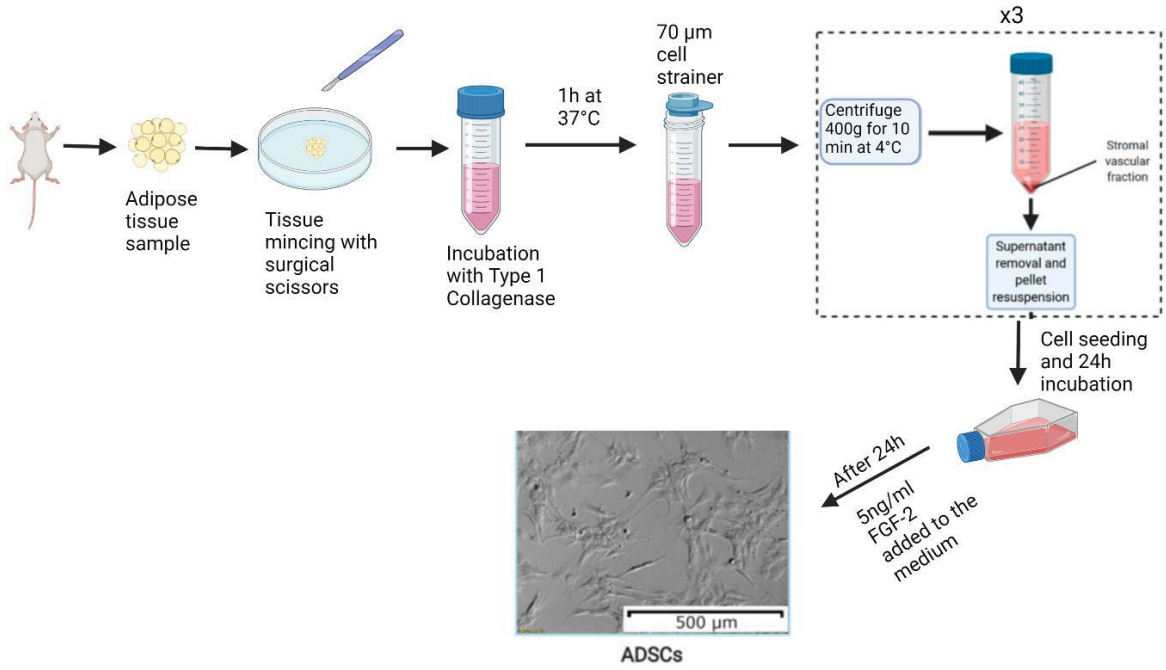

Figure 39: Schematic representation of isolation of EVs from AMSCs: The epididymal tissue is resected, cut into small pieces and homogenized. The tissue homogenate is digested using collagenase 1 for 1h at 37°C and passed through a cell strainer. The cells are washed and incubated in a culture flask with DMEM supplemented with 10% FBS + 1% P/S and 5ng/ml FGF-2

8.2.2. Isolation of EVs from AMSCs

The media was collected from culture wells seeded with 100,000 AMSCs after 24 hours of incubation at 37°C. The media was centrifuged at 300g for 10 minutes to pellet down the cell debris and the supernatant was transferred to a new falcon. The supernatant was centrifuged again at 2800g for 10 minutes for removing smaller debris particles and the supernatant was transferred to a new falcon. The supernatant was concentrated using Amicon Ultra-4, 10k tubes from Millipore at 2000g for 20 minutes. The concentrated media contained the extracellular vesicles.

8.2.3. AMSC derived EV treatment of RAW264.7 macrophages

100,000 adipose derived mesenchymal stem cells were seeded per well in 12 well plates, supplemented with DMEM (10%FBS + 1%P/S + 5ng/ml FGF2). On Day 2, the media was changed to starvation media (no FBS) and stimulants are added based on the conditions mentioned in **Table 9.** For conditions 3 and 4, transfection was conducted using Lipofectamine

reagent from ThermoFisher Scientific: Three reaction tubes were labelled as 1,2 and 3. In 1, 45µl of OptiMEM media and 2.5µl of Lipofectamine 3000 reagent was added for every well that needed to be transfected. In 2, 45µl of OptiMEM, 2µg of antimiR-155 and 4µl of P3000 reagent (2µl/µg nucleic acid to be transfected) were added. In tube 3, the contents of tubes 1 and 2 were mixed in equal proportions and incubated for 10 minutes at room temperature. 90-100µl of the contents of tube 3 were poured into each well and incubated at 37°C for at least 2 day. On Day 3, 250,000 RAW cells per well were seeded in 8, 24 well plates, supplemented with RPMI (10%FBS and 1%P/S). On Day 4, the media of the RAW cells was refreshed and stimulants were added to it based on **Table 10.** The cells were incubated for 6h at 37°C. After 48h of antimir-155 transfection into the AMSC, the EVs were collected based on the protocol mentioned earlier. After the 6h incubation of RAW cells, the media was aspirated and refreshed, while being supplemented with 55µl of concentrated EVs based on the table. The 24 well plates were incubated for 24h at 37°C. 300µl media was collected from each well for protein analysis and the cells were subjected to TRIzol based cell lysis for transcript analysis. Protein and transcript analysis samples were stored at -20°C.

Table 9: Conditions corresponding to different stimulants added to AMSC populations

Condition	Media and stimulants
1	Starvation media
2	Starvation media + 20ng/ml TNFα + 20ng/ml INFγ
3	Starvation media + AntimiR 155 transfection
4	Starvation media + 20ng/ml TNFα + 20ng/ml INFγ + AntimiR 155 transfection

Table 10: Conditions, stimulants and treatments for RAW264.7 macrophages

Condition	Stimulants added	EV treatment
M0	N/A	Control M0 – N/A
M2	10ng/ml IL-4 + 10ng/ml IL-13	Control M2 – N/A
M1	100ng/ml LPS + 20ng/ml TNFα	Control M1 – N/A
M1	100ng/ml LPS + 20ng/ml TNFα	concentrated untreated media
M1	100ng/ml LPS + 20ng/ml TNFα	concentrated media from starved AMSCs
M1	100ng/ml LPS + 20ng/ml TNFα	concentrated media from TNFα and INFγ stimulated AMSCs
M1	100ng/ml LPS + 20ng/ml TNFα	concentrated media from antimiR-155 transfected AMSCs
M1	100ng/ml LPS + 20ng/ml TNFα	concentrated media from antimiR-155 transfected and TNFα and INFγ stimulated AMSCs

8.3 Results and Discussion

8.3.1. Transcript analysis

In our study of treatment of RAW264.7 macrophages with AMSC derived EVs, we saw some interesting results for transcript analysis. Six genes were looked at in order to ascertain the immunomodulatory effect of the treatment based on literature, namely – TNFα, IL6, IL1β, MRC1, ARG1 and IL10. The former three being associated to pro inflammatory behaviors and the latter with anti-inflammatory(158–160). The quantitative profile for their expression can be seen in **Figure 40**.

TNFα and IL6 are well characterized inflammatory markers. The levels of TNFα have been shown to decrease by AMSC derived exosome treatment by Zhao et al. but in our experiment as seen in **Figure 40 (a)**, the EV treatment made no substantial difference(155). Although there was a considerable variation in the results, no discernable trend suggested the treatments working in direction of reducing TNFα levels. It could be due to low concentration of the EVs or the carry-over of proinflammatory cytokines from the AMSC treatment media. The EVs were concentrated and filtered but the cytokines can't be completely removed from it.

IL6 on the other hand did show a decrease in the M1 macrophages treated with stimulated AMSC derived EVs, both, with and without antimiR-155 transfection as observed in **Figure 40 (b)**. The EVs derived from stimulated AMSCs without transfection showed the best results, with the lowest IL6 levels than any of the other M1 populations(156,160,161). Thus, speaking in strictly decreasing pro-inflammatory characteristics, the EVs derived from stimulated AMSCs worked better than the ones from stimulated, antimiR-155 transfected AMSCs.

IL1β is another essential marker used for pro-inflammatory behavior characterization(159). Referring to **Figure 40 (c),** the EV treatments did show a trend of decrease in the IL1β levels, except the population treated with stimulated and transfected AMSC derived EVs, where the level went beyond the untreated M1 population(156). This could be due to change in cargo of the EVs. There has been research suggesting that different stimuli cause the cargo of the EVs to change, which changes how they affect the other cell populations(162).

Apart from the pro-inflammatory markers, the anti-inflammatory makers were taken into account as well. MRC1 or mannose receptor C type 1, ARG1 or arginase 1 and IL10, all three of them show similar trends in their graphs as observed in **Figure 40 (d), (e)** and **(f)**(155,161). The M1 population treated with stimulated and transfected AMSC derived EVs shows the highest levels of these transcripts, even higher than those found in the M2 macrophage population(151,163). This suggests a progressive change in the behavior of the M1 macrophage population. These levels are significantly higher than almost all the other M1 macrophage treatment conditions, pointing to the initiation of an anti-inflammatory microenvironment being propagated.

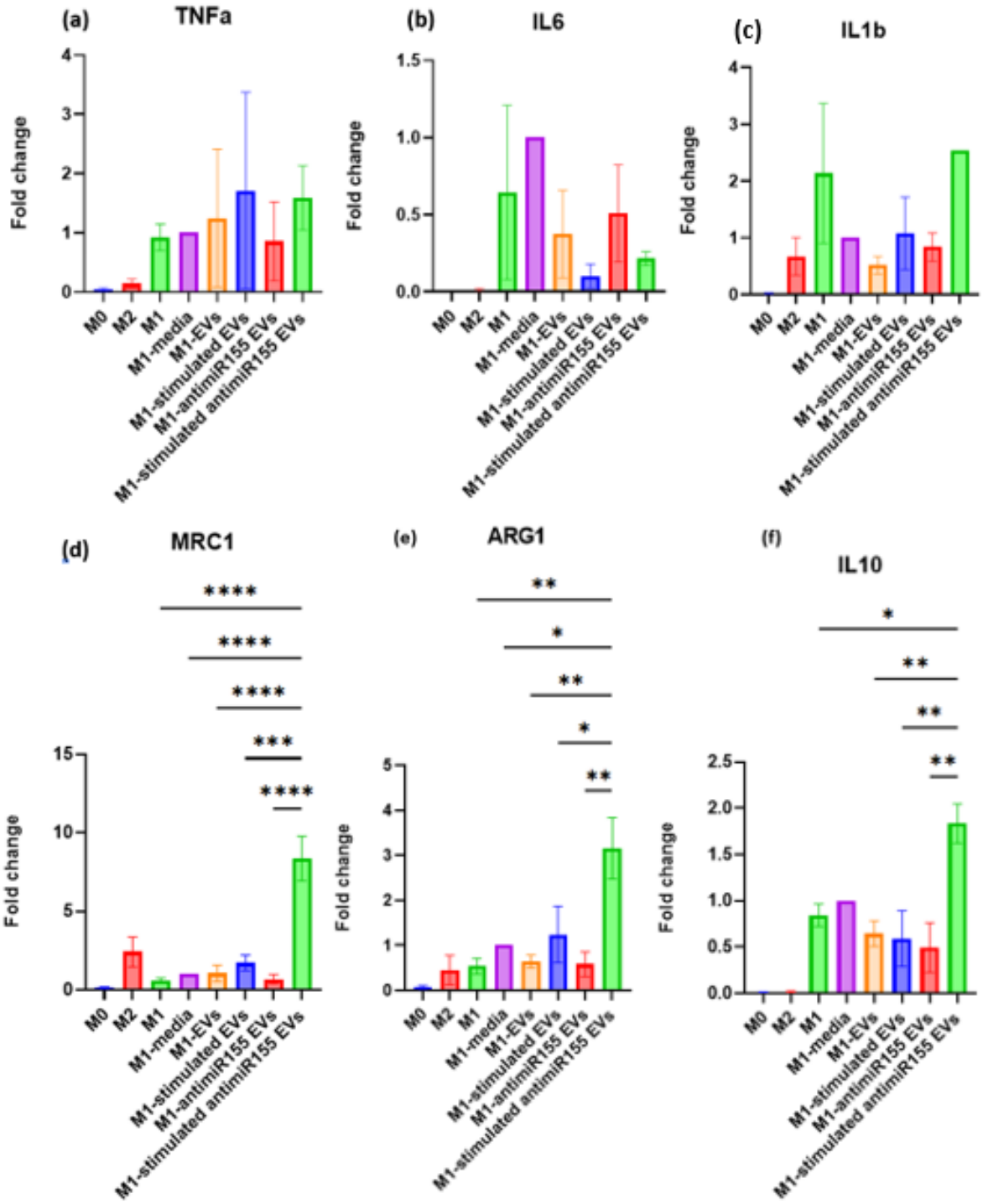

*Figure 40: Transcript levels for proinflammatory and anti-inflammatory genes in M0, M1 and M2 polarized RAW264.7 macrophages treated with AMSC derived EVs (a) TNFα levels (b) IL6 levels (c) IL1β levels (d) MRC1 levels (e) ARG1 levels (f) IL10 levels; M0-unstimulated RAW264.7 macrophages, M2-anti-inflammatory macrophages stimulated with 10ng/ml IL-4 + 10ng/ml IL-13, M1-proinflammatory RAW264.7 macrophages stimulated with100ng/ml LPS + 20ng/ml TNFα, M1-media – M1 macrophages treated with concentrated media, M1-EVs – M1 macrophages treated with EVs from unstimulated AMSCs, M1-stimulated EVs – M1 macrophages treated with TNFα and INFγ stimulated AMSC derived EVs, M1-antimiR155 EVs – M1 macrophages treated with antimiR-155 transfected AMSC derived EVs, M1-stimulated antimiR155 EVs – M1 macrophages treated with antimiR-155 transfected and TNFα+INFγ stimulated AMSC derived EVs | Significance levels tested using one way ANOVA * p<0.05*

8.3.2. Protein level analysis

Transcription and translation products do not have a linear relationship and in order to look at the protein levels of TNFα, IL6 and IL10, ELISA was performed, the results for which can be seen in **Figure 41**.

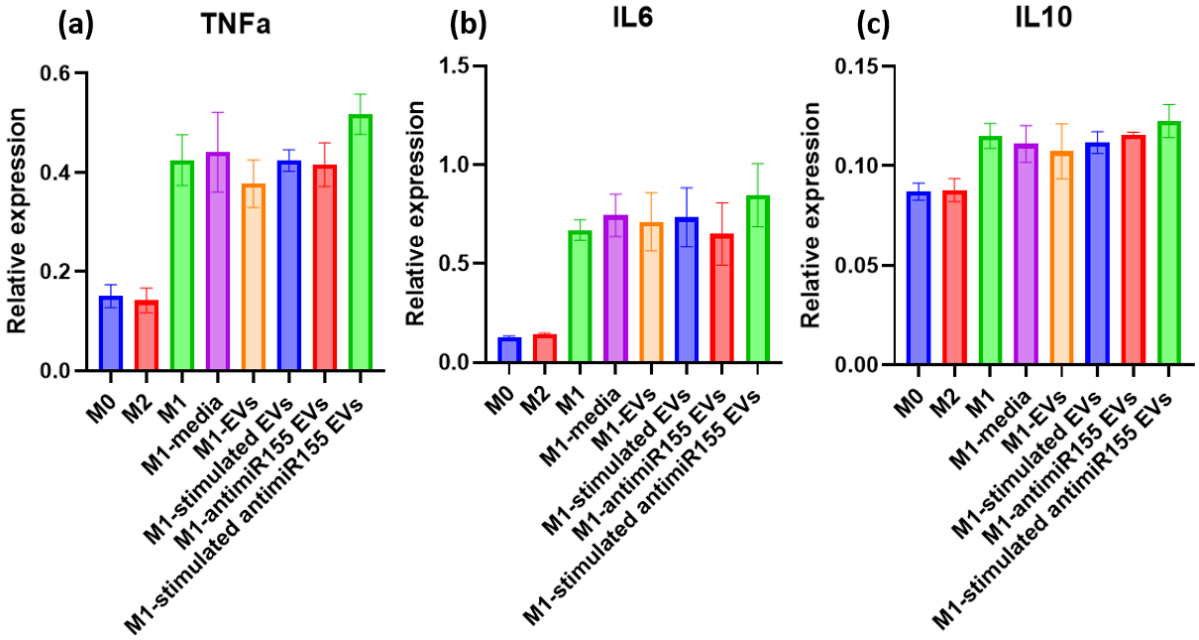

*Figure 41: Protein expression levels of TNFα, IL6 and IL10 measured using ELISA (a) TNFα levels (b) IL6 levels (c) IL10 levels; ; M0-unstimulated RAW264.7 macrophages, M2-anti-inflammatory macrophages stimulated with 10ng/ml IL-4 + 10ng/ml IL-13, M1-proinflammatory RAW264.7 macrophages stimulated with100ng/ml LPS + 20ng/ml TNFα, M1-media – M1 macrophages treated with concentrated media, M1-EVs – M1 macrophages treated with EVs from unstimulated AMSCs, M1-stimulated EVs – M1 macrophages treated with TNFα and INFγ stimulated AMSC derived EVs, M1-antimiR155 EVs – M1 macrophages treated with antimiR-155 transfected AMSC derived EVs, M1-stimulated antimiR155 EVs – M1 macrophages treated with antimiR-155 transfected and TNFα+INFγ stimulated AMSC derived EVs | Significance levels tested using one way ANOVA * p<0.05*

TNFα and IL6, both showed no difference in the different M1 populations, but were certainly higher than that of M0 and M2 phenotype. This could be due to the M1 macrophages responding to the EVs as foreign bodies and increasing their translation of the proinflammatory proteins, even though the IL6 transcript levels were low. For IL10, there were barely any differences in the levels for any of the populations. There was no significant difference observed over the span of the three ELISA assays conducted for the proteins. This could be due to the time of treatment not being enough. If the treatment was prolonged, the effects might be more pronounced at the translational level as in the transcript levels(164). Another possible explanation could be the interference due to EVs other than the exosomes. In order to characterize that, exosome isolation should be conducted and the experiment should be repeated with the treatment with them. The AMSCs were assumed to be a pure population but there is a chance that they weren't and the secondary population could contribute to the EV population, negating the therapeutic effect of the AMSC EVs. The AMSCs

should be stained with MSC markers like CD90 and CD105, sorted through FACS for a pure population and used for the production of EVs(165).

8.4. Conclusion

EVs were isolated from different AMSC population transfected with antimiR-155 and/or stimulated with pro-inflammatory cytokines (TNFα and INFγ) in order to assess the therapeutic efficacy of their treatment in RAW264.7 cells in context of inflammation. At the transcript level, TNFα did not show any effect of the treatment in any of the RAW264,7 populations. IL6 transcript levels were lowered in groups treated with EVs derived from AMSCs which were stimulated with TNFα and INFγ as compared to the transfected AMSC EV treatment, pointing to a better efficacy. IL1β transcript levels showed a decrease in all EV treatments except the ones derived from AMSCs stimulated with TNFα and INFγ as well as transfected with antimiR-155, possibly due to a drastic change in cargo with two major stimuli. The anti-inflammatory markers, MRC1, ARG1 and IL10 showed a similar trend of the highest levels to be found in the group treated with EVs derived from AMSCs stimulated with TNFα and INFγ as well as transfected with antimiR-155. These levels are significantly higher than almost all the other M1 macrophage treatment conditions, pointing to the initiation of an anti-inflammatory microenvironment being propagated. Unfortunately, the same results were not replicated at the protein level, where no differences were observed for TNFα, IL6 and IL10 levels in any of the M1 macrophage populations. Thus, the antimiR-155 transfection of AMSCs did play a role in the propagation of an anti-inflammatory microenvironment but the results are not conclusive and more experiments would be needed to make any concrete statements about the treatment strategy.

9. Appendix B – Protocol for RNA isolation from cells using TRIzol reagent

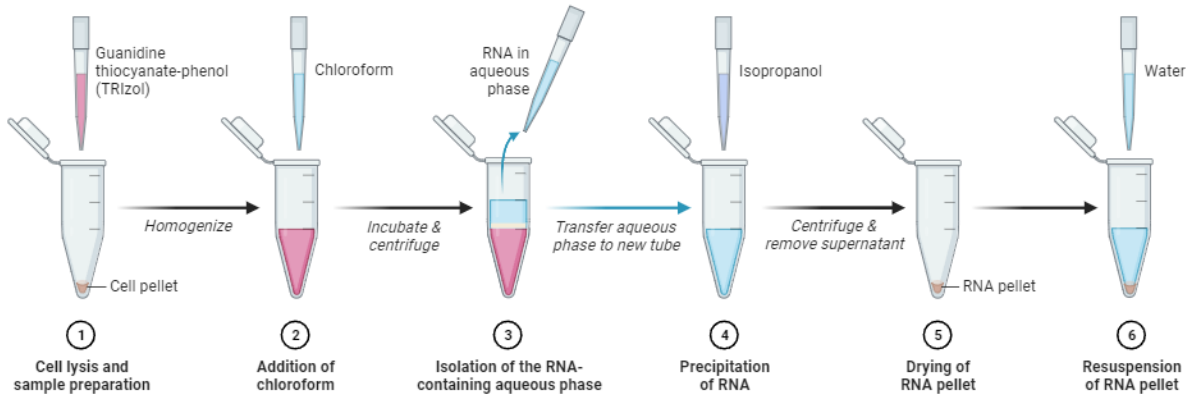

Figure 42: Schematic representation of RNA isolation using TRIzol reagent: Cells are suspended in TRIzol for homogenization and rupturing, followed by the addition of chloroform to form a second phase. The aqueous phase with RNA is transferred to a new tube. The tube is centrifuged and supernatant is discarded. The pellet is air dried and resuspended in RNase free water(71,166)

Figure 19: Schematic for RNA isolation using TRIzol reagent

1. The media is removed from the wells and TRIzol™ reagent is added. 300µl TRIzol™ reagent is used for 250,000 cells.
2. The lysate is pipetted up and down several times to homogenize and transferred to Eppendorfs.
3. Incubated for 5 minutes to allow complete dissociation of the nucleoproteins complex followed by addition of 60µl chloroform.
4. Incubated for 2–3 minutes and centrifuged the sample for 15 minutes at 12,000 × g at 4°C
5. Transferred the aqueous phase containing the RNA to a new tube by angling the tube at 45° and pipetted the solution out.
6. Added 150µl isopropanol on top of isolated RNA and Incubated for 10 minutes at 4°C
7. Centrifuged for 10 minutes at 12,000g at 4°C.
8. The supernatant is discarded with a micropipette
9. The pellet is resuspended in 300µl of 75% ethanol
10. The sample briefly vortexed, then centrifuged for 5 minutes at 7500 × g at 4°C.
11. The supernatant is discarded with a micropipettor.
12. The RNA is air dried for 10 minutes
13. The pellet is resuspended in 50 µL of RNase-free water.
14. Incubated in a water bath or heat block set at 55–60°C for 10–15 minutes and stored at -80°C

10. Appendix C – Protocol for cDNA synthesis and qPCR

cDNA synthesis protocol

1. The RNA concentration is quantified using the Nanodrop
2. 1000ng of RNA is used as the template for each sample and calculations are made to suspend 1000ng in 15ul. The volume is made up by the addition of RNase free water
3. The reverse transcription mix is prepared containing 4µl of reverse transcriptase reaction mix and 1µl of iScript reverse transcriptase enzyme for each sample
4. The mix is added to separate PCR tubes along with the RNA, with a total volume of 20µl
5. cDNA synthesis is run on preset conditions
6. The cDNA is stored at -20°C

qPCR protocol

1. The cDNA is diluted to a concentration of 10ng/µl
2. A master mix is made for each sample based on the **Table 11**

Table 11: Components of the master mix for qPCR

Sample	**1X**
H2O	1.9ul
Primers (Fr,Re)	0.05ul (each)
SYBR Green	4ul

3. The master mix is added to the 384 well PCR plate depending on the plate design
4. 2µl of cDNA is added to each of the wells from the respective PCR tubes to make the total volume of the wells to be 6µl
5. The plate is covered with a plastic adhesive sheet and spun to mix all the components
6. The qPCR is initiated based on preset conditions using the thermocycler
7. The data is visualized and quantified by the Bio-Rad program

11. Appendix D – Protocol for ELISA

1. 96 well Maxisorp plate is coated with 100µl of capture antibody/well overnight at room temperature
2. The next day, the wells are washed thrice with 200µl of 0.05% Tween in PBS
3. 200µl of 1% BSA in PBS is added for blocking and incubated for 1h at room temperature
4. The samples for testing are diluted using a solution of 1% BSA in PBS
5. The standard solutions for the calibration curve are made based by serially diluting the standard protein 8x, obtained along with the kit
6. The wells are washed thrice with 200µl of 0.05% Tween in PBS and the samples along with standards are added in a total volume of 100µl/well and incubated for 2h at room temperature
7. After the incubation, the wells are washed thrice with 200µl of 0.05% Tween in PBS
8. The detection antibody is diluted in 1% BSA in PBS and 100µl of it is put in the wells and incubated for 2h
9. The wells are washed thrice with 200µl of 0.05% Tween in PBS after the incubation
10. Working solution of streptavidin-HRP is made by diluting it with 1% BSA in PBS and 100µl of it is added to the wells for 20 minutes
11. The wells are washed thrice with 200µl of 0.05% Tween in PBS and 100Âµl of TMB substrate is added to each of them and incubated in the dark at room temperature for 20 minutes
12. The reaction is stop by adding 50µl of 10% 1.8M H_2SO_4 to the wells
13. The plate is visualized by a plate reader at 450nm and the calculations are performed based on the standard curve as well as the dilution of the sample

12. References

1. Rogers AB, Dintzis RZ. 13 - Hepatobiliary System. In: Treuting PM, Dintzis SM, Montine KS, editors. Comparative Anatomy and Histology (Second Edition) [Internet]. San Diego: Academic Press; 2018 [cited 2023 Aug 19]. p. 229–39. Available from: https://www.sciencedirect.com/science/article/pii/B9780128029008000130

2. Ishibashi H, Nakamura M, Komori A, Migita K, Shimoda S. Liver architecture, cell function, and disease. Semin Immunopathol. 2009 Sep 1;31(3):399–409.

3. Michalopoulos GK, Bhushan B. Liver regeneration: biological and pathological mechanisms and implications. Nat Rev Gastroenterol Hepatol. 2021 Jan;18(1):40–55.

4. What Is Liver Cancer? | Liver Cancer Types [Internet]. [cited 2023 Aug 17]. Available from: https://www.cancer.org/cancer/types/liver-cancer/about/what-is-liver-cancer.html

5. Ricken T, Werner D, Holzhütter HG, König M, Dahmen U, Dirsch O. Modeling function–perfusion behavior in liver lobules including tissue, blood, glucose, lactate and glycogen by use of a coupled two-scale PDE–ODE approach. Biomech Model Mechanobiol. 2015 Jun 1;14(3):515–36.

6. Racanelli V, Rehermann B. The Liver as an Immunological Organ. Hepatology. 2006 Feb;43:S54.

7. Meylan E, Tschopp J, Karin M. Intracellular pattern recognition receptors in the host response. Nature. 2006 Jul;442(7098):39–44.

8. Crispe IN. Liver antigen-presenting cells. J Hepatol. 2011 Feb 1;54(2):357–65.

9. Shahani T, Covens K, Lavend'homme R, Jazouli N, Sokal E, Peerlinck K, et al. Human liver sinusoidal endothelial cells but not hepatocytes contain factor VIII. J Thromb Haemost JTH. 2014 Jan;12(1):36–42.

10. Roderfeld M. Matrix metalloproteinase functions in hepatic injury and fibrosis. Matrix Biol J Int Soc Matrix Biol. 2018 Aug;68–69:452–62.

11. Omar R, Yang J, Liu H, Davies NM, Gong Y. Hepatic Stellate Cells in Liver Fibrosis and siRNA-Based Therapy. Rev Physiol Biochem Pharmacol. 2016;172:1–37.

12. Arriola Benitez PC, Pesce Viglietti AI, Elizalde MM, Giambartolomei GH, Quarleri JF, Delpino MV. Hepatic Stellate Cells and Hepatocytes as Liver Antigen-Presenting Cells during B. abortus Infection. Pathog Basel Switz. 2020 Jun 30;9(7):527.

13. Wilde B, Katsounas A. Immune Dysfunction and Albumin-Related Immunity in Liver Cirrhosis. Mediators Inflamm. 2019 Feb 25;2019:e7537649.

14. Friedman SL. Liver fibrosis – from bench to bedside. J Hepatol. 2003 Jan 1;38:38–53.

15. Martínez AK, Maroni L, Marzioni M, Ahmed ST, Milad M, Ray D, et al. Mouse Models of Liver Fibrosis Mimic Human Liver Fibrosis of Different Etiologies. Curr Pathobiol Rep. 2014 Dec 1;2(4):143–53.

16. Bataller R, Brenner DA. Liver fibrosis. J Clin Invest. 2005 Feb 1;115(2):209–18.

17. Puche JE, Saiman Y, Friedman SL. Hepatic stellate cells and liver fibrosis. Compr Physiol. 2013 Oct;3(4):1473–92.

18. Ying HZ, Chen Q, Zhang WY, Zhang HH, Ma Y, Zhang SZ, et al. PDGF signaling pathway in hepatic fibrosis pathogenesis and therapeutics. Mol Med Rep. 2017 Dec;16(6):7879–89.

19. Zeng T, Zhang CL, Xiao M, Yang R, Xie KQ. Critical Roles of Kupffer Cells in the Pathogenesis of Alcoholic Liver Disease: From Basic Science to Clinical Trials. Front Immunol [Internet]. 2016 [cited 2023 Aug 19];7. Available from: https://www.frontiersin.org/articles/10.3389/fimmu.2016.00538

20. Maher JJ, Zia S, Tzagarakis C. Acetalde hyde-Induced Stimulation of Collagen Synthesis and Gene Expression Is Dependent on Conditions of Cell Culture: Studies with Rat Lipocytes and Fibroblasts. Alcohol Clin Exp Res. 1994;18(2):403–9.

21. Bataller R, Paik YH, Lindquist JN, Lemasters JJ, Brenner DA. Hepatitis C virus core and nonstructural proteins induce fibrogenic effects in hepatic stellate cells. Gastroenterology. 2004 Feb;126(2):529–40.

22. McCaughan GW, George J. Fibrosis progression in chronic hepatitis C virus infection. Gut. 2004 Mar;53(3):318–21.

23. Ramadori G, Saile B. Portal tract fibrogenesis in the liver. Lab Investig J Tech Methods Pathol. 2004 Feb;84(2):153–9.

24. Wu H, Chen C, Ziani S, Nelson LJ, Ávila MA, Nevzorova YA, et al. Fibrotic Events in the Progression of Cholestatic Liver Disease. Cells. 2021 May 5;10(5):1107.

25. Schwabe RF, Tabas I, Pajvani UB. Mechanisms of Fibrosis Development in NASH. Gastroenterology. 2020 May;158(7):1913–28.

26. Takaki A, Kawai D, Yamamoto K. Multiple Hits, Including Oxidative Stress, as Pathogenesis and Treatment Target in Non-Alcoholic Steatohepatitis (NASH). Int J Mol Sci. 2013 Oct 15;14(10):20704–28.

27. Li J, Tuo B. Current and Emerging Approaches for Hepatic Fibrosis Treatment. Gastroenterol Res Pract. 2021 Jul 17;2021:6612892.

28. Hadi HE, Vettor R, Rossato M. Vitamin E as a Treatment for Nonalcoholic Fatty Liver Disease: Reality or Myth? Antioxidants. 2018 Jan 16;7(1):12.

29. Sumida Y, Naito Y, Tanaka S, Sakai K, Inada Y, Taketani H, et al. Long-term (>=2 yr) efficacy of vitamin E for non-alcoholic steatohepatitis. Hepatogastroenterology. 2013 Sep;60(126):1445–50.

30. Lippman SM, Klein EA, Goodman PJ, Lucia MS, Thompson IM, Ford LG, et al. Effect of selenium and vitamin E on risk of prostate cancer and other cancers: the Selenium and Vitamin E Cancer Prevention Trial (SELECT). JAMA. 2009 Jan 7;301(1):39–51.

31. Schürks M, Glynn RJ, Rist PM, Tzourio C, Kurth T. Effects of vitamin E on stroke subtypes: meta-analysis of randomised controlled trials. BMJ. 2010 Nov 5;341:c5702.

32. Meta-Analysis: High-Dosage Vitamin E Supplementation May Increase All-Cause Mortality | Annals of Internal Medicine [Internet]. [cited 2023 Aug 19]. Available from: https://www.acpjournals.org/doi/10.7326/0003-4819-142-1-200501040-00110

33. Loomba R, Lawitz E, Mantry PS, Jayakumar S, Caldwell SH, Arnold H, et al. The ASK1 inhibitor selonsertib in patients with nonalcoholic steatohepatitis: A randomized, phase 2 trial. Hepatol Baltim Md. 2018 Feb;67(2):549–59.

34. Shah ND, Bataller R. Cell-based therapy to reverse advanced alcoholic liver fibrosis. Ann Hepatol. 2016 Sep 1;15(5):806–8.

35. Zhao Z, Lin CY, Cheng K. siRNA- and miRNA-Based Therapeutics for Liver Fibrosis. Transl Res J Lab Clin Med. 2019 Dec;214:17–29.

36. Zeng XY, Zhang YQ, He XM, Wan LY, Wang H, Ni YR, et al. Suppression of hepatic stellate cell activation through downregulation of gremlin1 expression by the miR-23b/27b cluster. Oncotarget. 2016 Dec 27;7(52):86198–210.

37. Matsumoto Y, Itami S, Kuroda M, Yoshizato K, Kawada N, Murakami Y. MiR-29a Assists in Preventing the Activation of Human Stellate Cells and Promotes Recovery From Liver Fibrosis in Mice. Mol Ther J Am Soc Gene Ther. 2016 Oct;24(10):1848–59.

38. Xiao Y, Wang J, Chen Y, Zhou K, Wen J, Wang Y, et al. Up-regulation of miR-200b in biliary atresia patients accelerates proliferation and migration of hepatic stallate cells by activating PI3K/Akt signaling. Cell Signal. 2014 May;26(5):925–32.

39. Han J, Lee Y, Yeom KH, Kim YK, Jin H, Kim VN. The Drosha-DGCR8 complex in primary microRNA processing. Genes Dev. 2004 Dec 15;18(24):3016–27.

40. Okada C, Yamashita E, Lee SJ, Shibata S, Katahira J, Nakagawa A, et al. A High-Resolution Structure of the Pre-microRNA Nuclear Export Machinery. Science. 2009 Nov 27;326(5957):1275–9.

41. Yoda M, Kawamata T, Paroo Z, Ye X, Iwasaki S, Liu Q, et al. ATP-dependent human RISC assembly pathways. Nat Struct Mol Biol. 2010 Jan;17(1):17–23.

42. Winter J, Jung S, Keller S, Gregory RI, Diederichs S. Many roads to maturity: microRNA biogenesis pathways and their regulation. Nat Cell Biol. 2009 Mar;11(3):228–34.

43. Roy S, Benz F, Luedde T, Roderburg C. The role of miRNAs in the regulation of inflammatory processes during hepatofibrogenesis. Hepatobiliary Surg Nutr. 2015 Feb;4(1):24–33.

44. Benz F, Roderburg C, Vargas Cardenas D, Vucur M, Gautheron J, Koch A, et al. U6 is unsuitable for normalization of serum miRNA levels in patients with sepsis or liver fibrosis. Exp Mol Med. 2013 Sep;45(9):e42.

45. Kosaka N, Iguchi H, Yoshioka Y, Takeshita F, Matsuki Y, Ochiya T. Secretory Mechanisms and Intercellular Transfer of MicroRNAs in Living Cells♦. J Biol Chem. 2010 Jun 4;285(23):17442–52.

46. Roberts TC, Coenen-Stass AML, Betts CA, Wood MJA. Detection and quantification of extracellular microRNAs in murine biofluids. Biol Proced Online. 2014 Mar 14;16:5.

47. Sendi H, Mead I, Wan M, Mehrab-Mohseni M, Koch K, Atala A, et al. miR-122 inhibition in a human liver organoid model leads to liver inflammation, necrosis, steatofibrosis and dysregulated insulin signaling. PloS One. 2018;13(7):e0200847.

48. Zou Y, Cai Y, Lu D, Zhou Y, Yao Q, Zhang S. MicroRNA-146a-5p attenuates liver fibrosis by suppressing profibrogenic effects of TGFβ1 and lipopolysaccharide. Cell Signal. 2017 Nov 1;39:1–8.

49. Hu Y, Peng X, Du G, Zhang Z, Zhai Y, Xiong X, et al. MicroRNA-122-5p Inhibition Improves Inflammation and Oxidative Stress Damage in Dietary-Induced Non-alcoholic Fatty Liver Disease Through Targeting FOXO3. Front Physiol. 2022 Feb 11;13:803445.

50. Momen-Heravi F, Catalano D, Talis A, Szabo G, Bala S. Protective effect of LNA-anti-miR-132 therapy on liver fibrosis in mice. Mol Ther Nucleic Acids. 2021 Sep 3;25:155–67.

51. Blaya D, Aguilar-Bravo B, Hao F, Casacuberta-Serra S, Coll M, Perea L, et al. Expression of microRNA-155 in inflammatory cells modulates liver injury. Hepatol Baltim Md. 2018 Aug;68(2):691–706.

52. Mahesh G, Biswas R. MicroRNA-155: A Master Regulator of Inflammation. J Interferon Cytokine Res Off J Int Soc Interferon Cytokine Res. 2019 Jun;39(6):321–30.

53. Hu J, Huang S, Liu X, Zhang Y, Wei S, Hu X. miR-155: An Important Role in Inflammation Response. J Immunol Res. 2022 Apr 6;2022:7437281.

54. Alivernini S, Gremese E, McSharry C, Tolusso B, Ferraccioli G, McInnes IB, et al. MicroRNA-155—at the Critical Interface of Innate and Adaptive Immunity in Arthritis. Front Immunol [Internet]. 2018 [cited 2023 Aug 17];8. Available from: https://www.frontiersin.org/articles/10.3389/fimmu.2017.01932

55. Wang B, Majumder S, Nuovo G, Kutay H, Volinia S, Patel T, et al. Role of microRNA-155 at early stages of hepatocarcinogenesis induced by choline-deficient and amino acid–defined diet in C57BL/6 mice. Hepatology. 2009;50(4):1152–61.

56. Tang B, Lei B, Qi G, Liang X, Tang F, Yuan S, et al. MicroRNA-155-3p promotes hepatocellular carcinoma formation by suppressing FBXW7 expression. J Exp Clin Cancer Res. 2016 Jun 16;35(1):93.

57. Mohamed AA, Omar AAA, EL-Awady RR, Hassan SMA, Eitah WMS, Ahmed R, et al. MiR-155 and MiR-665 Role as Potential Non-invasive Biomarkers for Hepatocellular Carcinoma in Egyptian Patients with Chronic Hepatitis C Virus Infection. J Transl Intern Med. 2020 May 9;8(1):32–40.

58. Zhang L, Wang W, Li X, He S, Yao J, Wang X, et al. MicroRNA-155 promotes tumor growth of human hepatocellular carcinoma by targeting ARID2. Int J Oncol. 2016 Jun 1;48(6):2425–34.

59. Zhang Y, Wei W, Cheng N, Wang K, Li B, Jiang X, et al. Hepatitis C virus-induced up-regulation of microRNA-155 promotes hepatocarcinogenesis by activating Wnt signaling. Hepatology. 2012;56(5):1631–40.

60. Lin X, Chen L, Li H, Liu Y, Guan Y, Li X, et al. miR-155 accelerates proliferation of mouse hepatocytes during liver regeneration by directly targeting SOCS1. Am J Physiol-Gastrointest Liver Physiol. 2018 Oct;315(4):G443–53.

61. Csak T, Bala S, Lippai D, Kodys K, Catalano D, Iracheta-Vellve A, et al. MicroRNA-155 Deficiency Attenuates Liver Steatosis and Fibrosis without Reducing Inflammation in a Mouse Model of Steatohepatitis. PLOS ONE. 2015 Jun 4;10(6):e0129251.

62. Bala S, Marcos M, Kodys K, Csak T, Catalano D, Mandrekar P, et al. Up-regulation of MicroRNA-155 in Macrophages Contributes to Increased Tumor Necrosis Factor α (TNFα) Production via Increased mRNA Half-life in Alcoholic Liver Disease. J Biol Chem. 2011 Jan 14;286(2):1436–44.

63. Türkal M. Attenuating Inflammation by Modulation Microrna-155 Expression in Macrophages using Lipid Nanoparticles and Extracellular Vesicles [Internet]. University of Twente; 2022 [cited 2023 Aug 19]. Available from: http://essay.utwente.nl/92912/

64. Aleshcheva G, Pietsch H, Escher F, Schultheiss H. MicroRNA profiling as a novel diagnostic tool for identification of patients with inflammatory and/or virally induced cardiomyopathies. ESC Heart Fail. 2020 Nov 20;8(1):408–22.

65. Duroux-Richard I, Gagez AL, Alaterre E, Letestu R, Khalifa O, Jorgensen C, et al. miRNA profile at diagnosis predicts treatment outcome in patients with B-chronic lymphocytic leukemia: A FILO study. Front Immunol. 2022;13:983771.

66. Bajan S, Hutvagner G. RNA-Based Therapeutics: From Antisense Oligonucleotides to miRNAs. Cells. 2020 Jan;9(1):137.

67. Lee SWL, Paoletti C, Campisi M, Osaki T, Adriani G, Kamm RD, et al. MicroRNA delivery through nanoparticles. J Controlled Release. 2019 Nov 10;313:80–95.

68. Lennox KA, Owczarzy R, Thomas DM, Walder JA, Behlke MA. Improved Performance of Anti-miRNA Oligonucleotides Using a Novel Non-Nucleotide Modifier. Mol Ther Nucleic Acids. 2013 Aug;2(8):e117.

69. Lipid Nanoparticles–From Liposomes to mRNA Vaccine Delivery, a Landscape of Research Diversity and Advancement [Internet]. [cited 2023 Aug 19]. Available from: https://pubs.acs.org/doi/epdf/10.1021/acsnano.1c04996

70. Urits I, Swanson D, Swett MC, Patel A, Berardino K, Amgalan A, et al. A Review of Patisiran (ONPATTRO®) for the Treatment of Polyneuropathy in People with Hereditary Transthyretin Amyloidosis. Neurol Ther. 2020 Aug 12;9(2):301–15.

71. Scientific Image and Illustration Software | BioRender [Internet]. [cited 2023 Aug 17]. Available from: https://www.biorender.com/

72. Bezerra F, Saraiva MJ, Almeida MR. Modulation of the Mechanisms Driving Transthyretin Amyloidosis. Front Mol Neurosci. 2020 Dec 11;13:592644.

73. Xu L, Wang X, Liu Y, Yang G, Falconer RJ, Zhao CX. Lipid Nanoparticles for Drug Delivery. Adv NanoBiomed Res. 2022;2(2):2100109.

74. Li J, Wang X, Zhang T, Wang C, Huang Z, Luo X, et al. A review on phospholipids and their main applications in drug delivery systems. Asian J Pharm Sci. 2015 Apr 1;10(2):81–98.

75. Åslund AKO, Vandebriel RJ, Caputo F, de Jong WH, Delmaar C, Hyldbakk A, et al. A comparative biodistribution study of polymeric and lipid-based nanoparticles. Drug Deliv Transl Res. 2022 Sep 1;12(9):2114–31.

76. Hassett KJ, Higgins J, Woods A, Levy B, Xia Y, Hsiao CJ, et al. Impact of lipid nanoparticle size on mRNA vaccine immunogenicity. J Controlled Release. 2021 Jul 10;335:237–46.

77. Di J, Du Z, Wu K, Jin S, Wang X, Li T, et al. Biodistribution and Non-linear Gene Expression of mRNA LNPs Affected by Delivery Route and Particle Size. Pharm Res. 2022;39(1):105–14.

78. Van Haute D, Berlin JM. Challenges in realizing selectivity for nanoparticle biodistribution and clearance: lessons from gold nanoparticles. Ther Deliv. 2017 Sep;8(9):763–74.

79. Ngo W, Ahmed S, Blackadar C, Bussin B, Ji Q, Mladjenovic SM, et al. Why nanoparticles prefer liver macrophage cell uptake in vivo. Adv Drug Deliv Rev. 2022 Jun 1;185:114238.

80. Paunovska K, Gil CJ, Lokugamage MP, Sago CD, Sato M, Lando GN, et al. Analyzing 2000 in Vivo Drug Delivery Data Points Reveals Cholesterol Structure Impacts Nanoparticle Delivery. ACS Nano. 2018 Aug 28;12(8):8341–9.

81. Paunovska K, Da Silva Sanchez AJ, Sago CD, Gan Z, Lokugamage MP, Islam FZ, et al. Nanoparticles Containing Oxidized Cholesterol Deliver mRNA to the Liver Microenvironment at Clinically Relevant Doses. Adv Mater Deerfield Beach Fla. 2019 Apr;31(14):e1807748.

82. Tavares AJ, Poon W, Zhang YN, Dai Q, Besla R, Ding D, et al. Effect of removing Kupffer cells on nanoparticle tumor delivery. Proc Natl Acad Sci U S A. 2017 Dec 19;114(51):E10871–80.

83. Alavi M, Hamidi M. Passive and active targeting in cancer therapy by liposomes and lipid nanoparticles. Drug Metab Pers Ther [Internet]. 2019 Mar 1 [cited 2023 Aug 19];34(1). Available from: https://www.degruyter.com/document/doi/10.1515/dmpt-2018-0032/html?lang=en

84. LoPresti ST, Arral ML, Chaudhary N, Whitehead KA. The replacement of helper lipids with charged alternatives in lipid nanoparticles facilitates targeted mRNA delivery to the spleen and lungs. J Controlled Release. 2022 May 1;345:819–31.

85. Kulkarni JA, Myhre JL, Chen S, Tam YYC, Danescu A, Richman JM, et al. Design of lipid nanoparticles for in vitro and in vivo delivery of plasmid DNA. Nanomedicine Nanotechnol Biol Med. 2017 May;13(4):1377–87.

86. Zhang R, El-Mayta R, Murdoch TJ, Warzecha CC, Billingsley MM, Shepherd SJ, et al. Helper lipid structure influences protein adsorption and delivery of lipid nanoparticles to spleen and liver. Biomater Sci. 2021 Feb 23;9(4):1449–63.

87. Sago CD, Krupczak BR, Lokugamage MP, Gan Z, Dahlman JE. Cell Subtypes Within the Liver Microenvironment Differentially Interact with Lipid Nanoparticles. Cell Mol Bioeng. 2019 May 8;12(5):389–97.

88. Jensen K, Anderson JA, Glass EJ. Comparison of small interfering RNA (siRNA) delivery into bovine monocyte-derived macrophages by transfection and electroporation. Vet Immunol Immunopathol. 2014 Apr 15;158(3–4):224–32.

89. Chen D, Ganesh S, Wang W, Amiji M. The role of surface chemistry in serum protein corona-mediated cellular delivery and gene silencing with lipid nanoparticles. Nanoscale. 2019 May 9;11(18):8760–75.

90. Yanez Arteta M, Kjellman T, Bartesaghi S, Wallin S, Wu X, Kvist AJ, et al. Successful reprogramming of cellular protein production through mRNA delivered by functionalized lipid nanoparticles. Proc Natl Acad Sci. 2018 Apr 10;115(15):E3351–60.

91. Spadea A, Jackman M, Cui L, Pereira S, Lawrence MJ, Campbell RA, et al. Nucleic Acid-Loaded Lipid Nanoparticle Interactions with Model Endosomal Membranes. ACS Appl Mater Interfaces. 2022 Jul 6;14(26):30371–84.

92. Cui L, Renzi S, Quagliarini E, Digiacomo L, Amenitsch H, Masuelli L, et al. Efficient Delivery of DNA Using Lipid Nanoparticles. Pharmaceutics. 2022 Aug 15;14(8):1698.

93. Hoshyar N, Gray S, Han H, Bao G. The effect of nanoparticle size on in vivo pharmacokinetics and cellular interaction. Nanomed. 2016 Mar;11(6):673.

94. Clogston JD, Patri AK. Zeta Potential Measurement. In: McNeil SE, editor. Characterization of Nanoparticles Intended for Drug Delivery [Internet]. Totowa, NJ: Humana Press; 2011 [cited 2023 Aug 1]. p. 63–70. (Methods in Molecular Biology). Available from: https://doi.org/10.1007/978-1-60327-198-1_6

95. Bhattacharjee S. DLS and zeta potential - What they are and what they are not? J Control Release Off J Control Release Soc. 2016 Aug 10;235:337–51.

96. Hald Albertsen C, Kulkarni JA, Witzigmann D, Lind M, Petersson K, Simonsen JB. The role of lipid components in lipid nanoparticles for vaccines and gene therapy. Adv Drug Deliv Rev. 2022 Sep;188:114416.

97. Kiwada H, Matsuo H, Harashima H. Identification of proteins mediating clearance of liposomes using a liver perfusion system. Adv Drug Deliv Rev. 1998 Jun 8;32(1–2):61–79.

98. Walther J, Wilbie D, Tissingh VSJ, Öktem M, van der Veen H, Lou B, et al. Impact of Formulation Conditions on Lipid Nanoparticle Characteristics and Functional Delivery of CRISPR RNP for Gene Knock-Out and Correction. Pharmaceutics. 2022 Jan 17;14(1):213.

99. DeCarlo AN, Parrish J, Bridges W, Pratt S. 8 Assessment of consistency in quantification of ribonucleic acid across multiple methods. J Anim Sci. 2020 Nov 28;98(Suppl 2):35–6.

100. Thaller A, Schmauder L, Frieß W, Winter G, Menzen T, Hawe A, et al. SV-AUC as a stability-indicating method for the characterization of mRNA-LNPs. Eur J Pharm Biopharm. 2023 Jan;182:152–6.

101. Szebeni J, Kiss B, Bozó T, Turjeman K, Levi-Kalisman Y, Barenholz Y, et al. New insights into the structure of Comirnaty Covid-19 vaccine: A theory on soft nanoparticles with mRNA-lipid supercoils stabilized by hydrogen bonds [Internet]. bioRxiv; 2022 [cited 2023 Aug 15]. p. 2022.12.02.518611. Available from: https://www.biorxiv.org/content/10.1101/2022.12.02.518611v1

102. Kudsiova L, Lansley A, Scutt G, Allen M, Bowler L, Williams S, et al. Stability testing of the Pfizer-BioNTech BNT162b2 COVID-19 vaccine: a translational study in UK vaccination centres. BMJ Open Sci. 2021 Sep 12;5(1):e100203.

103. Lv H, Zhang S, Wang B, Cui S, Yan J. Toxicity of cationic lipids and cationic polymers in gene delivery. J Controlled Release. 2006 Aug 10;114(1):100–9.

104. Cui S, Wang Y, Gong Y, Lin X, Zhao Y, Zhi D, et al. Correlation of the cytotoxic effects of cationic lipids with their headgroups. Toxicol Res. 2018 Mar 22;7(3):473–9.

105. Ferraresso F, Strilchuk AW, Juang LJ, Poole LG, Luyendyk JP, Kastrup CJ. Comparison of DLin-MC3-DMA and ALC-0315 for siRNA Delivery to Hepatocytes and Hepatic Stellate Cells. Mol Pharm. 2022 Jul 4;19(7):2175–82.

106. Liu C, Liu XN, Wang GL, Hei Y, Meng S, Yang LF, et al. A dual-mediated liposomal drug delivery system targeting the brain: rational construction, integrity evaluation across the blood–brain barrier, and the transporting mechanism to glioma cells. Int J Nanomedicine. 2017 Mar 28;12:2407–25.

107. Bio-Rad. Bio-Rad. [cited 2023 Aug 17]. Autofluorescence - Flow Cytometry Guide. Available from: https://www.bio-rad-antibodies.com/flow-cytometry-autofluorescence.html

108. Zhang J, Zhang W, Yang L, Zhao W, Liu Z, Wang E, et al. Phytochemical gallic acid alleviates nonalcoholic fatty liver disease via AMPK-ACC-PPARa axis through dual regulation of lipid metabolism and mitochondrial function. Phytomedicine. 2023 Jan 1;109:154589.

109. Pattipeiluhu R, Arias-Alpizar G, Basha G, Chan KYT, Bussmann J, Sharp TH, et al. Anionic Lipid Nanoparticles Preferentially Deliver mRNA to the Hepatic Reticuloendothelial System. Adv Mater. 2022;34(16):2201095.

110. Rey-Giraud F, Hafner M, Ries CH. In Vitro Generation of Monocyte-Derived Macrophages under Serum-Free Conditions Improves Their Tumor Promoting Functions. PLOS ONE. 2012 Aug 6;7(8):e42656.

111. Edin S, Wikberg ML, Rutegård J, Oldenborg PA, Palmqvist R. Phenotypic Skewing of Macrophages In Vitro by Secreted Factors from Colorectal Cancer Cells. PLOS ONE. 2013 Sep 18;8(9):e74982.

112. Jones SW, Roberts RA, Robbins GR, Perry JL, Kai MP, Chen K, et al. Nanoparticle clearance is governed by Th1/Th2 immunity and strain background. J Clin Invest. 2013 Jul 1;123(7):3061–73.

113. Martinez FO, Gordon S, Locati M, Mantovani A. Transcriptional Profiling of the Human Monocyte-to-Macrophage Differentiation and Polarization: New Molecules and Patterns of Gene Expression1. J Immunol. 2006 Nov 15;177(10):7303–11.

114. Chen H, Yang WW, Wen QT, Xu L, Chen M. TGF-beta induces fibroblast activation protein expression; fibroblast activation protein expression increases the proliferation, adhesion, and migration of HO-8910PM [corrected]. Exp Mol Pathol. 2009 Dec;87(3):189–94.

115. Fernández-Borja M, Bellido D, Vilella E, Olivecrona G, Vilaró S. Lipoprotein lipase-mediated uptake of lipoprotein in human fibroblasts: evidence for an LDL receptor-independent internalization pathway. J Lipid Res. 1996 Mar;37(3):464–81.

116. Bhandari S, Larsen AK, McCourt P, Smedsrød B, Sørensen KK. The Scavenger Function of Liver Sinusoidal Endothelial Cells in Health and Disease. Front Physiol. 2021 Oct 11;12:757469.

117. Løvdal T, Andersen E, Brech A, Berg T. Fc receptor mediated endocytosis of small soluble immunoglobulin G immune complexes in Kupffer and endothelial cells from rat liver. J Cell Sci. 2000 Sep 15;113(18):3255–66.

118. Bala S, Zhuang Y, Nagesh PT, Catalano D, Zivny A, Wang Y, et al. Therapeutic inhibition of miR-155 attenuates liver fibrosis via STAT3 signaling. Mol Ther Nucleic Acids. 2023 Jul 15;33:413–27.

119. Merrill JR, Krajewski K, Yuan H, Frank JE, Lalush DS, Patterson C, et al. Data on biodistribution and radiation absorbed dose profile of a novel 64Cu-labeled high affinity cell-specific peptide for positron emission tomography imaging of tumor vasculature. Data Brief. 2016 Jun;7:480–4.

120. Esquinas PL, Shinto A, Kamaleshwaran KK, Joseph J, Celler A. Biodistribution, pharmacokinetics, and organ-level dosimetry for 188Re-AHDD-Lipiodol radioembolization based on quantitative post-treatment SPECT/CT scans. EJNMMI Phys. 2018 Dec 7;5(1):30.

121. Xiao K, Li Y, Luo J, Lee JS, Xiao W, Gonik AM, et al. The effect of surface charge on in vivo biodistribution of PEG-oligocholic acid based micellar nanoparticles. Biomaterials. 2011 May;32(13):3435–46.

122. Iwakiri Y, Shah V, Rockey DC. Vascular pathobiology in chronic liver disease and cirrhosis – Current status and future directions. J Hepatol. 2014 Oct 1;61(4):912–24.

123. Lautt WW. Regulatory processes interacting to maintain hepatic blood flow constancy: Vascular compliance, hepatic arterial buffer response, hepatorenal reflex, liver regeneration, escape from vasoconstriction. Hepatol Res Off J Jpn Soc Hepatol. 2007 Nov;37(11):891–903.

124. Guéguen C, Ben Chimol T, Briand M, Renaud K, Seiler M, Ziesel M, et al. Evaluating how cationic lipid affects mRNA-LNP physical properties and biodistribution. Eur J Pharm Biopharm [Internet]. 2023 Aug 12 [cited 2023 Aug 19]; Available from: https://www.sciencedirect.com/science/article/pii/S0939641123002059

125. Scholten D, Trebicka J, Liedtke C, Weiskirchen R. The carbon tetrachloride model in mice. Lab Anim. 2015 Apr 1;49(1_suppl):4–11.

126. Uemitsu N, Nakayoshi H. Evaluation of liver weight changes following a single oral administration of carbon tetrachloride in rats. Toxicol Appl Pharmacol. 1984 Aug;75(1):1–7.

127. Hoffmann KMV, Tonks NK, Barford D. The Crystal Structure of Domain 1 of Receptor Protein-tyrosine Phosphatase μ *. J Biol Chem. 1997 Oct 31;272(44):27505–8.

128. Ye N, Cai J, Dong Y, Chen H, Bo Z, Zhao X, et al. A multi-omic approach reveals utility of CD45 expression in prognosis and novel target discovery. Front Genet [Internet]. 2022 [cited 2023 Aug 20];13. Available from: https://www.frontiersin.org/articles/10.3389/fgene.2022.928328

129. Freitas-Lopes MA, Mafra K, David BA, Carvalho-Gontijo R, Menezes GB. Differential Location and Distribution of Hepatic Immune Cells. Cells. 2017 Dec 7;6(4):48.

130. Zwicker C, Bujko A, Scott CL. Hepatic Macrophage Responses in Inflammation, a Function of Plasticity, Heterogeneity or Both? Front Immunol. 2021 Jun 9;12:690813.

131. Crane MJ, Daley JM, Houtte O van, Brancato SK, Jr WLH, Albina JE. The Monocyte to Macrophage Transition in the Murine Sterile Wound. PLOS ONE. 2014 Jan 22;9(1):e86660.

132. Rose S, Misharin A, Perlman H. A novel Ly6C/Ly6G-based strategy to analyze the mouse splenic myeloid compartment. Cytom Part J Int Soc Anal Cytol. 2012 Apr;81(4):343–50.

133. Zheng C, Yang Q, Xu C, Shou P, Cao J, Jiang M, et al. CD11b regulates obesity-induced insulin resistance via limiting alternative activation and proliferation of adipose tissue macrophages. Proc Natl Acad Sci. 2015 Dec 29;112(52):E7239–48.

134. Duffield JS. Dendritic cells take on more tasks in the liver? Hepatol Baltim Md. 2012 Jan;55(1):16–9.

135. Hume DA, Robinson AP, MacPherson GG, Gordon S. The mononuclear phagocyte system of the mouse defined by immunohistochemical localization of antigen F4/80. Relationship between macrophages, Langerhans cells, reticular cells, and dendritic cells in lymphoid and hematopoietic organs. J Exp Med. 1983 Nov 1;158(5):1522–36.

136. Sun X, Jones HP, Dobbs N, Bodhankar S, Simecka JW. Dendritic Cells Are the Major Antigen Presenting Cells in Inflammatory Lesions of Murine Mycoplasma Respiratory Disease. PLoS ONE. 2013 Feb 4;8(2):e55984.

137. Sheng J, Chen Q, Soncin I, Ng SL, Karjalainen K, Ruedl C. A Discrete Subset of Monocyte-Derived Cells among Typical Conventional Type 2 Dendritic Cells Can Efficiently Cross-Present. Cell Rep. 2017 Oct;21(5):1203–14.

138. Chow A, Schad S, Green MD, Hellmann MD, Allaj V, Ceglia N, et al. Tim-4+ Cavity-Resident Macrophages Impair Anti-Tumor CD8+ T cell Immunity. Cancer Cell. 2021 Jul 12;39(7):973-988.e9.

139. Schmid MC, Khan SQ, Kaneda MM, Pathria P, Shepard R, Louis TL, et al. Integrin CD11b activation drives anti-tumor innate immunity. Nat Commun. 2018 Dec 19;9:5379.

140. Yao X, Dong G, Zhu Y, Yan F, Zhang H, Ma Q, et al. Leukadherin-1-Mediated Activation of CD11b Inhibits LPS-Induced Pro-inflammatory Response in Macrophages and Protects Mice Against Endotoxic Shock by Blocking LPS-TLR4 Interaction. Front Immunol [Internet]. 2019 [cited 2023 Aug 17];10. Available from: https://www.frontiersin.org/articles/10.3389/fimmu.2019.00215

141. Bain CC, Scott CL, Uronen-Hansson H, Gudjonsson S, Jansson O, Grip O, et al. Resident and pro-inflammatory macrophages in the colon represent alternative context-dependent fates of the same Ly6Chi monocyte precursors. Mucosal Immunol. 2013 May;6(3):498–510.

142. Shan Z, Ju C. Hepatic Macrophages in Liver Injury. Front Immunol. 2020 Apr 17;11:322.

143. Xue Q, Yan Y, Zhang R, Xiong H. Regulation of iNOS on Immune Cells and Its Role in Diseases. Int J Mol Sci. 2018 Nov 29;19(12):3805.

144. Kostrzewski T, Snow S, Battle AL, Peel S, Ahmad Z, Basak J, et al. Modelling human liver fibrosis in the context of non-alcoholic steatohepatitis using a microphysiological system. Commun Biol. 2021 Sep 15;4(1):1–15.

145. Iredale JP, Thompson A, Henderson NC. Extracellular matrix degradation in liver fibrosis: Biochemistry and regulation. Biochim Biophys Acta BBA - Mol Basis Dis. 2013 Jul 1;1832(7):876–83.

146. Feng X, Bao J, Song C, Xie L, Tan X, Li J, et al. Functional role of miR-155 in physiological and pathological processes of liver injury (Review). Mol Med Rep. 2021 Oct 1;24(4):1–8.

147. Théry C, Amigorena S, Raposo G, Clayton A. Isolation and Characterization of Exosomes from Cell Culture Supernatants and Biological Fluids. Curr Protoc Cell Biol. 2006;30(1):3.22.1-3.22.29.

148. Batrakova EV, Kim MS. Using exosomes, naturally-equipped nanocarriers, for drug delivery. J Controlled Release. 2015 Dec 10;219:396–405.

149. Morhayim J, Rudjito R, van Leeuwen JP, van Driel M. Paracrine Signaling by Extracellular Vesicles via Osteoblasts. Curr Mol Biol Rep. 2016;2(1):48–55.

150. Qi J, Zhou Y, Jiao Z, Wang X, Zhao Y, Li Y, et al. Exosomes Derived from Human Bone Marrow Mesenchymal Stem Cells Promote Tumor Growth Through Hedgehog Signaling Pathway. Cell Physiol Biochem. 2017 Aug 16;42(6):2242–54.

151. Buzas EI. The roles of extracellular vesicles in the immune system. Nat Rev Immunol. 2023 Apr;23(4):236–50.

152. Hidalgo-Garcia L, Galvez J, Rodriguez-Cabezas ME, Anderson PO. Can a Conversation Between Mesenchymal Stromal Cells and Macrophages Solve the Crisis in the Inflamed Intestine? Front Pharmacol [Internet]. 2018 [cited 2023 Aug 20];9. Available from: https://www.frontiersin.org/articles/10.3389/fphar.2018.00179

153. Arabpour M, Saghazadeh A, Rezaei N. Anti-inflammatory and M2 macrophage polarization-promoting effect of mesenchymal stem cell-derived exosomes. Int Immunopharmacol. 2021 Aug 1;97:107823.

154. Lee H, Hong I. Double-edged sword of mesenchymal stem cells: Cancer-promoting versus therapeutic potential. Cancer Sci. 2017 Oct;108(10):1939–46.

155. Zhao H, Shang Q, Pan Z, Bai Y, Li Z, Zhang H, et al. Exosomes From Adipose-Derived Stem Cells Attenuate Adipose Inflammation and Obesity Through Polarizing M2 Macrophages and Beiging in White Adipose Tissue. Diabetes. 2017 Nov 13;67(2):235–47.

156. Domenis R, Cifù A, Quaglia S, Pistis C, Moretti M, Vicario A, et al. Pro inflammatory stimuli enhance the immunosuppressive functions of adipose mesenchymal stem cells-derived exosomes. Sci Rep. 2018 Sep 6;8(1):13325.

157. Chen YT, Sun CK, Lin YC, Chang LT, Chen YL, Tsai TH, et al. Adipose-Derived Mesenchymal Stem Cell Protects Kidneys against Ischemia-Reperfusion Injury through Suppressing Oxidative Stress and Inflammatory Reaction. J Transl Med. 2011 May 5;9(1):51.

158. Bocsan IC, Milaciu MV, Pop RM, Vesa SC, Ciumarnean L, Matei DM, et al. Cytokines Genotype-Phenotype Correlation in Nonalcoholic Steatohepatitis. Oxid Med Cell Longev. 2017 Aug 9;2017:e4297206.

159. Mirea AM, Tack CJ, Chavakis T, Joosten LAB, Toonen EJM. IL-1 Family Cytokine Pathways Underlying NAFLD: Towards New Treatment Strategies. Trends Mol Med. 2018 May 1;24(5):458–71.

160. Wang J, Xia J, Huang R, Hu Y, Fan J, Shu Q, et al. Mesenchymal stem cell-derived extracellular vesicles alter disease outcomes via endorsement of macrophage polarization. Stem Cell Res Ther. 2020 Sep 29;11(1):424.

161. Harrell CR, Jovicic N, Djonov V, Arsenijevic N, Volarevic V. Mesenchymal Stem Cell-Derived Exosomes and Other Extracellular Vesicles as New Remedies in the Therapy of Inflammatory Diseases. Cells. 2019 Dec;8(12):1605.

162. Racchetti G, Meldolesi J. Extracellular Vesicles of Mesenchymal Stem Cells: Therapeutic Properties Discovered with Extraordinary Success. Biomedicines. 2021 Jun 10;9(6):667.

163. Li H, Jiang T, Li MQ, Zheng XL, Zhao GJ. Transcriptional Regulation of Macrophages Polarization by MicroRNAs. Front Immunol [Internet]. 2018 [cited 2023 Aug 20];9. Available from: https://www.frontiersin.org/articles/10.3389/fimmu.2018.01175

164. Wiklander OPB, Brennan MÁ, Lötvall J, Breakefield XO, Andaloussi SE. Advances in therapeutic applications of extracellular vesicles. Sci Transl Med. 2019 May 15;11(492):eaav8521.

165. Ghaneialvar H, Soltani L, Rahmani HR, Lotfi AS, Soleimani M. Characterization and Classification of Mesenchymal Stem Cells in Several Species Using Surface Markers for Cell Therapy Purposes. Indian J Clin Biochem. 2018 Jan;33(1):46–52.

166. Addgene: Kit Free RNA Extraction [Internet]. [cited 2023 Aug 20]. Available from: https://www.addgene.org/protocols/kit-free-rna-extraction/